2009

EFFECTS OF OXIDATIVE MODIFICATIONS ON SUBUNIT INTERACTIONS IN HEMOGLOBIN

Brian L. Boys

EFFECTS OF OXIDATIVE MODIFICATIONS ON SUBUNIT INTERACTIONS IN HEMOGLOBIN

(Spine title: Protein Oxidation and Hemoglobin Disassembly)

(Thesis format: Integrated-Article)

by

Brian L. Boys

Graduate Program
in
Chemistry

A thesis submitted in partial fulfillment
of the requirements for a degree of
Master of Science

School of Graduate and Postdoctoral Studies
The University of Western Ontario
London, Ontario, Canada

Table of Contents

List of Appendices

List of Symbols and Abbreviations

A_λ – absorbance at wavelength λ

A_L - left-circularly polarized light

A_R - right-circularly polarized light

A^+ - positively charged analyte ion

α – alpha helix

α^a - apo-α-globin

αHb - apo-α-globin (Chapter 3)

α^h - holo-α-globin

β^a - apo-β-globin

βHb - apo-β-globin (Chapter 3)

β^h - holo-β-globin

β^a_{ox} - oxidatively damaged apo-β-globin

β – beta sheet

ε – dielectric constant

ε_o – permittivity of vacuum ($8.8541878 \times 10^{-12}$ C^2 J^{-1} m^{-1})

ε_λ – molar extinction coefficient

θ, ψ – bond torsion angles

θ_1, θ_2 – progress variables in protein folding, i.e., torsion angles

γ – surface tension

γ – electrolytic load (Chapter 3)

b – path length through optical cuvette

c, [ ] – concentration in mol L^{-1}

CD – circular dichroism

CE – counter electrode

CID – collision induced dissociation

C_p – heat capacity

D – denaturant

DPG- 2-3-diphosphoglycerate

E_{on} – electric field required for onset of electrospray

E^o – equilibrium standard reduction potential

ESI - electrospray ionization

FRET - Förster resonance energy transfer

f_u – fraction unfolded

G^o - standard Gibb's free energy

ΔG^o - standard Gibb's free energy change

$\Delta G^{\ddagger}$ - standard Gibb's free energy of activation

$\Delta G^o{}_{N\to U}(0)$ - standard Gibb's unfolding free energy in absence of denaturant

$\Delta G^o{}_{N\to U}(D)$ - apparent standard Gibb's unfolding free energy with denaturant D

k_B – Boltzmann constant

k_f – first-order folding rate constant

k_u - first-order unfolding rate constant

h – Planck's constant

Hb – hemoglobin

^{cyanomet}Hb - ferri (Fe^{3+}) hemoglobin with heme iron ligated by CN^-

^{met}Hb - ferri (Fe^{3+}) hemoglobin

^{oxy}Hb - ferro (Fe^{2+}) hemoglobin with heme iron ligated by O_2

I_o – intensity of incident radiation

I – intensity of emergent radiation (Chapter 1.4.1.1)

I – nuclear spin number (Chapter 1.4.1.4)

I_{ESI} – electrospray current without corona contribution

I_{corona} – corona contribution to observed electrospray current

I_{tot} – overall electrospray current

K_d – dissociation constant

LC – liquid chromatography

m - $\delta \Delta G^{o}_{N \rightarrow U}(D) / \delta[D]$

m_z – magnetic spin quantum number

M - mass

MS – mass spectrometry

m/z – mass to charge ratio

N – native state

NMR – nuclear magnetic resonance

P_N – population of proteins in the native state

P_U – population of proteins in the unfolded state

P_a – population of proteins in unfolded macrostate

q – point charge

Q – quadrupole mass filter

r – distance separating two entities

r_c – outer radius of a metal electrospray capillary

R – amino acid side group

R- gas constant

R – relaxed state of oxygenated Hb

RBC – red blood cell

RNS – reactive nitrogen species

ROS – reactive oxygen species

SCE – saturated calomel reference electrode

T – temperature in Kelvin

T – tense state of deoxygenated Hb

TOF – time of flight mass analyzer

TS – transition state

U – unfolded state

U – potential energy

v_f - flow rate

V_o – voltage applied to ESI capillary

$V_{M/L}$ – interfacial potential drop at a metal-liquid interface

WE – working electrode

X – optical signal (Chapter 1)

X – nebulizer gas (Chapter 3)

Abstract

Much is known regarding the folding reactions of small, single domain proteins. However, the extent to which these principles apply to the folding of large, multi-domain proteins, and multi-subunit protein complexes, remains to be seen. Monitoring the (un)folding reactions of such proteins poses unique challenges, and requires instrumentation capable of distinguishing intramolecular contacts from intermoleculer interactions.

Electrospray ionization (ESI) mass spectrometry (MS) offers enormous potential to the study of multi-subunit protein complexes, as it simultaneously detects and resolves coexisting protein species and conformers in solution. Such high selectivity combined with excellent sensitivity makes ESI-MS a primary tool in the study of higher-order protein folding reactions.

The work herein examines the unfolding reaction of the multi-subunit oxygen transport protein hemoglobin (Hb) using ESI-MS in combination with UV-Vis spectroscopy. The results strongly support a symmetrical dissociation mechanism, which contradicts a previously proposed mechanism supporting an asymmetric disassembly. This apparent contradiction is attributed to non-native oxidative modifications which destabilize the native state.

Due to the nature of ESI, instrument-induced analyte oxidation is a concern. The process of ESI-induced analyte oxidation is discussed and the mechanism of which is determined. Prevention strategies are therefore put forth, since given the effects of

oxidation on folding, it is vital to distinguish solution phase analyte oxidation from instrument-induced oxidation.

Keywords: protein folding, hemoglobin, disassembly mechanism, electrospray ionization mass spectrometry, UV-Vis spectroscopy, equilibrium, oxidation, corona discharge, electrochemistry

Statement of Co-Authorship

The work in Chapter 2 was published in the following article:

> Brian L. Boys, Mark C. Kuprowski, and Lars Konermann (2007). Symmetric Behaviour of Hemoglobin α- and β- Subunits During Acid-Induced Denaturation Observed by Electrospray Mass Spectrometry. *Biochemistry,* 46(37), 10675-10684. Reproduced with permission. © 2007 American Chemical Society

The work in Chapter 3 has been accepted for publication:

> Brian L. Boys, Mark C. Kuprowski, James J. Noël, and Lars Konermann (2009). Protein Oxidative Modifications During Electrospray Ionization: Solution Phase Electrochemistry or Corona Discharge-Induced Radical Attack? *Anal. Chem.* (in press). Reproduced with permission. Unpublished work © 2009 American Chemical Society

The original draft for each of the above articles was prepared by the author. Subsequent revisions were by Dr. Lars Konermann and the author. The tryptic peptide mapping and LC-ESI-MS/MS analysis presented in Figure 2.9 was conducted by Mark C. Kuprowski. All other experimental work was performed by the author.

Acknowledgements

My *super*visor, Dr. Lars Konermann, and everyone along the way...

Chapter 1 – Introduction

1.1 Proteins: From Primary Structure to Intricate Machines

The living cell is an amazing self replicating entity, containing proteins and many other bio-organic molecules within a viscous cytosol. Proteins, being the direct output of the genetic code as entailed by the central dogma of biology, form the structural moieties of cells and organisms, and also guide the chemical reactions that allow physical life as we know it to exist [1]. Proteins are chiral-biological polymers of varying size that consist of combinations of 19 L-amino acids and L-proline (an imino acid). Prior to function, proteins must fold into very specific structures [2-5]. The architecture of proteins can be divided into four hierarchical levels (Figure 1.1). The *primary structure* defines the linear sequence of amino acids linked by coplanar peptide (amide) bonds; the *secondary structure* refers to the local arrangement of the peptide backbone into α-helices, β-sheets, turns, and coiled regions; *tertiary structure*, the highest level of spatial organization for individual protein chains, defines the three-dimensional fold of all parts of the constituent chain. Beyond the complete folding of monomeric chains, for some proteins there exists a higher level of molecular organization through interaction with other protein chains (subunits). This final level of molecular assembly on a microscopic level is called *quaternary structure.*

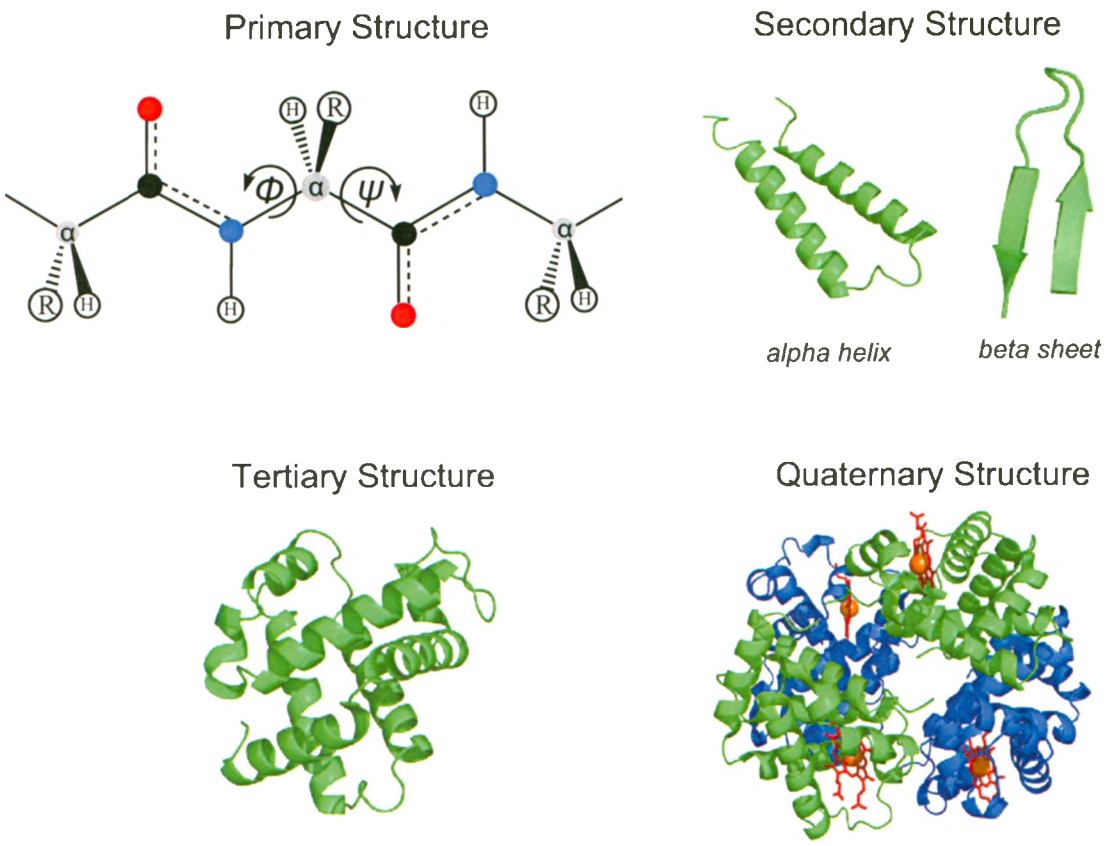

Figure 1.1: Depiction of the four hierarchical levels of protein structure. *Primary structure*: the partial double bond character of the coplanar peptide bond and Φ, ψ torsion angles adjacent the α-carbon is shown. Notation: α-carbon (grey), carbonyl carbon (black), oxygen (red), nitrogen (blue), amino acid defining functionality (R), hydrogen (H). *Secondary structure*: cartoon depiction of a helix-loop-helix and an anti-parallel beta-sheet, two common folding motifs. *Tertiary structure*: cartoon depiction of an alpha-helical protein. *Quaternary structure*: cartoon depiction of the alpha helical protein Hb containing four subunits and four porphyrin cofactors.

1.1.1 Protein Folding: A Brief History

Pauling, Mirsky and Anson in the 1930's described a theory pertaining to the structure of the native and denatured states of proteins [6]. Pauling and colleagues were later able to anticipate α-helical secondary structure in proteins, and for this in part received the 1954 Nobel Prize in chemistry [7]. The next revolution in the understanding of protein structure came in the 1960's from atomic-resolution X-ray crystal structures of the proteins myoglobin and hemoglobin [8].

The work of Anfinsen on the *in vitro* folding of ribonuclease a decade later was instrumental in that it showed for the first time that the native structure of a protein is a thermodynamically stable state, which depends only on the totality of intra- and interatomic interactions of the polypeptide chain as prescribed by the amino acid sequence and facilitated through solvent interactions [9]. To show that it was possible to refold a denatured protein in a test tube by restoring physiologic solvent conditions, outside the cell and away from ribosomes or chaperones, was to give birth to a new field of research pertaining to the physical understanding of proteins. For his work on the principles that govern the folding of protein chains, Anfinsen shared part of the 1972 Nobel Prize in chemistry.

Anfinsen developed the thermodynamic hypothesis of protein folding, implying that there is a folding code based on the liner sequence of amino acids. However, an apparent problem pointed out by Levinthal pertaining to the kinetics of the folding process struck much curiosity, as the following paradox is quoted in nearly every protein folding review [10]. Consider the peptide backbone of a small protein of 101 amino acids. Assuming the torsion angles Φ and ψ adjacent each α-carbon (Figure 1.1) sample three

angles each during folding, 3^{200} (10^{95}) possible conformations exist. If a folding protein were to search these conformations in an unbiased and random fashion until the native conformation was reached, even in the absence of an activation barrier, proceeding at the maximum rate possible given by k_BT/h (~ 6.25×10^{12} s^{-1} if T = 300K) [11], the protein would take ~10^{75} years to fold! Of course a more whimsical way of thinking using this line of logic would be to calculate how much it would cost for a monkey to earn a degree if all exams were multiple choice. Just as it is understood that a student doesn't obtain a mark of 100% by chance, that is, successful students aren't monkeys, it is understood that proteins do not fold by pure random walk, and that each unfolded conformer need not sample all possible conformations [12]. Unguided searching through vast space, conformational space in the case of Levinthal's protein, or information space in the case of the monkey, equates impossibility. These paradoxes disappear with the notion of an energy landscape, guided folding or meaningful knowledge. Biological proteins are programmed for efficient folding, where directed and efficient sampling of conformational space enables denatured proteins to circumvent the 'Levinthal paradox' via funneled energy landscapes (section 1.1.2) [13].

Much progress has been made in understanding the 'protein folding problem' of 50 years ago, namely, the tertiary structure of each protein being a function of its primary structure. This global optimization problem is separable to (a) Anfinsen's thermodynamic hypothesis, the thermodynamic intra- and interatomic interactions directing folding and function and (b) the kinetics of the folding process, how do proteins go about circumventing the Levinthal paradox once they leave the ribosome [14, 15]. The

'hunt for the unicorn' is the aspiration to develop an algorithm to predict native structure from primary sequence [16].

1.1.2 *The Protein Folding Landscape: the 'new view'*

To gain insight into the folding process, researchers typically employ *in vitro* folding and unfolding studies on purified proteins [5]. Such experiments are carried out under kinetic or equilibrium conditions [17]. Additionally, as computer processor speed has advanced, simulations based on homology algorithms or molecular dynamics are being developed to model (un)folding processes *in silico* [16]. *In vitro* kinetic studies reveal protein folding reactions to be very fast, commencing on the order of milliseconds to seconds, with a few ultra-fast folding proteins relaxing on the microsecond time scale [18-21].

The (un)folding reaction of some small, single-domain proteins appear to behave as a two-state process [22-26]. Two-state, by definition, means that only two populations of species are ever detected. For the two-state mass action model:

$$U \xrightarrow{k_f} N \tag{1.1}$$

the rate equation for the native state N can be described by:

$$\frac{dP_N}{dt} = k_f P_u \qquad with \quad P_N + P_u = 1 \tag{1.2}$$

where P_N and P_U are the fractions of proteins in the native and unfolded state, respectively. The folding first-order rate constant is denoted as k_f. The situation described

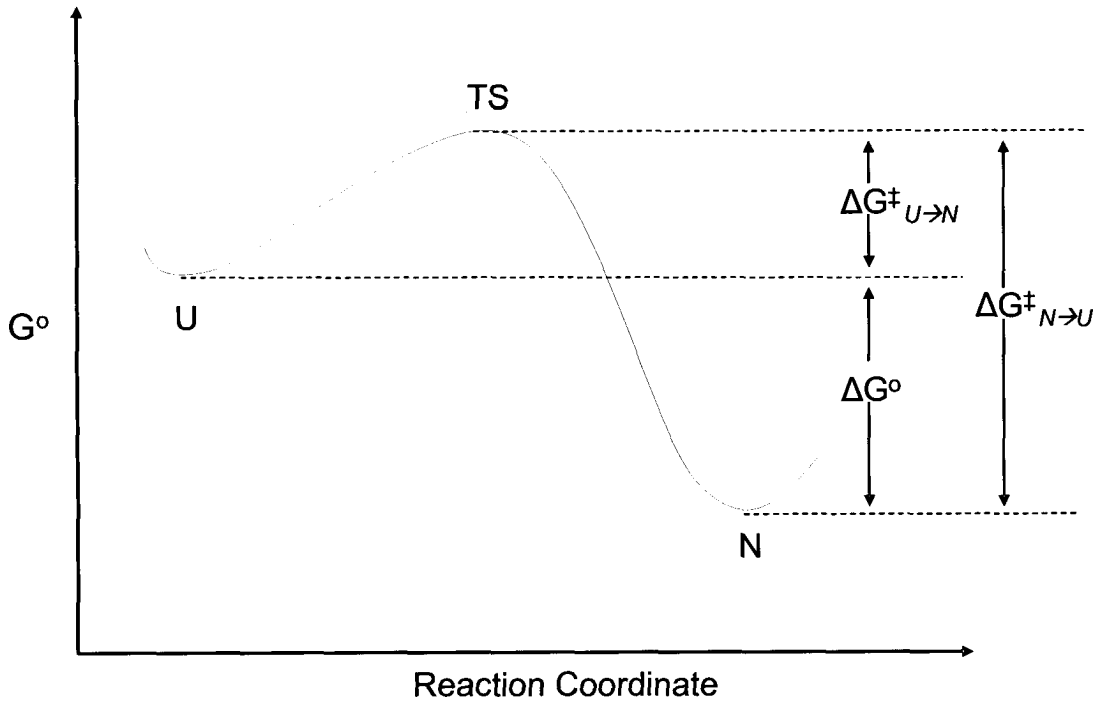

Figure 1.2: Arrhenius diagram of a two-state process, such as protein folding from an unfolded state U to the native state N. The obligatory transition state TS barrier results in single exponential behaviour of the process $U \rightarrow N$. The change in standard Gibs free energy ΔG^o between U and N as a function of a single reaction coordinate is indicated. The heights of the folding $U \rightarrow N$ and unfolding $N \rightarrow U$ TS barriers under native solvent conditions are indicated.

in eq 1.1 and 1.2 can be understood in a macroscopic sense through the Arrhenius diagram presented in Figure 1.2, which is often used to describe classical chemical reactions of a single reaction coordinate. Figure 1.2 represents a situation favouring the native state *N*, where the folding process $U \rightarrow N$ is shown to occur along a single pathway via three distinct molecular structures *U, TS*, and *N* appearing in sequential order. A thermodynamic energy barrier ($>3k_BT$) to an improbable transition state *TS* structure explains the often observed single exponential folding kinetics [27, 28]. This 'old view' or 'sequential micropath view' of protein folding was used to understand experimental data in a macroscopic sense [29].

Even though two-state (un)folding is often *observed* and modeled in a macroscopic sense using eq. 1.1 and 1.2 (also thermodynamically, see section 1.2.1), how could this line up with our understanding of what proteins are on a microscopic level, both in unfolded (denatured) and native states? There is no theoretical basis as to a protein (un)folding reaction having a single dominant free energy barrier as opposed to many smaller distributed barriers [30]. In protein folding terms, the word *state* denotes a region of conformational space, whereby 'native state' represents a large free energy minima on the kinetically relevant energy landscape. In a 'two-state' view, the 'unfolded state' represents the remaining large number of conformations (or microstates) in rapid local equilibrium, occupying shallow energy wells separated by $< k_BT$ [18]. Thus, a more general form of the rate equation governing two-state protein folding would be one that included parallel microscopic folding routes [31]:

$$\frac{dP_N}{dt} = \sum_{a \neq N} k(a \rightarrow N) P_a \qquad with \quad P_N + \sum_{a \neq N} P_a = 1 \tag{1.3}$$

where P_N and P_a are the fractions of proteins in the native state and all other 'unfolded states', respectively. All pathways leading to the native state from unfolded states are represented by the sum $\sum_{a \neq N}$.

The realization that folding proceeds via multiple parallel routes, as described in eq 1.3, was a cornerstone in the 'new view' or 'ensemble view' of protein folding, and may be visualized in three-dimensions through funneled energy landscapes [15, 32, 33], an example of which is presented in Figure 1.3. Folding funnels plot interaction free energy G as a function of two progress variables θ_1 and θ_2, such as torsion angles. The vertical axis or depth of the funnel is a function of all energetic and entropic contributions affecting protein stability (section 1.2), excluding chain conformational entropy, which within the framework of funnel models is depicted in θ space as the width of the funnel. It is important to keep in mind the extreme multidimensionality of protein folding, two dimensional folding funnels fall short of this. Nonetheless, the funneled energy landscape of Figure 1.3 is a more accurate reflection of the protein folding process in comparison to the Arrhenius diagram presented in Figure 1.2 in that (1) a multitude of parallel folding trajectories are possible, reflecting the enormous multiplicity of the unfolded macrostate, (2) the drastic reduction in conformational entropy which accompanies folding is depicted and (3) the experimental observation that some proteins fold in a two-state fashion is accounted for by the multiplicity of parallel pathways decreasing as proteins fold down the funneled energy landscape [14, 26, 34], not as a result of a single microscopic energy barrier as in Figure 1.2.

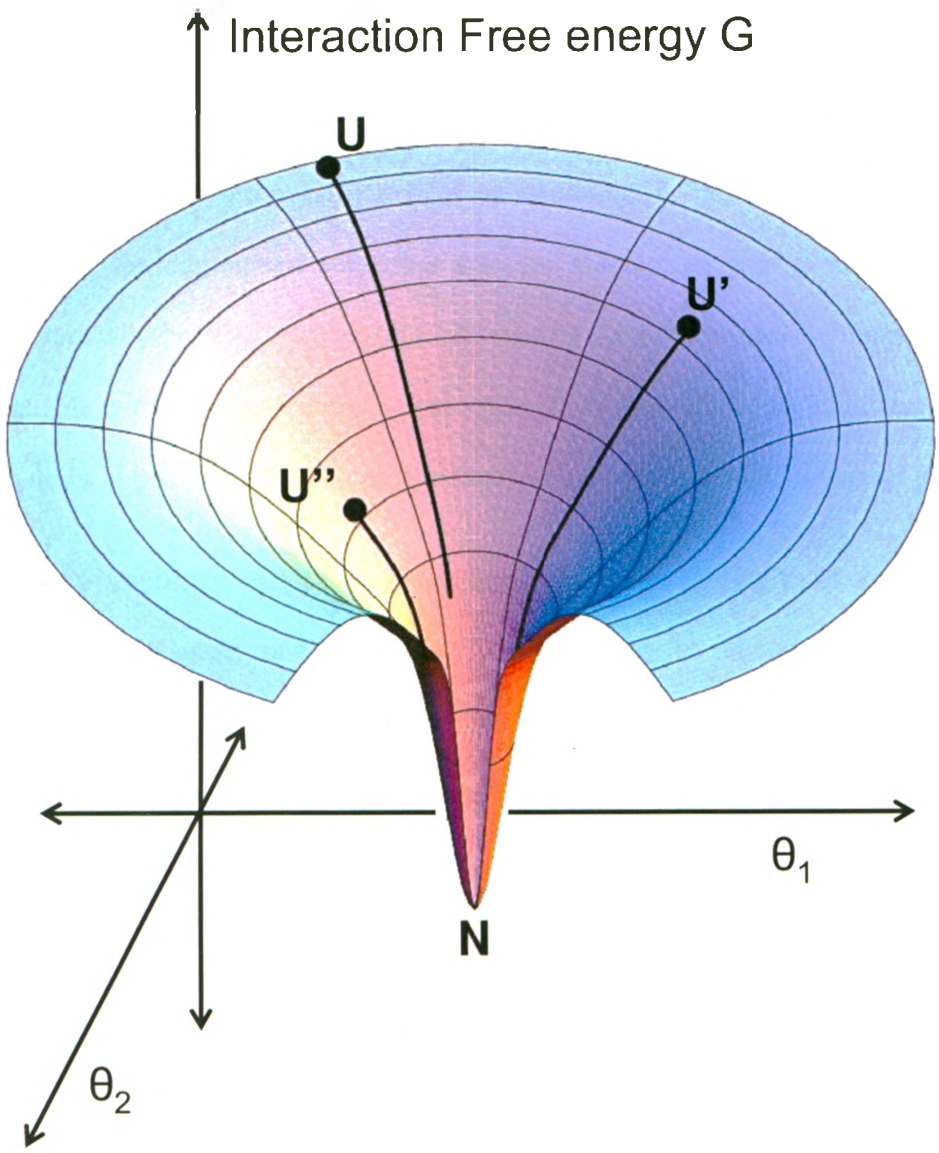

Figure 1.3: A cartoon representation of a funneled energy landscape depicting the 'new view' of the protein folding reaction $U \rightarrow N$. Interaction free energy G is plotted as a function of two progress variables, θ_1 and θ_2. Taken and modified from www.dillgroup.ucsf.edu/

1.2 Protein Stability

A basic tenet from Anfinsen's hypothesis was that the native state adopted by a protein under physiological conditions corresponds to the conformation with the lowest free energy [9]. However, it appears that this notion is only partially correct, as many proteins will slowly aggregate, especially at high concentration [5, 35, 36]. Under such conditions, it may be the aggregated state that has the global free energy minima, whilst the physiologically-healthy native state occupies a local free energy minima, i.e., it is metastable with respect to pathological aggregate forms. The misfolding and aggregation of proteins is known to be a hallmark of several age-related chronic diseases [37].

An important part of understanding a protein's folding mechanism is knowing how stable it is under native conditions. Compared to the strength of a typical carbon-carbon single bond (346 kJ mol^{-1}), or the average O-H bond strength in water (459 kJ mol^{-1}) [38], native proteins are only marginally stable under physiological conditions, with typical unfolding free energies in the absence of denaturant $\Delta G^{o}_{N\to U}(0)$ on the order of tens of kJ mol^{-1}. Some $\Delta G^{o}_{N\to U}(0)$ include: 24 kJ mol^{-1} for myoglobin [39], 31 kJ mol^{-1} for cytochrome c [39], and 39 kJ mol^{-1} for lysozyme [40].

1.2.1 Calculating Unfolding Free Energy $\Delta G^{o}_{N\to U}$

Given an infinite amount of time, the extent of the process for the isolated system

$$N \longleftrightarrow U \tag{1.4}$$

is governed by thermodynamics, where in order for spontaneity, the change in Gibb's free energy ΔG^o must meet the requirement:

$$\Delta G^o < 0 \qquad (1.5)$$

where (°) indicates standard state conditions. The Gibbs free energy is a combined restatement of the second law of thermodynamics in a way that focuses on the 'system' for convenience:

$$\Delta G^o = \Delta H^o - T\Delta S^o \qquad (1.6)$$

where the change in enthalpy and entropy at temperature T in Kelvin is represented as ΔH^o and ΔS^o at standard state, respectively.

For a reactive species perturbed from equilibrium, the direction of spontaneous change can be determined from:

$$\Delta G^o = -RT \ln K \qquad (1.7)$$

where R is the universal gas constant, T is the temperature in Kelvin, and K is the equilibrium constant. For the protein (un)folding reaction described in eq 1.4

$$K = \frac{[U]}{[N]} = \frac{k_u}{k_f} \qquad (1.8)$$

where [*N*] and [*U*] denote the concentrations of species *N* and *U*, respectively. The folding and unfolding rate constants are k_f and k_u, respectively.

Unfolding free energies under native conditions are routinely measured for purified proteins using the linear extrapolation method [25], which assumes two-state unfolding behaviour obeying eq.1.4 and a linear dependence of the apparent unfolding free energy $\Delta G^o_{N\to U}(D)$ on the denaturant concentration *D:*

$$\Delta G^o_{N\to U}(D) = \Delta G^o_{N\to U}(0) - m[D] \qquad (1.9)$$

where $\Delta G^o_{N\to U}(D)$ is the apparent unfolding free energy at denaturant concentration *D*; $\Delta G^o_{N\to U}(0)$ is the unfolding free energy in the absence of denaturant, and *m* is the gradient $\delta \Delta G^o_{N\to U}(D)/\delta[D]$, a constant proportional to a protein's increase in solvent accessible surface area (ASA) upon unfolding [41]. Unfolding is done in an equilibrium fashion, employing any one of a variety of chemical or physical denaturants (section 1.2.3). In classical experiments, the relative concentration of *U* (or *N*) can be measured by various spectroscopic techniques [42]. The optical signal *X* at denaturant concentration *D* is plotted on a relative scale, most commonly as fraction unfolded, f_U:

$$f_U = \frac{X - X_N}{X_U - X_N} = \frac{[U]}{[U]+[N]} \qquad (1.10)$$

where $f = 0$ for $X = X_N$ represents 100% *N* and $f = 1$ for $X = X_U$ represents 100% *U*. Expressing eq 1.10 in terms of eq. 1.7 and 1.8 gives:

$$f_U = \frac{\exp\left(\frac{(-\Delta G^o{}_{N\to U}}{RT}\right)}{\exp\left(\frac{(-\Delta G^o{}_{N\to U}}{RT}\right)+1} \qquad (1.11)$$

Assuming the linear approximation method of eq 1.9, $\Delta G^o_{N\to U}$ is substituted with $\Delta G^o_{N\to U}(D)$ to give

$$f_U = \frac{\exp\left(\frac{(m[D]-\Delta G^o{}_{N\to U}(0)}{RT}\right)}{\exp\left(\frac{(m[D]-\Delta G^o{}_{N\to U}(0)}{RT}\right)+1} \qquad (1.12)$$

Thus, the experimentally measured two-state f_U curve is a function of two parameters, m and $\Delta G^o_{N\to U}(0)$, which can be obtained through regression analysis. As predicted from eq 1.12, a large m value would result in a lower apparent value for $\Delta G^o_{N\to U}(0)$. This is observed experimentally [41] and accounted for by the fact that m values show strong liner correlation with the solvent accessible surface area exposed upon unfolding, which chaotropic denaturants interact favourably with (section 1.2.3). Thus, one must be careful when comparing $\Delta G^o_{N\to U}(0)$ of proteins of different size in the absence of corresponding m values, as larger proteins will exhibit a stronger dependence of $\Delta G^o_{N\to U}$ on denaturant D than smaller proteins.

The equilibrium unfolding curves for two single-domain proteins of similar size, cyt c and the slightly larger lysozyme, are presented in Figure 1.4. Figure 1.4 A is a plot of eq 1.12, where m = 11.7 kJ mol^{-1} M^{-1} and $\Delta G^{o}_{N\rightarrow U}(0)$ = 31 kJ mol^{-1} for cyt c [39] and m = 12.1 kJ mol^{-1} M^{-1} and $\Delta G^{o}_{N\rightarrow U}(0)$ = 39 kJ mol^{-1} for lysozyme [40]. Figure 1.4 B plots eq 1.9 and indicates linear extrapolation to $[D] = 0$ so as to obtain $\Delta G^{o}_{N\rightarrow U}(0)$. Even with a slightly larger m value, lysozyme is observed to be more stable when analyzed with this two-state equilibrium unfolding criteria.

Calculating $\Delta G^{o}_{N\rightarrow U}(0)$ via the linear extrapolation method works reasonably well for small single-domain proteins that (un)fold in an *apparent* two-state fashion. Deviations from two-state (un)folding complicate the analysis [39, 43, 44]. Nonetheless, useful information regarding the *apparent* stability of model proteins shown to (un)fold in a two-state fashion can be obtained in this way [40, 42].

1.2.2 Noncovalent Interactions

The stability of a folded protein under native solvent conditions is a subtle balance between stabilizing and destabilizing contributions [45]. Indeed, protein folding is a compromising process, obeying the principle of 'minimum frustration' and the limitations imposed through steric hindrance. Because of a native protein's marginal stability over its denatured state, every stabilizing interaction of the native state is important.

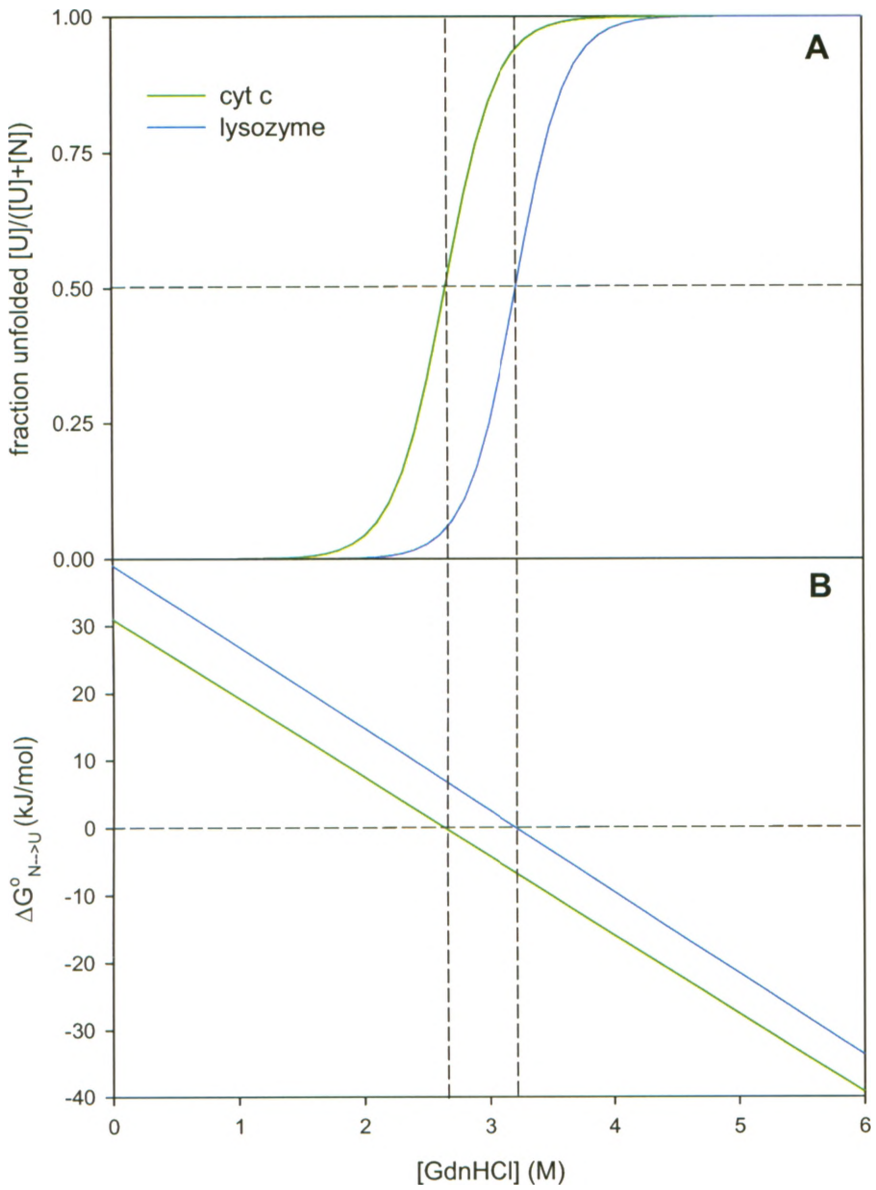

Figure 1.4: Equilibrium unfolding curves demonstrating the use of the linear approximation method in determining the unfolding free energy under native conditions $\Delta G^{o}_{N\rightarrow U}(0)$. (A) Normalized optical signal shows the fraction of unfolded protein during the $U \rightarrow N$ transition (eq. 1.12 in section 1.2.1). (B) The liner relationship between the apparent unfolding free energy at denaturant concentration D (eq 1.9 in section 1.2.1) where extrapolation to $[D]$=0 gives $\Delta G^{o}_{N\rightarrow U}(0)$. Values used to fit eq 1.12 were taken from [39, 40].

1.2.2.1 Electrostatic Interactions

The electrostatic potential energy U between two point charges q_1 and q_2 separated by a distance r is given by Coulomb's Law:

$$U(r) = \frac{q_1 q_2}{4\pi\varepsilon_o \varepsilon r} \qquad (1.13)$$

where ε_o is the permittivity of vacuum and ε is the dielectric constant of the medium. The dielectric constant for vacuum has been normalized to 1.000, with typical values for nonpolar liquid hydrocarbons being ~2, and for liquid water ~80 [46]. Thus, the nature of the solvating medium has significant affect on the magnitude of *U(r)*. ε for the internal hydrophobic core of a folded protein ranges from 1 to 8 [47].

Often charge-dipole or dipole-dipole interactions are present in proteins. The potential of these interactions do not scale as r^{-1}, as do charge-charge interactions (eq 1.13). Their strength is weaker at larger distances, scaling at r^{-3} for charge-dipole and r^{-6} for dipole-induced dipole interactions [48].

Once thought to be a dominant driving force for protein folding, electrostatic attraction and repulsion of formal/partial charges is now thought to play a lesser role, with estimates of ~10 kJ mol^{-1} enthalpic stabilization per ion pair. An effect for most proteins which is about an order of magnitude less than the free energy stabilization provided via hydrophobic interactions (section 1.2.2.4)[45].

1.2.2.2 London Attraction

London attraction, London dispersion, and induced dipole - induced dipole are synonymous in that they describe the instantaneous attractive potential that all polarizable atoms and molecules have for one another, that is, if they are not too close. This short-range, fleeting potential can be expressed as [46]:

$$U(r) = -\frac{A_{ij}}{r_{ij}^{6}} \qquad (1.14)$$

where r_{ij} is separation distance of atom or molecules i and j; A_{ij} is a positive constant (units KJ m^6 mol^{-1}) proportional to the ionization energy and polarizability of atoms or molecules i and j [49]. Although London attraction may occur between non-polar and polar molecules, such as regions of an unfolded protein with water, due to the low polarizability of oxygen, such interactions are weak.

When the distance separating atoms or molecules approaches the sum of their van der Waals radii, an exponential repulsive potential scaling as r_{ij}^{-12}, an effect of Pauli's exclusion principle, results. Combining long-range London attraction with short-range van der Waals repulsion results in a Lennard-Jones potential of the form:

$$U(r) = -\frac{A_{ij}}{r_{ij}^{6}} + \frac{B_{ij}}{r_{ij}^{12}} \qquad (1.15)$$

where B_{ij} is a positive constant (units kJ m^{12} mol^{-1}) dependant upon the interacting atoms or molecules [50].

Lennard-Jones interactions in the tightly-packed hydrophobic core of folded proteins have been found to play a significant role in the stabilization of the native state under folding conditions [51].

1.2.2.3 Hydrogen Bonding

Mirsky and Pauling were the first to predict the α-helical secondary structure based on the notion that it maximized intramolecular hydrogen bonding between the amide NH and carbonyl C=O groups of the peptide backbone [6]. Such hydrogen bonding between amides contributes a bond enthalpy ~ 15 kJ mol^{-1} [46]. Hydrogen bonding is a vital driving force in the formation of alpha helical and beta sheet secondary structure elements. However, in order for a particular stabilizing contribution to be considered a vital driving force for global folding, it must account for the stability of the native state, and unfolded proteins are capable of forming strong hydrogen bonds with water. Additionally, the intramolecular hydrogen bonding in native proteins requires a very ordered arrangement of the backbone as well as side chain functionalities [52]. Such an entropic penalty is likely to overwhelm the intramolecular hydrogen bonding payoff at high temperatures (eq 1.6), resulting in unfolding [45].

The hierarchical model for protein folding, where acquisition of secondary structure precedes and directs tertiary contacts, as implied in Figure 1.1, is now thought not to be generally applicable [53]. Secondary structural stability can take on a range of values, and in some cases may be inherently unstable in the absence of tertiary interactions. For such proteins, folding is thought to proceed in a nucleation-condensation fashion, as opposed to hierarchical in a 'framework' sense, where elementary tertiary contacts facilitate acquisition of certain secondary structure motifs [53, 54]. Nonetheless,

for small proteins, rapid acquisition of secondary structure, particularly α-helices, is noted to be very fast [27]. This can be partially attributed to rapid acquisition of intrapeptide hydrogen bonds, which in some instances are favoured over peptide-water hydrogen bonds under native conditions [27, 55].

The presence of C^{α}—H····O=C hydrogen bonds in proteins has been established with a strength of roughly half that of amide N—H····O=C hydrogen bonds [56]. Noticeable strengths of C^{α}—H····O=C hydrogen bonds may, in some proteins, contribute to the stabilization of the native state [57].

1.2.2.4 Hydrophobic Effect

The hydrophobic effect, literally meaning 'water hating', refers to the tendency of a single non-polar solute in water to be extracted into a non-polar medium. Oil and water don't mix. This macroscopic observation was used by Lord Rayleigh in 1890 while making one of the first estimates of molecular size [58] The hydrophobic effect should be distinguished from the term 'hydrophobic interaction', which "refers to the association of two non-polar moieties in water" [58]. Such an association has enthalpic, through London attraction, and entropic contributions to free energy.

Hydrophobic interaction at *room temperature* is entropically driven, a result of the ordering of water molecules around non-polar solutes [59]. The first-shell waters around non-polar moieties encapsulate them with a hydrogen-boded clathrate-like cage. Such ordering has been coined 'iceberg water'[58].

Hydrophobic interactions are now considered to be the dominant force in protein folding, where estimates of free energy gain are in the range 5-10 kJ mol^{-1} upon transfer of a non-polar side chain from water into a non-polar media [14]. Such an energy gain per

hydrophobic residue equates to a large stabilization for a global fold featuring a hydrophobic core under physiological conditions.

1.2.3 Denaturation

Under denaturing conditions, the highly-disordered unfolded state will have the lowest free energy [60]. Thus, a 'denaturant' is any physical or chemical agent that affects the delicate balance between protein-protein interactions and protein-solvent interactions enough so as to disrupt the intra- and intermolecular interactions that stabilize the native state [60].

Physical denaturants such as extremes of temperature or high pressure are capable of inducing unfolding. Thermal denaturation is a popular method for studying protein (un)folding, both kinetically and under equilibrium conditions. This approach affords rapid temperature jump experiments, facilitating ultra-fast experimental kinetic measurements. Also, measurements of heat capacity C_p and ΔC_p through calorimetry provide useful information regarding the unfolding transition. High temperatures destabilize the native state by enhancing the entropic penalty of folding (eq 1.6).

Extremes of pH are also very popular in studying (un)folding; typically, jumps to-and-from low pH are favoured. The high proton diffusion coefficient facilitates pH jump kinetic experiments. The low concentration of acid required to denature most proteins affords well to equilibrium type studies, such as those conducted in Chapter 2 on hemoglobin (Hb). By altering the charge on proteins via extremes of pH, Columbic repulsion (eq 1.13) is sufficient to destabilize the native fold.

Chemical denaturants or chaotropes ("disorder-makers") include organic co-solvents (alcohols, acetonitrile, etc.) urea and gunidinium salts. Despite the long history

and widespread use of chaotropic denaturing agents, the molecular mechanism of their action remains unclear [61, 62]. It is sometimes claimed that chaotropic denaturation results from favouarble interaction with a protein's surface [61, 63]. Thus, the (un)folding equilibrium will shift so as to populate the conformer which exposes the most surface area, the denatured state. A second hypothesis is that a denaturant can attenuate hydrophobic interaction by disrupting hydrogen-bonds in water [63, 64], thereby increasing the solubility of a protein's hydrophobic core, reducing the largest driving force to folding [14].

1.2.4 Oxidative Modifications

It is well established that nonenzymatic posttranslational protein modifications have a hand in the aging process [65-67]. As organisms age, the level of covalently modified DNA, lipids, and proteins resulting from the constant attack by a host of reactive species, including reactive oxygen species (ROS), reactive nitrogen species (RNS), and the reactive by-products of metabolism, accumulates. Of particular interest is the effect that age-related posttranslational modifications of proteins, including protein carbonylation, cross-linking, and oxidation has on function [66].

Oxidization of proteins has been shown to affect stability [68], folding [69] and surface hydrophobicity [70]. Increased levels of protein-protein cross linkages, aggregation, and compromised biological activity are just a few detrimental effects that oxidized proteins incur [65]. In Chapter 2, the effects of oxidative modifications on subunit interactions in Hb are discussed.

1.3 Multi-Subunit Assemblies

Much regarding the folding of small proteins has been delineated over the past decade [4, 13, 14, 32, 71]. In particular, the gap between the fastest folding events measured experimentally and the longest folding events modeled computationally has narrowed from both ends as computational power has improved and ultra-fast folding proteins are now able to be monitored experimentally [71]. It is generally accepted that the hydrophobic effect plays a dominant role in the folding of small globular proteins. However, there is yet no universal agreement as to the dominant forces driving protein-protein association. It is now the era where we see if the principles learned about the folding of small proteins also apply to the folding and assembly of larger proteins/complexes.

Multi-subunit (un)folding and (dis)assembly studies are far from trivial, as off pathway aggregation often occurs during such experiments [5, 72, 73]. Indeed, it is difficult to replicate experimentally the *in vivo* environment in which proteins fold. Many specialized cellular machines exist to catalyze disulfide bond formation and isomerization of peptide bonds adjacent to proline residues. Moreover, molecular chaperones and ubiquitin mediated degradation are thought to keep potentially hazardous misfolded proteins 'in check' [32, 74].

Protein-protein interactions that stabilize quaternary structure are vital for the functioning of protein complexes. There exist general similarities and differences between the interior of globular proteins and binding interfaces [75, 76]. Notable similarities include (1) comparable packing densities and (2) the presence of hydrogen-boned networks and hydrophobic interactions. Notable differences include (1) a weaker hydrophobic effect for protein-protein interfaces and (2) the presence of salt-bridges and a

larger fraction of polar residues at many protein-protein interfaces as compared to protein cores, where such electrostatic interactions have been shown to be destabilizing [47]. However, despite these 'general' characteristics of protein-protein interfaces, dissociation constants for multi-subunit protein complexes vary from 10^{-3} M < K_d < 10^{-15} M [75]. Although it is not yet clear how orders of magnitude variation in K_d can be explained, it is suspected that each K_d has been designed to fit a particular biological role [77, 78].

1.3.1 Hemoglobin: A Model System

Hemoglobin A (Hb) is a highly conserved oxygen transport protein found within mammalian red blood cells (RBCs) at a tetramer concentration of around 5 mM [79]. Hb is composed of two heme containing α- and β-globin dimers (αβ) arranged in a tetrahedral 'dimer of dimers' fashion, as shown in Figure 1.5 [80, 81]. Vertebrate α- and β-globin share roughly 50 % sequence homology [82]. The α- and β-subunits are equally divergent form the oxygen storage protein myoglobin, with a globin fold comprising seven and eight helices, respectively [82, 83]. The noncovalent contacts that stabilize tetrameric Hb are located along two distinct interfaces and encompass Lennard-Jones interactions, hydrogen bonds, and salt bridges [83]. α and β interacting along the $\alpha_1\beta_1$ ($\alpha_2\beta_2$) "packing" interface form contacts that involve some 34 residues [84-86]. The $\alpha_1\beta_2$ ($\alpha_2\beta_1$) "sliding" interface is characterized by somewhat weaker contacts, involving only about 19 residues [80, 86]. The specific architecture of this $\alpha_1\beta_2$ ($\alpha_2\beta_1$) interface provides the structural basis for cooperative oxygen binding. More extensive salt bridges are present in the T (tense) or deoxy state than in the R (relaxed) or oxy state [81]. This structural change leads to a

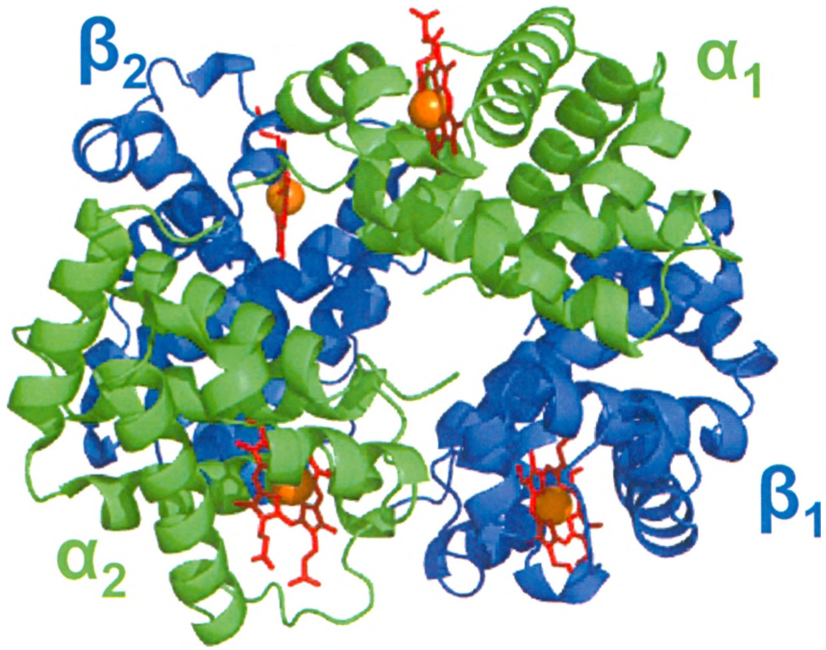

Figure 1.5: Cartoon rendered crystal structure of Hb (PDB file 1G09). α (green) and β (blue) chains are shown bound to their prosthetic heme cofactor (red). The subscripts 1and 2 on the α- and β- chains point out the packing ($\alpha_1\beta_1$) and sliding ($\alpha_1\beta_2$) interfaces of Hb.

remarkable increase in the tetramer-dimer dissociation constant upon oxygenation, from ca. 10^{-11} M in the T state to about 10^{-6} M in the R state [79, 87].

Hb also serves as an important model system for exploring the mechanisms by which multi-subunit complexes assemble from their monomeric constituents. This is explored in detail in Chapter 2.

1.4 Instrumentation for Monitoring Protein Folding Reactions

There exists an arsenal of biophysical methodologies with which to glean pertinent information regarding the (un)folding reactions of proteins [49]. In analogy to the tale of "the blind men and the elephant", there is no one 'gold standard' technique with which the biophysical experimentalist gains full insight into the reactions at hand. Instead, a complementary approach is often used, where combinations of techniques are employed. However, a due justice to the description of each herein would not be feasible nor relevant to the works of chapters 2 and 3. Instead, attention will be paid to the instrumental techniques employed during my studies on the unfolding of Hb (Chapter 2), with particular emphasis on the use of electrospray ionization (ESI) mass spectrometry (MS) for this purpose (Chapter 3). Having said this, some techniques not employed in chapters 2 or 3, but whose utility in protein science cannot go unrecognized, will be discussed briefly.

1.4.1 Optical Spectroscopy

The ways in which the spectrum of electromagnetic radiation interacts with matter is broad, providing the biophysical chemist with a variety of probes into the structure, folding, and dynamics of proteins. The following section on optical spectroscopy is by no means exhaustive, intended to provide the reader with a brief synopsis of some commonly used optical probes for studying protein folding.

1.4.1.1 UV-Visible Absorption Spectroscopy

The electronic absorption of ultraviolet (UV) and visible (Vis) radiation by a molecule in solution is linearly related to its concentration at a fixed path length under ideal conditions through the Beer-Lambert Law [88]:

$$A_\lambda = \log\frac{I_o}{I} = \varepsilon_\lambda bc \qquad (1.16)$$

where A_λ is the absorption at wavelength λ, I_o is the intensity of incident radiation, I is the intensity of emergent radiation, ε_λ is the wavelength specific molar extinction coefficient, b is the path length through the optical cuvette and c is the concentration of the absorbing species.

Since UV-Vis spectroscopy is sensitive to the concentration of absorbing species, it is very useful in determining unknown concentrations when a defined ε_λ is known. For proteins without metal or organic cofactors, broad absorption of the peptide backbone is observed around 190 nm. Proteins containing the highly conjugated aromatic amino acids tryptophan, tyrosine, and phenylalanine absorb around 280 nm, with tryptophan having an $\varepsilon_{280} > 5000 M^{-1} cm^{-1}$ [46]. If metal or organic cofactors are present, UV-Vis spectroscopy is often very useful as a highly specific probe into their particular chemical environment.

One particular drawback of UV-Vis spectroscopy for following protein (un)folding reactions pertains to its low selectivity. Optical signals for coexisting protein conformers are often broad and similar, thus confusing analysis for species without distinct absorption bands.

1.4.1.2 Fluorescence spectroscopy

Fluorescence, the immediate emission of light from an excited electronic state, is widely exploited in the analysis of biological substances. As with absorption, fluorescence is highly sensitive to the local chemical environment of the fluorophore, but not selective. Luminating amino acids include tryptophan, tyrosine, and phenylalanine, of which tryptophan gives the highest emission centered around 350 nm due to its high absorptivity at 280 nm.

What makes fluorescence spectroscopy particularly well suited for the study of protein conformation is the phenomena of excitation transfer, or Förster resonance energy transfer (FRET) [89]. The ability to transfer excitation from one chromophore to another scales with the distance separating them as r^{-6} [46]. Thus, for proteins in an environment where the emission from one chromophore overlaps the absorption band of another, FRET can be used as a type of 'molecular ruler', a probe of conformation using the relative distance between juxtaposed chromophores [27, 73].

1.4.1.3 Circular Dichrosim Spectroscopy

Chiral structures can be detected and characterized with polarized light [46]. Biological molecules are chiral. Specifically, biological molecules exhibit homochirality, an example of which includes the observation that all α-carbons of proteins are of the L-enantiomer. Chirality is also present in the higher-order structures of proteins, where the periodic conformation of the backbone imparts enantioselectivity. Examples include the secondary structural α-helical and β-sheet elements.

Natural light is unpolarized, that is, its electric vector may oscillate in any direction orthogonal to the axis of propagation. Light can be polarized such that only

specific oscillations of the electric vector are retained. The tip of the electric vector of circularly polarized light sweeps out a helix as it swirls around the axis of propagation. Light can be circularly polarized in a left or right handed fashion. Molecular chirality can be detected and characterized by circular dichroism (CD) spectroscopy by comparing the differential absorption of left- and right-circularly polarized light:

$$\Delta A = A_L - A_R \qquad (1.17)$$

where A_L and A_R refer to the absorbance of left- and right-circularly polarized light, respectively.

Probing the far-UV absorption bands of the peptide bonds in proteins using CD spectroscopy gives information relating to secondary structure [46, 48]. Right-handed α-helices give characteristic negative CD peaks at 222 and 208 nm. Proteins rich in β-sheets are characterized by a single broad negative peak centered between 210-230 nm. Random coils exhibit a single negative peak centered below 210 nm. A major drawback of CD spectroscopy, like other forms of spectroscopy, stems from the fact that its signal is an average of all species/conformers present in solution, making it a 'low selectivity' technique. Nonetheless, valuable insight is gleaned when combined with other forms of spectroscopy or instrumentation capable of resolving solution phase conformers [73].

1.4.1.4 Nuclear Magnetic Resonance Spectroscopy

Just as electrons have spin states (± ½), so do nuclei (0, ½, 1, or greater). The spin number I of a nucleus depends on the number of protons and neutrons. For many nuclei, however, the magnetic dipoles cancel, giving $I = 0$. Nuclei with nonzero spin numbers will align their net magnetic dipole in an external magnetic field in certain quantized orientations and begin to precess about the axis of the external field. The number of possible orientations is given by $2I + 1$. For spin ½ nuclei (i.e., ^{1}H, ^{13}C, ^{15}N, ^{31}P) two possible orientations of the magnetic spin quantum number m_z exist, which in the absence of the external field are degenerate [46, 49]. In the presence of the external magnetic field, these spin states split and are roughly of equal population. Thus the energy spacing is very small; it only takes a low frequency radio wave of the correct energy to cause excitation. Nuclear magnetic resonance (NMR) spectroscopy monitors the change in the nuclear spin state caused from the absorption of radio frequency radiation in an applied magnetic field. Interaction of nuclei with other nuclei, and with electrons, influences the frequency of absorption. Thus, NMR is a powerful tool in that it probes the local environment of every spin active nucleus.

NMR spectroscopy has contributed a plethora of information to the field of protein science. One particular example is the use of NMR spectroscopy in protein structure determination under near-physiological conditions in solution [90]. For his contribution to the development of NMR spectroscopy for determining the 3D structure of biological macromolecules in solution, Kurt Wüthrich received ½ of the 2002 Nobel Prize in chemistry.

Besides 3D structure determination, NMR spectroscopy is routinely used in studies on the folding interactions, allosteric nature, and dynamics of proteins smaller

than ~25 kDa [90, 91]. Complications arise for the analysis of proteins larger than ~25 kDa. As protein size increases, so does the number of NMR peaks, and in combination with line broadening and loss of sensitivity, analysis is tedious if not impossible. Much effort has been put into alleviating this problem, raising the current 'high-end' practical mass limit of NMR to over 100 kDa [90].This has been achieved via (1) increasing the magnetic field strength, (2) multidimensional NMR combining 2D ^{1}H-^{1}H nuclear Overhauser effect spectroscopy (NOESY) with uniformly labeled ^{15}N and/or ^{13}C NMR to give 3D or 4D spectra, (3) new NMR techniques such as transverse relaxation-optimized spectroscopy (TROSY) [90, 92]. However, despite these advancements, the use of NMR spectroscopy for studying higher-order protein assembly remains challenging, as distinguishing intramolecular interactions from intermolecular contacts is often problematic.

1.4.2 Electrospray Ionization Mass *Spectrometry*

The experimental analysis of multi-subunit (dis)assemblies requires instrumentation capable of resolving intramolecular structural changes from intermolecular contacts. Although traditional spectroscopic techniques such as UV-Vis, fluorescence, and CD are very useful probes for what they measure, their utility as primary methods for studying protein (un)folding/(dis)assembly reactions is limited since they measure information averaged across the entire analyte population and are thus unable to resolve coexisting protein conformers [5].

Direct insights into the structure and dynamics of protein complexes can be obtained by electrospray ionization (ESI) mass spectrometry (MS). The gentle nature of

the ESI process allows a wide range of noncovalent assemblies to be transferred into the gas-phase, such that their composition can be determined from their mass [93-96].

1.4.2.1Electrospray Ionization

The traditional electrospray ionization (ESI) source, introduced over twenty years ago, consisted of a small bore (100 μM ID) conductive tube held at high (3-5 kV) positive or negative potential relative to the mass spectrometer orifice some centimeters away [97, 98]. For his part in developing ESI as an ion source for mass spectrometry, John Fenn received ¼ of the 2002 Nobel Prize in chemistry. Since the main stream introduction of ESI, much advancement has been made to the development of unique modes of operation particular for different applications spanning a great scope of disciplines [99-101]. However, despite these evolutionary advancements, a steep electric gradient around a pointed needle electrode through which a conductive solution flows remains a fundamental requirement for ESI.

Electrospray processes work via an electrophoretic charge separation, where the electric field in the vicinity of the pointed needle tip induces migration of preformed ions in solution [102]. An ESI source operating in the positive ion mode, by far the most common mode of operation for studying proteins, is depicted in Figure 1.6. In positive ion mode, preformed positive ions migrate towards the tip of the electrospray needle, where a balance of surface tension and Columbic repulsion culminates in the emission of a filament of positively charged droplets in a fashion dependent on spray conditions and fluid properties [103].

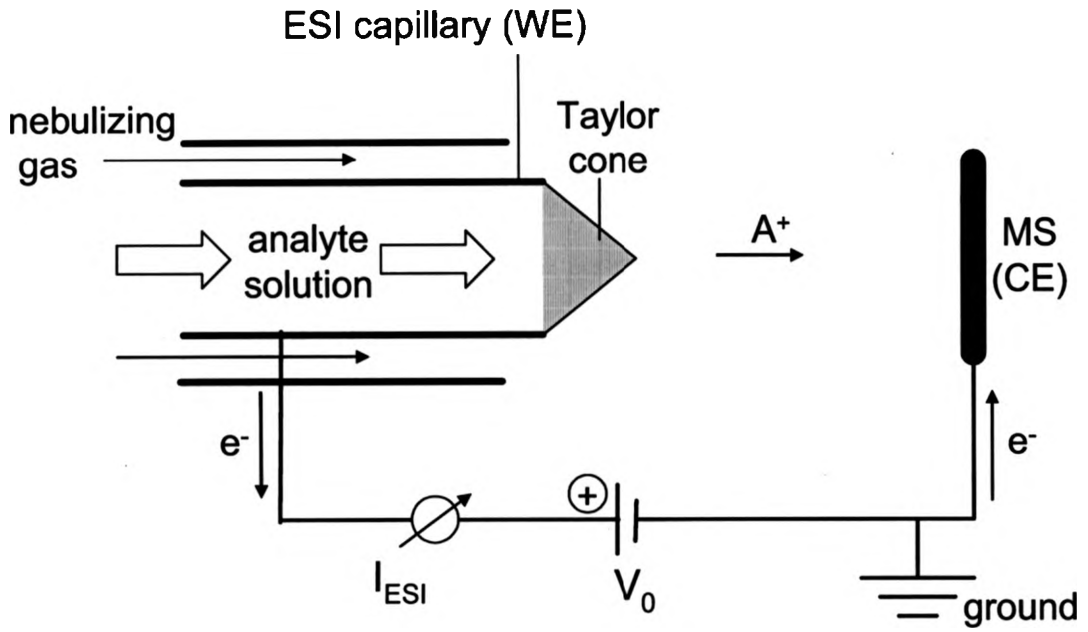

Figure 1.6: Schematic depiction of an ESI source in positive ion mode. Positively charged solvent droplets are ejected from the tip of the Taylor cone. Subsequent evapouration, aided by a coaxial sheath of hot nebulizing gas, and fission events give rise to positively charged analyte ions (A^+). Notation: MS, mass spectrometer; CE, counter electrode; WE, working electrode.

The theoretical electric field required for the onset of electrospray has been estimated [104]:

$$E_{on} \approx \left(\frac{2\gamma \cos\theta}{\varepsilon_o r_c} \right)^{\frac{1}{2}} \tag{1.18}$$

where γ is the solvent surface tension, θ is the half angle of the Taylor cone, r_c is the outer radius of the metal capillary, and ε_o is the permittivity of vacuum. With all else equal, one can see from eq 1.18 that for two solvents, the change in E_{on} can be estimated by taking the square root of the quotient of the surface tensions.

ESI can be thought of as a special kind of electrolytic flow cell, where current is governed by the passage of charged droplets through a neutral gas, a very large resister indeed. This mode of operation is depicted in Figure 1.6, where the total current is low (<< 1μA) and *only* a result of eletrophoretic charge separation sustained via oxidation of solvent, capillary, or analyte at the metal/liquid working electrode (WE) interface (anode) [105]. The circuit is completed via reduction of the charged droplets/ions on collision with various parts of the mass spectrometer, serving as the counter electrode (CE, cathode) in Figure 1.6. A second regime involving the occurrence of a corona discharge is often silently present, especially when solutions of high surface tension (i.e., water) are sprayed. The occurrence of corona discharge during ESI, its artifacts, and prevention strategies is the topic of Chapter 3.

1.4.2.2 Electrospray Ionization of Proteins

In positive ion mode, from analyte containing positively charged droplets, intact gas-phase ions are formed, the mechanism of which is still a matter of debate [106-109]. By far the most readily detected analytes via this process are those that are ionic in solution and/or include functionalities that demonstrate reasonable activity towards Brønsted or Lewis acid/base chemistry, giving rise to ions of the type $[M+nH]^{n+}$. However, charging with protons is not ubiquitous, as any cation species could serve as a charge carrier. Indeed, despite significant effort to rid samples of non-volatile salts, Na^+ and K^+ adducts are routinely observed in ESI-MS spectra.

Mass spectrometers do not measure mass; rather, they measure the mass-to-charge ratio (*m/z*) of ions. Given the nature of the charging process, every protein species and conformer in solution will acquire a characteristic charge state distribution of the form:

$$\frac{m}{z} = \frac{M + \sum_i n_i m_i}{\sum_i n_i} \qquad (1.19)$$

where *m/z* is a particular mass-to-charge ratio, m_i is the mass of charge carrier *i*, and n_i is the number of charges of type *i*. From eq 1.19, the mass *m* and charge *z* of an analyte ion can be calculated from three adjacent *m/z* peaks. ESI of proteins often give many such peaks, allowing for accurate mass determination. The multiple charging nature of ESI also facilitates the analysis of very large complexes. The acquired charge state distribution provides a highly sensitive probe for changes in the overall protein conformation. Unfolded solution-phase proteins have been shown experimentally [110,

111] and by computation [112] to acquire a higher mean charge state as well as a more broad distribution of charging units during positive ion ESI than their tightly folded counterparts. As a result, ESI-MS is able to simultaneously detect coexisting conformers in solution, something that traditional biophysical probes often fail to do. These features, together with the virtually unlimited mass range of ESI-MS [113], make this technique particularly well suited for the study of multi-subunit complex (dis)assemblies, as well as other avenues in structural biology [111]. Having said this, due to the enormous complexity of protein structures, one single method of instrumentation is usually insufficient for gaining comprehensive insights into a particular folding process. Often a variety of complementary approaches must be employed in order to obtain a more 'complete picture' of protein folding and interaction processes.

1.4.2.2 Mass Spectrometry

Once gas phase ions have been generated, they can be introduced into the high vacuum environment of a mass spectrometer. Using electric and magnetic fields, mass spectrometers manipulate the trajectories of ions such that *m/z* can be measured [114, 115].

There exists a variety of types of mass analyzers for use in mass spectrometry, each with unique advantages and drawbacks. Furthermore, multiple mass analyzers can be joined in series, facilitating ion selection, ion fragmentation via collision-induced dissociation, and *m/z* analysis of the resulting ion species. A mass spectrometer with a particular combination of mass analyzers for use in the study of protein folding is depicted in Figure 1.7. This hybrid mass spectrometer consists of a quadrupole (Q) mass filter separated from a time-of-flight (TOF) mass analyzer by a hexapole collision cell,

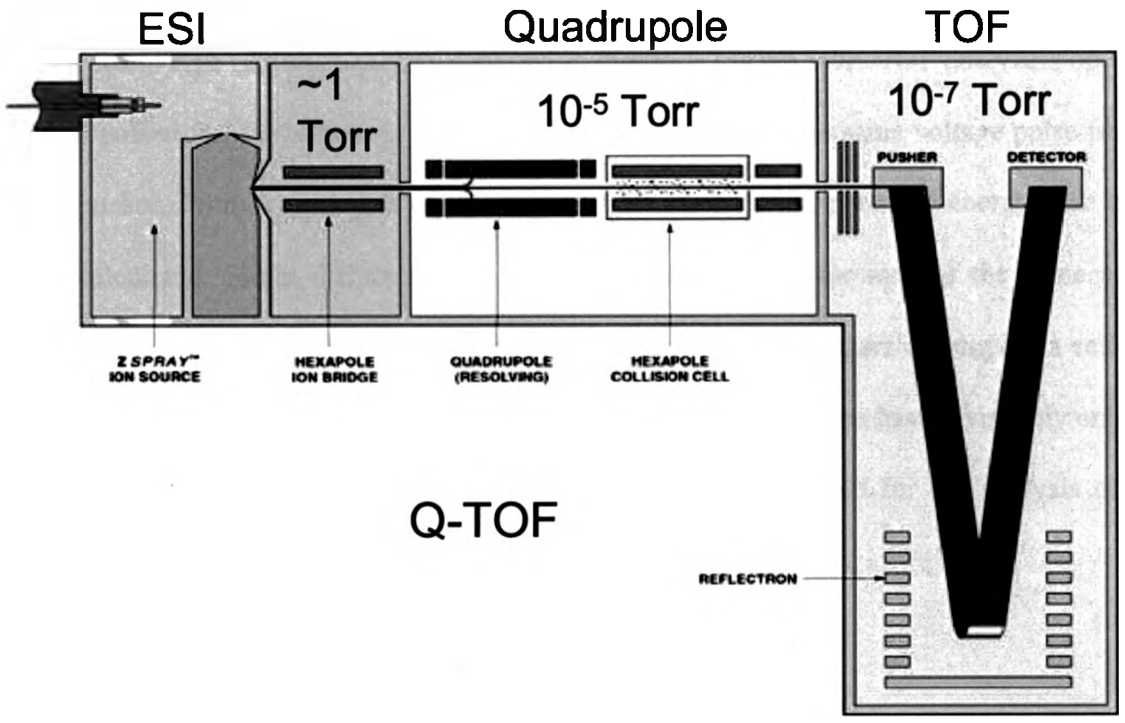

Figure 1.7: Schematic depiction of a Q-TOF mass spectrometer capable of MS-MS analysis via collision-induced dissociation (CID). A hexapole collision cell separates a quadrupole mass filter (Q) from a time-of-flight mass analyzer (TOF). Typical pressures of the various interfaces are indicated in Torr (1 atm = 760 Torr). Taken and modified from www.waters.com

where the introduction of a small quantity of an inert gas such as Ar results in collision-induced dissociation. Quadrupole mass filters allow selection of a particular *m/z* by destabilizing the trajectories of the remaining ions [116]. By stabilizing the trajectory of selected ions, quadrupole mass filters are often found upstream of collision cells. The second type of mass analyzer depicted in Figure 1.7 is the TOF. TOF analyzers operate in a pulsed fashion, where at each cycle all ions experience the same voltage pulse from the pusher. From knowledge of the flight time and imparted potential energy, *m/z* can be calculated. Slight differences in acquired kinetic energy for ions of the same *m/z* are accounted for with the use of a reflectron [117]. TOF analyzers employing a reflectron offer excellent resolution (~10,000). In addition, TOF analyzers have a virtually unlimited upper *m/z* range [113], making them particularly well suited for the analysis of large multi-subunit complexes.

1.5 Scope of Thesis

This work examines the disassembly mechanism of freshly prepared bovine Hb using ESI-MS in combination with UV-Vis spectroscopy (Chapter 2). The powerful nature of ESI-MS for following high-order protein folding reactions is demonstrated. A symmetric disassembly mechanism is supported which contradicts the existence of a previously proposed obligatory intermediate. Apparent contradictions are discovered to be a result of posttranslational oxidative modifications. The detrimental effects of protein oxidation on the stability of the native state, and on folding reactions, are reinforced. The necessity of determining the oxidation status of the protein in solution prior to folding studies is found to be paramount.

The possible implications of the inherent oxidative nature of positive ion mode ESI are discussed and the mechanism of ESI-induced protein oxidation is determined (Chapter 3). An often silently present corona discharge regime during 'typical' ESI conditions is brought into light, with its known effects being resolved from suspicions pertaining to the electrolytic environment of the ESI capillary.

The work presented herein reinforces the utility of ESI-MS in the study of high-order protein folding reactions using Hb as a model system. A heightened understanding of the operation of an ESI source is obtained, and guidelines for preventing unwanted artifacts are established.

1.6 References

1. Crick, F. (1970) Central Dogma of Molecular Biology, *Nature. 227*, 561-563.

2. Voet, D. V., J. G., and Pratt, C.W. (2004) *Fundamentals of Biochemistry, 2nd Edition*, John Wiley & Sons.

3. Baker, D. (2000) A surprising simplicity to protein folding, *Nature. 405*, 39-42.

4. Onuchic, J. N. & Wolynes, P. G. (2004) Theory of protein folding, *Curr. Opin. Struct. Biol. 14*, 70-75.

5. Seckler, R. (2000) Assembly of multi-subunit structures in *Mechanisms of Protein Folding* (Pain, R. H., ed), Oxford University Press, Oxford.

6. Mirsky, A. E. & Pauling, L. (1936) On the strcture of native, denatured, and coagulated proteins, *Proc. Natl. Acad. Sci. U.S.A. 22*, 439-447.

7. Pauling, L., Corey, R. B. & Branson, H. R. (1951) The structure of proteins: two hydrogen-bonded helical configurations of the polypeptide chain, *Proc. Natl. Acad. Sci. 37*, 205-211.

8. Perutz, M. F. (1965) Structure and Function of Haemoglobin I. A Tentative Atomic Model of Horse Oxyhaemoglobin, *J. Mol. Biol. 13*, 646-668.

9. Anfinsen, C. B. (1973) Principles that Govern the Folding of Protein Chains, *Science. 181*, 223-230.

10. Levinthal, C. (1969) Mossbauer Spectroscopy in Biological Systems in *Proceedings of a Meeting Held at Allerton House, Monticello, Illinois* (DeBrunner, J. T. P. & Munck, E., eds) pp. 22-24, University of Illinois Press, Chicago.

11. Noggle, J. H. (1996) *Physical Chemistry*, third edn, HarperCollins, New York.

12. Zwanzig, R., Szabo, A. & Bagchi, B. (1992) Levinthal's paradox, *Proc. Natl. Acad. Sci. U.S.A. 89*, 20-22.

13. Daggett, V. & Fersht, A. (2003) The present view of the mechanism of protein folding, *Nat. Rev. Mol. Cell Biol. 4*, 497-502.

14. Dill, K. A., Ozkan, S. B., Shell, M. S. & Weikl, T. R. (2008) The Protein Folding Problem, *Annu. Rev. Biophys. Biomol. Struct. 37*, 289-316.

15. Dinner, A. R., Sali, A., Smith, L. J., Dobson, C. M. & Karplus, M. (2000) Understanding protein folding via free-energy surfaces from theory and experiment, *Trends Biochem. Sci. 25*, 331 - 339.

16. Kryshtafovych, A., Venclovas, C., Fidelis, K. & Moult, J. (2005) Progress Over the First Decade of CASP Experiments, *Proteins. Suppl 7*, 225-236.

17. Chamberlain, A. K. & Marqusee, S. (2000) Comparison of Equilibrium and Kinetic Approaches for Determining Protein Folding Mechanisms, *Adv. Prot. Chem. 53*, 283-328.

18. Ghosh, K., Ozkan, S. B. & Dill, K. A. (2007) The Ultimate Speed Limit to Protein Folding Is Conformational Searching, *J. Am. Chem. Soc. 129*, 11920-11927.

19. Kubelka, J., Henry, E. R., Cellmer, T., Hofrichter, J. & Eaton, W. A. (2008) Chemical, physical, and theoretical kinetics of an ultrafast folding protein, *Proc. Natl. Acad. Sci. U.S.A. 105*, 18655-18662.

20. Kubelka, J., Hofrichter, J. & Eaton, W. A. (2004) The protein folding 'speed limit', *Curr. Opin. Struct. Biol. 14*, 76-88.

21. Arora, P., Oas, T. G. & Myers, J. K. (2004) Fast and faster: A designed variant of the B-domain of protein A folds in 3 μsec, *Protein Sci. 13*, 847-853.

22. Fersht, A. R. (1999) *Structure and Mechanism in Protein Science*, W. H. Freeman & Co., New York.

23. Jackson, S. E. & Fersht, A. (1991) Folding of Chymotrypsin Inhibitor 2. 1. Evidence for a Two-State Transition, *Biochem. 30*, 10428-10435.

24. Burton, R. E., Myers, J. K. & Oas, T. G. (1998) Protein Folding Dynamics: Quantitative Comparison between Theory and Experiment, *Biochemistry. 37*, 5337-5343.

25. Santoro, M. M. & Bolen, D. W. (1988) Unfolded Free Energy Changes Determined by the Linear Extrapolation Method. 1. Unfolding of Phenylmethanesulfonyl α-Chymotrypsin Using Different Denaturants, *Biochem. 27*, 8063-8068.

26. Schonbrun, J. & Dill, K. A. (2003) Fast protein folding kinetics, *Proc. Natl. Acad. Sci. USA. 100*, 12678-12682.

27. Sinha, K. K. & Udgaonkar, J. B. (2008) Barrierless evolution of structure during the submillisecond refolding reaction of a small protein, *Proc. Natl. Acad. Sci. U.S.A. 105*, 7998-8003.

28. Hammond, G. S. (1953) A correlation of reaction rates, *J. Am. Chem. Soc. 77*, 334-338.

29. Dill, K. A. (1999) Polymer principles and protein folding, *Protein Sci. 8*, 1166-1180.

30. Karplus, M. (2000) Aspects of Protein Reaction Dynamics: Deviations from Simple Behavior, *J. Phys. Chem. B. 104*, 11-27.

31. Zwanzig, R. (1997) Two-state models of protein folding kinetics, *Proc. Natl. Acad. Sci. U.S.A. 94*, 148-150.

32. Dobson, C. M. (2004) Experimental investigation of protein folding and misfolding, *Methods. 34*, 4-14.

33. Dill, K. A. & Chan, H. S. (1997) From Levinthal to pathways to funnels, *Nat. Struct. Biol. 4*, 10-19.

34. Konermann, L. (2006) Exploring the Relationship Between Funneled Energy Landscapes and Two-State Protein Folding, *Proteins. 65*, 153-163.

35. Baynes, B. M., Wang, C. & Trout, B. L. (2005) Role of arginine in the stabilization of proteins against aggregation, *Biochemistry. 44*, 4919-4925.

36. Mishra, R., Seckler, R. & Bhat, R. (2005) Efficient Refolding of Aggregation-prone Citrate Synthase by Polyol Osmolytes, *J. Biol. Chem. 280*, 15553-15560.

37. Dobson, C. M. (2003) Protein folding and misfolding, *Nature. 426*, 884-890.

38. Lide, D. R. (2001) *CRC Handbook of Chemistry and Physics*, 82nd edn, CRC Press, Boca Raton, London, New York, Washington.

39. Dai, S. Y. & Fitzgerald, M. C. (2006) A Mass Spectrometry-Based Probe of Equilibrium Intermediates in Protein-Folding Reactions, *Biochemistry. 45*, 12890-12897.

40. Haezebrouck, P., Noyelle, K. & Van Dael, H. (1998) Equilibrium and kinetic folding of pigeon lysozyme, *Biochemistry. 37*, 6772-6780.

41. Myers, J. K., Pace, C. N. & Schotz, J. M. (1995) Denaturant *m* values and heat capacity changes: Relation to changes in accessible surface areas of protein unfolding, *Protein Sci. 4*, 2138-2148.

42. Nicholson, E. M. & Scholtz, M. (1996) Conformational Stability of the Escherichia coli HPr Protein: Test of the Linear Extrapolation Method and a Thermodynamic Characterisation of Cold Denaturation, *Biochemistry. 35*, 11369-11378.

43. Ghaemmaghami, S., Fitzgerald, M. C. & Oas, T. G. (2000) A quantitative, high-throughput screen for protein stability, *Proc. Natl. Acad. Sci. USA. 97*, 8296-8301.

44. Powell, K. D. & Fitzgerald, M. C. (2003) Accuracy and precision of a new H/D exchange- and mass spectrometry-based technique for measuring the thermodynamic properties of protein-peptide complexes, *Biochemistry. 42*, 4962-4970.

45. Dill, K. A. (1990) Dominant Forces in Protein Folding, *Biochemistry. 29*, 7133-7155.

46. Tinoco, I., Sauer, K. & Wang, J. C. (1995) *Physical Chemistry: Principles and Applications in Biological Sciences*, 3rd edn, Simon & Schuster Company, London.

47. Hendsch, Z. S. & Tidor, B. (1994) Do salt bridges stabilize proteins? A continuum electrostatic analysis, *Protein Sci. 3*, 211-226.

48. Kaltashov, I. A. & Eyles, S. J. (2005) *Mass Spectrometry in Biophysics*, John Wiley and Sons, Inc., Hoboken, NJ.

49. van Holde, K., Johnson, W. & Shing Ho, P. (2006) *Principles of Physical Biochemistry*, second edn, Pearson Prentice Hall.

50. Berendsen, H. J. C., Grigera, J. R. & Straatsma, T. P. (1987) The missing term in effective pair potentials, *J. Phys. Chem. 91*, 6269-6271.

51. Chen, J. & Stites, W. E. (2001) Packing Is a Key Selection Factor in the Evolution of Protein Hydrophobic Cores, *Biochem. 40*, 15280-15289.

52. Chellgren, B. W. & Creamer, T. P. (2006) Side-Chain Entropy Effects on Protein Secondary Structure, *Proteins. 62*, 411-420.

53. Bond, C. J., Wong, K.-B., Clarke, J., Fersht, A. R. & Daggett, V. (1997) Characterization of residual structure in the thermally denatured state of barnase by simulation and experiment: Description of the folding pathway, *Proc. Natl. Acad. Sci. USA. 94*, 13409-13413.

54. Daggett, V. & Fersht, A. R. (2003) Is there a unifying mechanism for protein folding?, *Trends Biochem. Sci. 28*, 18-25.

55. Moglich, A., Joder, K. & Kiefaber, T. (2006) End-to-end distance distributions and intrachain diffusion constants in unfolded polypeptide chains indicate intramolecular hydrogen bond formation, *Proc. Nat. Acad. Sci. 103*, 12394-12399.

56. Vargas, R., Garza, J., Dixon, D. A. & Hay, B. P. (2000) How Strong is the Cα-H...O=C Hydrogen Bond?, *J. Am. Chem. Soc. 122*, 4750-4755.

57. Derewenda, Z., Lee, L. & Derewenda, U. (1995) The Occurence of C-H...O Hydrogen Bonds in Proteins, *J. Mol. Biol. 252*, 248-262.

58. Southall, N. T., Dill, K. A. & Haymett, A. D. J. (2002) A View of the Hydrophobic Effect, *J. Phys. Chem. B. 106*, 521-533.

59. Sharp, K. A. & Madan, B. (1997) Hydrophobic Effect, Water Structure, and Heat Capacity Changes, *J. Phys. Chem. B. 101*, 4343-4348.

60. Konermann, L. (2003) Protein Unfolding and Denaturants in *Encyclopedia of Life Sciences* (www.els.net), Nature Publishing Group, London.

61. Dunbar, J., Yennawat, H. P., Banerjee, S., Luo, J. & Farber, G. K. (1997) The effect of denaturants on protein structure, *Protein Sci. 6*, 1727-1733.

62. Dobson, C. M. & Karplus, M. (1999) The fundamentals of protein folding: bringing together theory and experiment, *Curr. Opin. Struct. Biol. 9*, 92-101.

63. Batchelor, J. D., Olteanu, A., Tripathy, A. & Pielak, G. J. (2004) Impact of Protein Denaturants and Stabilizers on Water Structure, *J. Am. Chem. Soc. 126*, 1958-1961.

64. Russo, D. (2008) The impact of kosmotropes and chaotropes on bulk and hydration shell water dynamics in a model peptide solution, *Chem. Phys. 345*, 200-211.

65. Stadtman, E. R. (2006) Protein oxidation and aging, *Free Radical Research. 40*, 1250-1258.

66. Soskic, V., Groebe, K. & Schrattenholz, A. (2008) Nonenzymatic posttranslational protein modifications in ageing, *Exp. Gerontol. 43*, 247-257.

67. Grimsrud, P. A., Xie, H., Griffin, T. J. & Bernlohr, D. A. (2008) Oxidative Stress and Covalent Modification of Protein with Bioactive Aldehydes, *J. Bio. Chem. 283*, 21837-21841.

68. Kim, Y. H., Berry, A. H., Spencer, D. S. & Stites, W. E. (2001) Comparing the effect on protein stability of methionine oxidation versus mutagenesis: steps toward engineering oxidative resistance in proteins, *Protein Eng. 14*, 343 - 347.

69. Chugha, P., Sage, H. J. & Oas, T. G. (2006) Methionine oxidation of monomeric λ repressor: The denatured state ensemble under nondenaturing conditions, *Protein Sci. 15*, 533-542.

70. Chao, C.-C., Ma, Y.-S. & Stadtman, E. R. (1997) Modification of protein surface hydrophobicity and methionine oxidation by oxidative systems, *Proc. Natl. Acad. Sci. U.S.A. 94*, 2969-2974.

71. Dyer, R. B. (2007) Ultrafast and downhill protein folding, *Curr. Op. Struct. Biol. 17*, 38-47.

72. Meldrum, N. U. (1931) The acid-denaturation of haemoglobin, *T. Biochem. J. 25*, 1498-1512.

73. Boys, B. L. & Konermann, L. (2007) Folding and Assembly of Hemoglobin Monitored by Electrospray Mass Spectrometry Using an On-line Dialysis System, *J. Am. Soc. Mass Spectrom. 18*, 8-16.

74. Luzzatto, L. & Notaro, R. (2002) Haemoglobin's chaperone, *Nature. 417*, 703-704.

75. Dong, F. & Zhou, H.-X. (2006) Electrostatic Contribution to the Binding Stability of Protein-Protein Complexes, *Proteins. 65*, 87-102.

76. Tsai, C.-J. & Nussinov, R. (1997) Hydrophobic folding units at protein-protein interfaces: Implications to protein folding and to protein-protein association, *Protein Sci. 6*, 1426-1437.

77. Brooijmans, N., Sharp, K. A. & Kuntz, I. D. (2002) Stability of macromolecular complexes, *Proteins. 48*, 645-653.

78. Conte, L. C., Chothia, C. & Janin, J. (1999) The Atomic Structure of Protein-Protein Recognition Sites, *J. Mol Biol. 285*, 2177-2198.

79. Riggs, A. F. (1998) Self-association, cooperativity and supercooperativity of oxygen binding by hemoglobins, *J. Exper. Biol. 201*, 1073-1084.

80. Eaton, W. A., Henry, E. R., Hofrichter, J. & Mozzarelli, A. (1999) Is cooperative oxygen binding by hemoglobin really understood, *Nat. Struct. Biol. 6*, 351 - 358.

81. Perutz, M. F. (1970) Stereochemistry of Cooperative Effects in Haemoglobin, *Nature. 228*, 726-739.

82. Hardison, R. C. (1996) A brief history of hemoglobins: plant, animal, protist, and bacteria, *Proc. Natl. Acad. Sci. U.S.A. 93*, 5675-5679.

83. Antonini, E. & Brunori, M. (1971) *Hemoglobin and Myoglobin in Their Reactions With Ligands*, North-Holland Publishing Company, Amsterdam, London.

84. Edelstein, S. J., Rehmar, M. J., Olson, J. S. & Gibson, Q. H. (1970) Functional aspects of the subunit association-dissociation equilibria of hemoglobin, *J. Biol. Chem. 245*, 4372-4381.

85. Schaeffer, J. R., McDonald, M. J., Turci, S. M., Dinda, D. M. & Bunn, H. F. (1984) Dimer-Monomer Dissociation of Human Hemoglobin A, *J. Biol. Chem. 259*, 14544-14547.

86. Santiveri, C. M., Perez-Canadillas, J. M., Viadivelu, M. K., Allen, M. D., Rutherford, T. J., Watkins, N. A. & Bycroft, M. (2004) NMR structure of the α-Hemoglobin Stabilizing Protein, *J. Biol. Chem. 279*, 34963-34970.

87. White, S. L. (1975) The molecular dissociation of ferrihemoglobin derivatives, *J. Biol. Chem. 250*, 1263-1268.

88. Skoog, D. A. (1998) *Principles of Instrumental Analysis*, Brooks/Cole Thomson Learning, Toronto.

89. dos Remedios, C. G. & Moens, P. D. J. (1995) Fluorescence Resonance Energy Transfer Spectroscopy Is a Reliable "Ruler" for Measuring Structural Changes in Proteins, *J. Struct. Biol. 115*, 175 - 185.

90. Wüthrich, K. (2001) Nuclear Magnetic Resonance Spectroscopy of Proteins in *Encyclopedia of Life Sciences* (www.els.net), Nature Pulishing Group, London.

91. Song, X.-j., Simplaceanu, V., Ho, N. T. & Ho, C. (2008) Effector-Induced Structural Fluctuation Regulates the Ligand Affinity of an Allosteric Protein: Binding of Inositol

Hexaphosphate Has Distinct Dynamic Consequences for the T and R States of Hemoglobin, *Biochem. 47*, 4907-4915.

92. Arrowsmith, C. H. & Wu, Y. (1998) NMR of large (>25 kDa) proteins and protein complexes, *Progr. Nucl. Mag. Res. Spectr. 32*, 277-286.

93. Loo, J. A. (2005) Noncovalent Protein-Ligand Complexes in *The Encyclopedia of Mass Spectrometry* (Gross, M. L. & Caprioli, R. M., eds) pp. 289-299, Elsevier, Amsterdam.

94. Donald, L. J., Stokell, D. J., Holliday, N. J., Ens, W., Standing, K. G. & Duckworth, H. W. (2005) Multiple equilibria of the Escherichia coli chaperonin GroES revealed by mass spectrometry, *Protein Sci. 14*, 1375-1379.

95. Fändrich, M., Tito, M. A., Leroux, M. R., Rostom, A. A., Hartl, F. U., Dobson, C. M. & Robinson, C. V. (2000) Observation of the noncovalent assembly and disassembly pathways of the chaperone complex MtGimC by mass spectrometry, *Proc. Natl. Acad. Sci. USA. 97*, 14151-14155.

96. Heck, A. J. R. & Van den Heuvel, R. H. H. (2004) Investigation of intact protein complexes by mass spectrometry, *Mass Spectrom. Rev. 23*, 368-389.

97. Yamashita, M. & Fenn, J. B. (1984) Electrospray Ion Source. Another variation on the Free-Jet Theme, *J. Phys. Chem. 88*, 4451-4459.

98. Yamashita, M. & Fenn, J. B. (1984) Negative Ion Production with the Electrospray Ion Source, *J. Phys. Chem. 88*, 4671-4675.

99. Pan, P., Gunawardena, H. P., Yu, X. & McLuckey, S. A. (2004) Nanospray ionization of protein mixtures: solution pH and protein pI, *Anal. Chem. 76*, 1165-1174.

100. Van Berkel, G. J. & Kertesz, V. (2007) Electrochemistry/spray Ion Source, *Anal. Chem. 79*, 5511-5520.

101. Van Berkel, G. (2008) Established and emerging atmospheric pressure surface sampling/ionization techniques for mass spectrometry, *J. Mass Spectrom. 43*, 1161-1180.

102. Blades, A. T., Ikonomou, M. G. & Kebarle, P. (1991) Mechanism of Electrospray Mass Spectrometry. Electrospray as an Electrolysis Cell, *Anal. Chem. 63*, 2109-2114.

103. Nemes, P., Marginean, I. & Vertes, A. (2007) Spraying Mode Effect on Droplet Formation and Ion Chemistry in Electrosprays, *Anal. Chem. 79*, 3105-3116.

104. Ikonomou, M. G., Blades, A. & Kebarle, P. (1991) Electrospray Mass Spectrometry of Methanol and Water Solutions Supression of Electric Discharge with SF6 Gas, *J. Am. Soc. Mass Spectrom. 2*, 497-505.

105. Van Berkel, G. J. (2000) Insights into Analyte Electrolysis in an Electrospray Emitter from Chronopotentiometry Experiments and Mass Transport Calculations, *J. Am. Soc. Mass Spectrom. 11*, 951-960.

106. de la Mora, F. J. (2000) Electrospray Ionization of large multiply charged species proceeds via Dole's charged residue mechanism, *Anal. Chim. Acta. 406*, 93-104.

107. Adak, S., Wang, Q. & Stuehr, D. J. (2000) Molecular Basis for Hyperactivity in Tryptophan 409 Mutants of Neuronal NO Synthase, *J. Biol. Chem. 275*, 17434-17439.

108. Wang, G. & Cole, R. B. (2000) Charged residue versus ion evaporation for formation of alkali metal halide clusters ions in ESI, *Anal. Chim. Acta. 406*, 53-65.

109. Kebarle, P. & Peschke, M. (2000) On the Mechanisms by which the charged droplets produced by electrospray lead to gas phase ions, *Anal. Chim. Acta. 406*, 11-35.

110. Chowdhury, S. K., Katta, V. & Chait, B. T. (1990) Probing Conformational Changes in Proteins by Mass Spectrometry, *J. Am. Chem. Soc. 112*, 9012-9013.

111. Kaltashov, I. A. & Eyles, S. J. (2002) Studies of Biomolecular Conformations and Conformational Dynamics by Mass Spectrometry, *Mass Spectrom. Rev. 21*, 37-71.

112. Konermann, L. (2007) A Minimalist Model for Exploring Conformational Effects on the Electrospray Charge State Distribution of Proteins, *J. Phys. Chem. B. 111*, 6534-6543.

113. Sobott, F. & Robinson, C. V. (2002) Protein complexes gain momentum, *Curr. Op. Struct. Biol. 12*, 729-734.

114. Roboz, J. (1968) *Mass Spectrometry: Instrumentation and Techniques*, Wiley, New York.

115. Watson, J. T. (1997) *Introduction to Mass Spectrometry*, Lippincott - Raven, Philadelphia, New York.

116. Siuzdak, G. (1996) *Mass Spectrometry for Biotechnology*, Academic Press, San Diego, New York, Boston, London, Sydney, Tokyo, Toronto.

117. Karas, M. & Bahr, U. (1996) Matrix-Assisted Laser Desorption-Ionization (MALDI) Mass Spectrometry of Biological Molecules in *Mass Spectrometry in Biomolecular Sciences* (Caprioli, R. M., Malorni, A. & Sindona, G., eds) pp. 33-49, Kluwer, Dordrecht, Boston, London.

Chapter 2 - Symmetric Behavior of Hemoglobin α- and β- Subunits During Acid-Induced Denaturation Observed by Electrospray Mass Spectrometry

2.1 Introduction

Hemoglobin (Hb) serves as an important model system for exploring the mechanisms by which multi-subunit complexes assemble from their monomeric constituents. Studies of this kind have been carried out *in vitro* [1-3], in cell-free systems [4], as well as *in vivo* [5]. A total of eight moieties, namely two apo-α-chains (α^a), two apo-β-chains (β^a), and four heme groups are required for the formation of the intact $(\alpha^h\beta^h)_2$ tetramer (subscripts "a" and "h" refer to apo- and heme-bound holo states, respectively). For many previous *in vitro* experiments the assembly of Hb has been triggered by mixing initially separated α^h and β^h subunits under native solvent conditions. Prior to mixing, the isolated subunits form noncovalent $(\alpha^h)_2$ and $(\beta^h)_4$ complexes, respectively. Dissociation of these species into monomers allows the formation of αβ heterodimers to occur, which can then form the native $(\alpha^h\beta^h)_2$ structure [1, 6-10]. Electrostatic interactions play an important role in guiding these assembly processes [11-13]. The *in vivo* mechanism of Hb formation likely involves co-translational folding and heme binding of the individual subunits. A chaperone (AHSP, α-hemoglobin-stabilizing protein) binds to nascent monomeric α^h, thereby preventing the formation of cytotoxic α-globin aggregates [14-20]. Interestingly, the assembly of intact ^{met}Hb from extensively unfolded monomeric subunits and free heme can proceed *in vitro* even in the absence of AHSP [21]. The overall picture that

emerges from these previous studies, as well as from equilibrium experiments [22], is that the Hb assembly mechanism follows the general sequence $2\ \alpha + 2\ \beta \rightarrow 2\ \alpha\beta \rightarrow (\alpha\beta)_2$ [14, 23, 24]. It is undisputed that native $(\alpha^h\beta^h)_2$ is generated by the binding of two $\alpha^h\beta^h$ heterodimers to each other. However, the question whether $\alpha^h\beta^h$ is preceded by another heterodimeric species is still a matter of debate [25]. Soret absorption measurements and other spectroscopic experiments suggest that the assembly process at near-neutral pH may involve semi-α-hemoglobin ($\alpha^h\beta^a$) as a major intermediate for both human and bovine Hb [4, 25-30].

In principle, both α- and β-globin can exist in various conformations, heme binding states and quaternary structures, resulting in an vast number of possible species that could potentially be involved in the assembly process. Based on conventional spectroscopic measurements it is challenging to obtain clear-cut evidence for the existence of certain reaction pathways, and to prove or disprove the existence of specific intermediates. Electrospray ionization (ESI) mass spectrometry (MS), on the other hand, is a highly selective technique that allows the detection of multiple co-existing protein species [31]. The gentle nature of the ESI process implies that intact ligand-protein and protein-protein complexes can be transferred into the gas phase, such that the composition of these assemblies can be deduced from their mass [31-36]. At the same time, the charge state distributions of the observed protein ions provide information on the overall compactness of the corresponding solution-phase conformations. Unfolded proteins generally result in higher protonation states than tightly folded conformers [31, 37, 38].

In an interesting study, Griffith and Kaltashov [39] recently employed ESI-MS for monitoring the response of ^{met}Hb to increasing acid concentrations. A stepwise decrease

in pH from 8 to 3 resulted in a gradual decay of the $(\alpha^h\beta^h)_2$ signal. α^h and $\alpha^h\beta^h$ were the major species observed around pH 5. Below pH 4, unfolded α^a and β^a chains were dominant. These experiments suggested characteristic differences in the behavior of α- and β-globin. The former was able to bind heme independent of its association state, apparent by the observation of monomeric α^h. In contrast, monomeric β-globin was seen exclusively in its apo-state. Based on these observations it was proposed that β-globin exhibits heme-binding competency only while in association with α^h chains, in either a dimeric or tetrameric complex. Another notable result was the observation of a heme-deficient dimer ($\alpha^h\beta^a$), which was interpreted as a key intermediate of the (dis)assembly process. It was suggested that the apparent asymmetric behavior of the two subunits during acid-induced unfolding might have general implications for the assembly of Hb under non-denaturing conditions both *in vitro* and *in vivo* [28, 39, 40]. A subsequent study from our laboratory came to somewhat different conclusions. Upon monitoring the refolding of ^{met}Hb at slightly basic pH it was found that both monomeric α- and β-globin were capable of binding heme. Moreover, these refolding data did not support the notion that $\alpha^h\beta^a$ is an obligatory intermediate en route towards the native $(\alpha^h\beta^h)_2$ complex [21].

The bulk of the existing ESI-MS literature on Hb, as well as a number of optical studies, involved the use of protein samples obtained commercially as lyophilized powder. It has been pointed out previously that ^{met}Hb treated in this way contains considerable levels of chemical modifications [41, 42]. While studies on these samples can undoubtedly provide interesting information, it is imperative to explore in how far the history of the protein affects its biochemical properties. This work revisits the mechanism of acid-induced Hb denaturation. Using ESI-MS, it is shown that the behavior of freshly

prepared Hb is dramatically different from that of lyophilized protein from commercial sources. We study the response to changes in pH for three forms, ^{oxy}Hb (oxygen-bound with heme iron in the Fe^{2+} oxidation state), ^{met}Hb (physiologically inactive, with heme iron in the Fe^{3+} oxidation state), and ^{cyanomet}Hb (^{met}Hb with heme iron distally ligated by CN^-) [43]. The pH profiles obtained in this way reveal a remarkably symmetrical behavior for both α- and β-globin. In particular, it is found that $\alpha^h\beta^a$ dimers are virtually undetectable under all conditions.

2.2 **Experimental**

2.2.1 Materials

Bovine ^{oxy}Hb was prepared from fresh hemolysate via standard procedures [43]. Briefly, fresh blood was collected from a Holstein heifer [44] into a chilled glass vial containing sodium citrate as an anticoagulant to a final concentration of 0.3% (w/v). Centrifugation at 5,500 g for 20 min gave a RBC pellet. Plasma and buffy coat (containing white blood cells and platelets) were removed with suction. Isolated RBCs were resuspended and washed in isotonic 0.9% w/v sodium chloride, and then centrifuged again at 5,500 g for 20 min. This washing step was repeated four times to rid the samples of plasma proteins and cellular debris. Hemolysate was obtained through osmotic shock, and stromal impurities were extracted into an organic phase. This was achieved by mixing the packed RBCs with an equal volume of distilled water containing 10% v/v toluene. Centrifugation at 15,000 g for 30 min yielded an aqueous layer of purified hemolysate which was then dialyzed at 4 °C against 10 mM ammonium acetate over a period of 36 h with multiple buffer exchanges. The total concentration of the purified ^{oxy}Hb stock solution obtained in this way was determined via the pyridine hemochromogen method to be 1.7 mM (as tetramer) [45]. Analyses employing UV-Vis spectroscopy on ^{cyanomet}Hb with, ε_{540} = 44 mM^{-1} cm^{-1} (as tetramer), were in agreement with this result [46, 47]. In contrast to human Hb, the bovine protein interacts only weakly with 2-3-diphosphoglycerate (DPG), and the 2-3-DPG levels in bovine RBCs are relatively low [48, 49]. Inductively coupled plasma MS revealed that the dialysis procedure outlined above further lowered the concentration of organophosphates in the hemolysate by roughly one order of magnitude. In order to minimize auto-oxidation of ^{oxy}Hb to ^{met}Hb, the protein stock solutions were flash frozen

in liquid nitrogen in 10 mM ammonium acetate. Rapid thawing was practiced in accordance with previous studies [50]. The percentage of ^{met}Hb in the thawed ^{oxy}Hb stock solutions was *ca.* 2 %, as determined by measuring the absorbance decrease at 620 nm upon addition of KCN [51-53]. Aliquots of freshly prepared ^{oxy}Hb were purposely converted to ^{met}Hb by oxidation with a 1.2-fold stoichiometric excess of potassium ferricyanide for 5 min at 25 °C. A fraction of the ^{met}Hb was then further derivatized to ^{cyanomet}Hb by exposing it to a 1.2-fold stoichiometric excess of neutralized potassium cyanide for 2 min at 25 °C. All derivatized Hb species were desalted on a 3 x 25 cm G-25 Sephadex column prior to analysis.

Commercial bovine ^{met}Hb was purchased as lyophilized powder (Sigma, St. Louis, MO) and was dialyzed against 10 mM ammonium acetate. All commercial stock Hb solutions were made to 1 mM (as tetratmer) and were centrifuged to remove small amounts of insoluble debris. Post-dialysis samples were flash frozen in liquid nitrogen and stored at -80°C. The percentage of ^{met}Hb in the commercially obtained stock was found to be around 99 %. All experiments in this work were carried out on Hb solutions containing ammonium acetate at a final concentration of 10 mM. Absorption measurements were carried out on a Carry-300 Varian UV-Vis spectrophotometer (Palo Alto, CA), using a protein concentration of 15 μM (as tetramer) and a cuvette with a 1 mm optical path length.

2.2.2 Mass Spectrometry

Mass spectra were recorded on a Q-TOF Ultima API instrument (Waters/Micromass, Manchester, UK) utilizing a standard Z-spray ESI source operating in positive ion mode. All MS parameters were optimized to give the highest Hb tetramer signal at pH 6.8. A

capillary voltage of 3.5 kV, cone voltage of 45 V, and RF lens 1 voltage of 20 V were found to be optimal. The desolvation and source temperatures were kept low (30 and 80° C, respectively) to minimize tetramer dissociation. Samples were introduced into the mass spectrometer at a flow rate of 5 μL min^{-1} via a syringe pump. Hb samples analyzed by ESI-MS were of high concentration (60 μM as tetramer) to minimize the dissociation of noncovalent complexes in solution. All Hb samples were diluted from the corresponding stock solution and the pH was adjusted with formic acid, allowing an equilibration period of 1 h prior to analysis. The mass spectrometer was calibrated with CsI. The ion optics were adjusted to provide uniform transmission in the m/z range of interest. All data were acquired and analyzed using MassLynx software provided by the instrument manufacturer. Consistent with previous reports, the subunit masses of the protein were found to be 15,053 and 15,954Da for α^a and β^a, respectively [54, 55]. The heme prosthetic group accounts for an additional 616 Da for each subunit.

The locations of oxidative modification sites in commercial ^{met}Hb were determined by tryptic peptide mapping and LC-ESI-MS/MS. 50 μM ^{met}Hb was digested with trypsin for 4 h at 37° C using a 10:1 ^{met}Hb:trypsin ratio by weight. The digest was loaded into a 25 μL sample loop and separated on a Symmetry C18 column (Waters). Tryptic peptides were separated using a Waters 1525μ HPLC pump at a flow rate of 100 μL min^{-1}, employing a linear water/acetonitrile gradient in the presence of 0.05% trifluoroacetic acid. The acetonitrile content of the mobile phase was ramped from 2% to 60% within 60 min. Peptides of interest were analyzed by ESI-MS/MS as they eluted from the column by operating the Q-TOF instrument in data-dependent acquisition mode.

2.3 Results and Discussion

2.3.1 Comparison of Different Hemoglobin Samples

The ESI mass spectrum recorded for commercially obtained ^{met}Hb at pH 6.8 (Figure 2.1A) resembles data reported in previous ESI-MS studies [39, 41]. It shows a host of different species, including $(\alpha^h\beta^h)_2$ tetramers, $\alpha^h\beta^h$ dimers, heme deficient dimers ($\alpha^h\beta^a{}_{ox}$), monomeric α^h, β^h, $\beta^a{}_{ox}$, as well as free heme. The subscript "ox" is used for ions exhibiting a molecular mass that is 32 Da higher than expected based on the amino acid sequence. This phenomenon is attributed to oxidative modifications [21, 41], as discussed in more detail below. The occurrence of a tetramer-dimer equilibrium for ^{met}Hb is well established [22, 56, 57], such that the observation of dimeric species in Figure 2.1A is not surprising. A K_d value of 4 μM has been reported for the $(\alpha^h\beta^h)_2 \leftrightarrow 2\ \alpha^h\beta^h$ dissociation, whereas the corresponding value for ^{cyanomet}Hb is 1 μM at pH 7 [58]. The presence of significant amounts of monomeric globin ions in Figure 2.1A is unexpected, considering the results of previous experiments carried out in bulk solution [22, 56, 57]. It might be suspected that some of the monomeric and dimeric species in the spectrum are fragmentation products generated during ESI. Recent hydrogen/deuterium exchange studies, however, have revealed that this is not the case. Instead, all of the ionic signals mentioned so far correspond to protein species that exist in solution [42]. Figure 2.1A also reveals the presence of hexamers $(\alpha^h\beta^h)_3$, octamers $(\alpha^h\beta^h)_4$, decamers $(\alpha^h\beta^h)_5$, and dodecamers $(\alpha^h\beta^h)_6$.

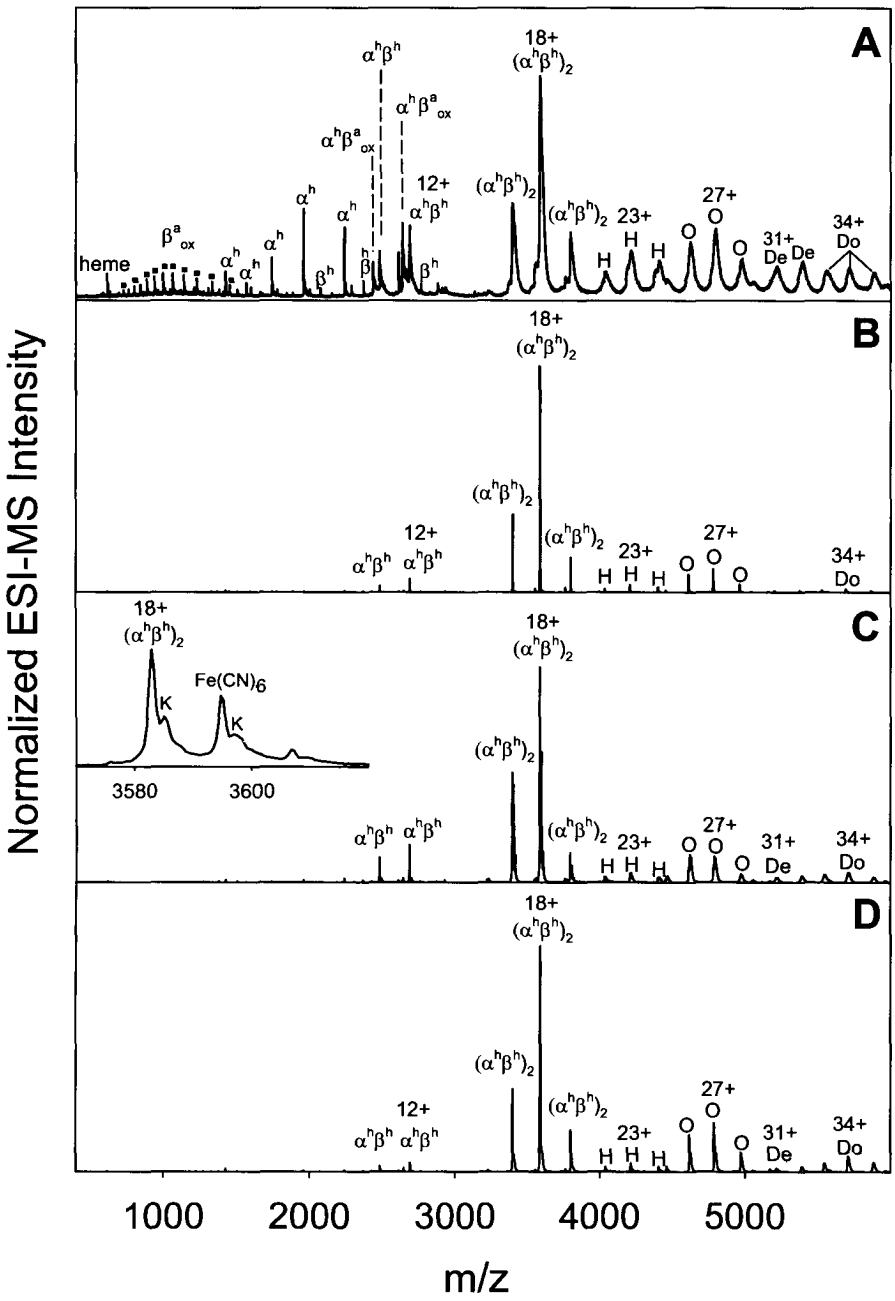

Figure 2.1: ESI mass spectra of different Hb derivatives recorded under native solvent conditions (pH 6.8) at a tetramer concentration of 60 μM. (A) ^{met}Hb obtained commercially as a lyophilized powder. The other three panels show data for Hb freshly prepared from bovine blood, (B) ^{oxy}Hb; (C) ^{met}Hb; (D) ^{cyanomet}Hb. Notation: H, O, De, Do hexamers, octamers, decamers, and dodecamers, respectively. Peaks labeled with black squares represent (apo-β +32) Da species (β^{a}_{ox}). The inset in (C) shows a ferrocyandide and potassium (K) adduct bound to ^{met}Hb tetramers.

Although there is evidence for the possible formation of higher order Hb assemblies under some conditions [59], the $(\alpha^h\beta^h)_n$ species (with $n > 2$) observed here likely represent clusters generated during ionization, a common occurrence in ESI-MS [42, 60, 61].

Compared to the data for commercial ^{met}Hb, the ESI mass spectrum of freshly prepared ^{oxy}Hb has a much simpler appearance (Figure 2.1B), being strongly dominated by $(\alpha^h\beta^h)_2$ ions. The contributions of $\alpha^h\beta^h$ and larger aggregates are greatly reduced. Monomeric species, as well as heme-deficient dimers are virtually undetectable. The measured mass corresponds to that of de-oxygenated Hb, that is, O_2 binding is not maintained during the ESI process, although the protein is infused into the ion source in its fully oxygenated form. The peak width is significantly reduced due to vast improvements in desolvation behavior. Signal broadening caused by the presence of residual solvent adducts is frequently observed in ESI mass spectra of large noncovalent complexes, as exemplified in Figure 2.1A [33, 62, 63]. The observation of much more favorable desolvation properties for freshly prepared ^{oxy}Hb (Figure 2.1B) is remarkable.

To investigate whether the different ESI-MS behavior of the two samples is related to the oxidation state of the heme iron, freshly prepared ^{oxy}Hb was converted to ^{met}Hb by addition of potassium ferricyanide. The resulting spectrum (Figure 2.1C) is very similar to that obtained for ^{oxy}Hb, albeit with slightly elevated intensities for dimers and larger aggregates (hexamer to dodecamer). Close inspection of the tetramer signals reveals peak splitting due to a residual $Fe(CN)_6$ adduct (Figure 2.1C, inset). This behavior is consistent with the known tendency of Hb to accommodate ferrocyanide in its organophosphate binding site, which lies between the two β subunits in the tetrameric complex [43, 64]. Dimers do not possess this binding site, consistent with the observation

that $\alpha^h\beta^h$ does not form a ferrocyanide adduct. For completeness, we also investigated the properties of ^{cyanomet}Hb, which was obtained by incubation of ^{met}Hb with a slight molar excess of neutralized KCN (see the Experimental procedures section). The overall differences between the ESI mass spectra of freshly prepared ^{cyanomet}Hb (Figure 2.1D) and ^{met}Hb (Figure 2.1C) are relatively small. However, Figure 2.1D shows a lower contribution of $\alpha^h\beta^h$, consistent with the fact that heme ligation with CN^- reduces the K_d of $(\alpha^h\beta^h)_2$ by a factor of four, as mentioned above [58].

In additional experiments, freshly prepared ^{oxy}Hb was lyophilized, followed by redissolution and extended storage of the resulting samples. Mass spectra obtained for protein treated in this way resembled that of commercial ^{met}Hb (Figure 1A), with prominent monomer, dimer, and $\alpha^h\beta_{ox}$ signals (data not shown).

2.3.2 Acid-Induced Denaturation.

Figure 2.2 depicts the changes in the ESI mass spectrum upon acidification of freshly prepared ^{oxy}Hb. Lowering the pH from 6.8 to 4.4 (Figure 2.2A, B) results in a dramatic shift of the tetramer-dimer equilibrium, such that $\alpha^h\beta^h$ becomes the dominant species. In addition, ionic signals corresponding to monomeric α^h and β^h are observed. The low charge states (around 7+) of these monomer ions indicate that they represent highly compact protein conformers in solution [38, 65]. Upon decreasing the pH to 4.0 the relative signal intensities of α^h and β^h increase further. At the same time, highly charged α^a and β^a ions appear in the spectrum, indicating the presence of significantly unfolded apo-globin chains in solution (Figure 2.2C).

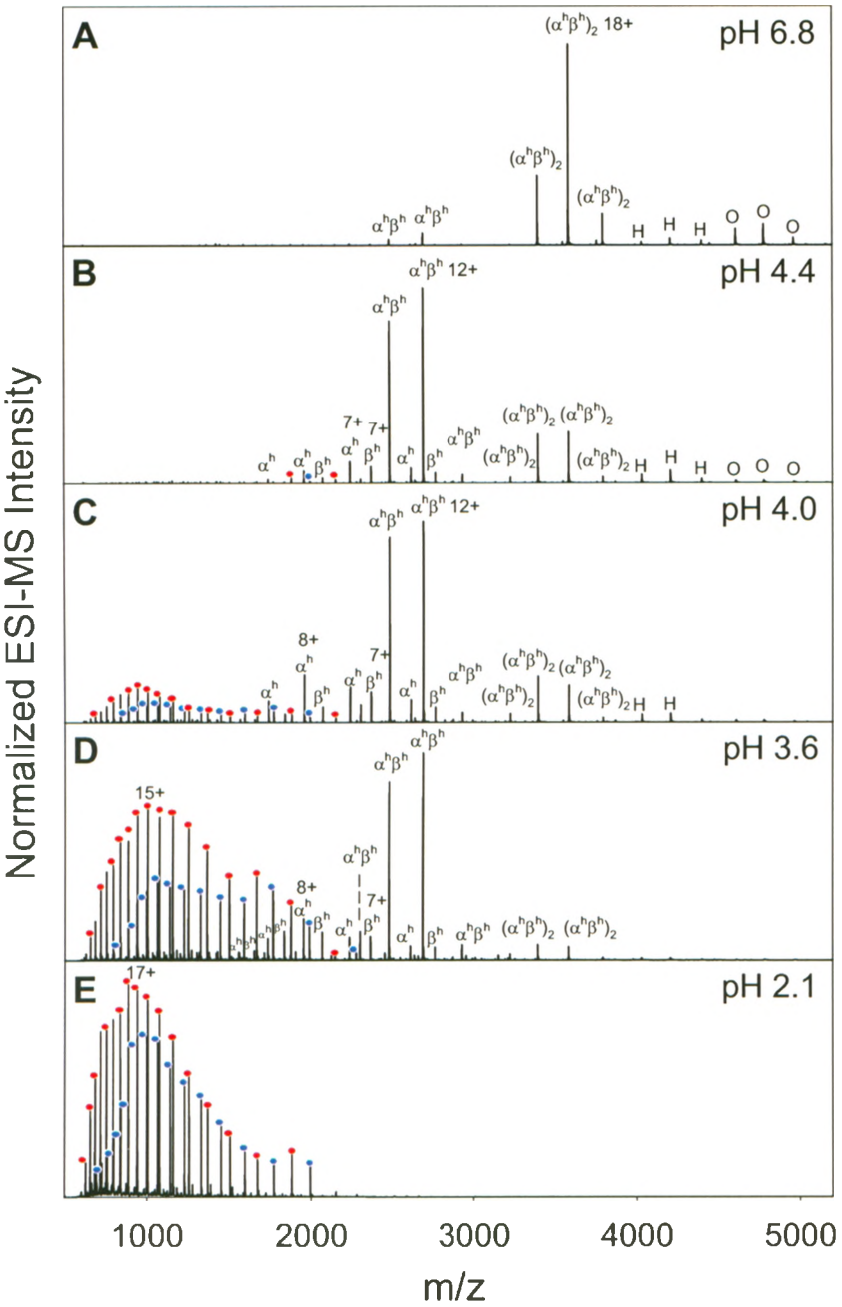

Figure 2.2. ESI mass spectra of freshly prepared ^{oxy}Hb recorded at different pH (as indicated). Notation: same as in Figure 2.1; red and blue symbols represent α^a and β^a ions, respectively. The charge states of selected ions are indicated.

This trend continues upon further acidification (Figure 2.2D). Figure 2.2E represents the end point of the titration. The spectrum under these conditions (pH 2.1) exclusively shows α^a and β^a ions, with charge state distributions that have their maxima around 17+. These data reflect the fact that at pH 2.1 all quaternary contacts and heme-protein interactions have been disrupted, and that the monomeric subunits are extensively unfolded in solution [38, 65]. The higher signal intensities for α^a than for β^a can be attributed to ion suppression effects, as well as differences in the desolvation behavior of the two globin chains [66]. The heme released during denaturation is not detectable in Figures 2 C-E due to rapid aggregation of the free porphyrin under acidic conditions [67, 68]. ESI mass spectra very similar to those depicted in Figure 2.2 were obtained during the acid-induced denaturation of freshly prepared ^{met}Hb and ^{cyanomet}Hb, demonstrating that the overall denaturation mechanism of the three forms studied here is largely insensitive to changes in heme oxidation and ligation state. Detailed ESI-MS titration data for the two ferri Hb derivatives are not shown due to space limitations, however, selected spectra for ^{met}Hb will be discussed below (Figure 2.7).

Complementary information on the acid-induced denaturation of the three freshly prepared Hb derivatives can be obtained by UV-Vis spectroscopy. The absorbance changes accompanying the titration of ^{oxy}Hb are depicted in Figure 2.3. At neutral pH the protein shows bands at 577 and 541 nm, and a dominant Soret signal at 415 nm. The presence of these so-called α, β, and γ bands confirms that the protein is indeed in its fully oxygenated low-spin Fe^{2+} state [43]. Acidification leads to a gradual disappearance of the 577/541 nm doublet, and the Soret peak shifts to 405 nm. This spectral transition reflects a change in heme oxidation state to Fe^{3+}, corresponding to that of ^{met}Hb. The

onset of this process occurs around pH 4, that is, in the range where monomeric α^h, β^h, and free apoprotein start to occur in the ESI mass spectrum (Figure 2.2C). These changes reflect the fact that the highly specific structural environment of the native heme binding pocket in ^{oxy}Hb protects the heme iron from autoxidation [69]. Disruption of the binding pocket during denaturation allows the $Fe^{2+} \rightarrow Fe^{3+}$ transition to occur under the aerobic solution conditions used here. Further acidification leads to a broad spectrum that is blue shifted even further, characteristic of heme that has been released from the protein and undergone acid aggregation [70-72].

The spectral changes accompanying the acid-induced denaturation of freshly prepared ^{met}Hb exhibit an isosbestic point at 380 nm (Figure 2.4). This suggests that the ferri-heme chromophore experiences a two-state transition, from protein-bound to aggregated in acidic solution. Since these spectral changes only probe the heme environment, the apparent two-state nature of the optical transition does not contradict the observation of various protein oligomerization states (monomers, dimers, and tetramers) by ESI-MS. In the range between pH 4 and pH 2.1 the data for ^{cyanomet}Hb (Figure 2.5) are very similar to those for ^{met}Hb (Figure 2.4), reflecting the transition from protein-bound ferri-heme to the acid-denatured state of Hb. In the case of ^{cyanomet}Hb, however, this process is preceded by the loss of cyanide, apparent from an absorbance decrease around 540 nm, as well as a shift of the Soret band from 419 to 405 nm (Figure 2.5) [43]. Presumably, the driving force for this reaction is the protonation of cyanide at low pH. This cyanide loss is a gradual process that can be monitored directly by ESI-MS (Figure 2.6). In the near-neutral range the mass spectra show $(\alpha^h\beta^h)_2$ bound to up to four CN^- groups.

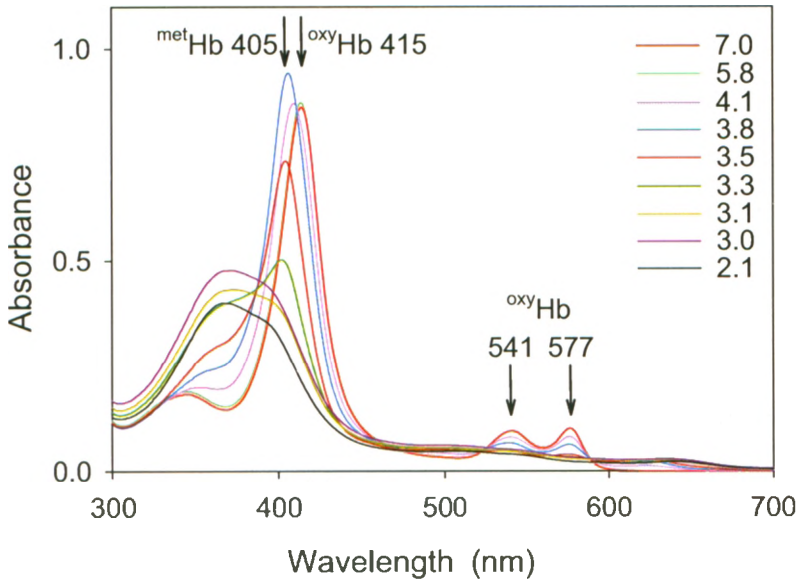

Figure 2.3: UV-Vis spectral changes accompanying the acid-induced denaturation of freshly prepared ^{oxy}Hb. The pH values for the individual spectra are indicated. Also shown are the characteristic absorption maxima for ^{oxy}Hb and ^{met}Hb [43].

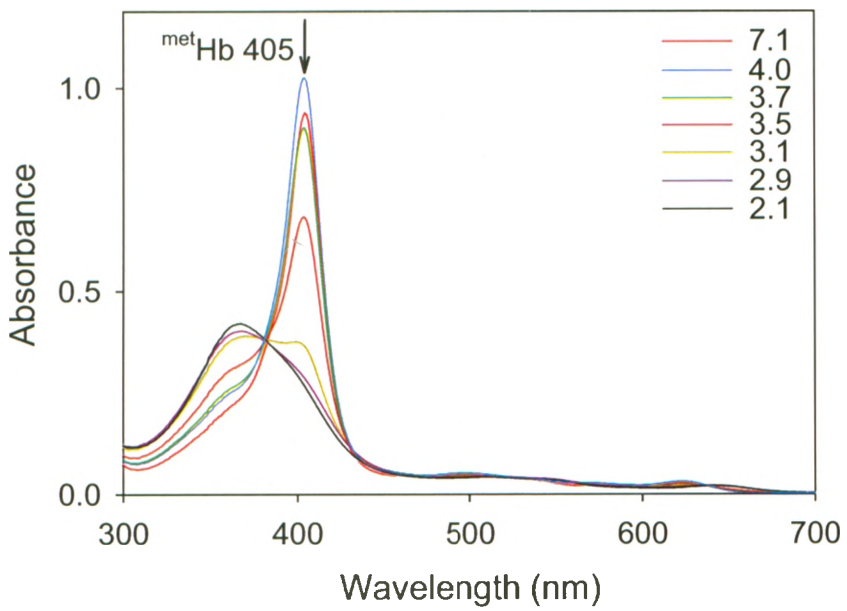

Figure 2.4: UV-Vis spectral changes accompanying the acid-induced denaturation of freshly prepared ^{met}Hb.

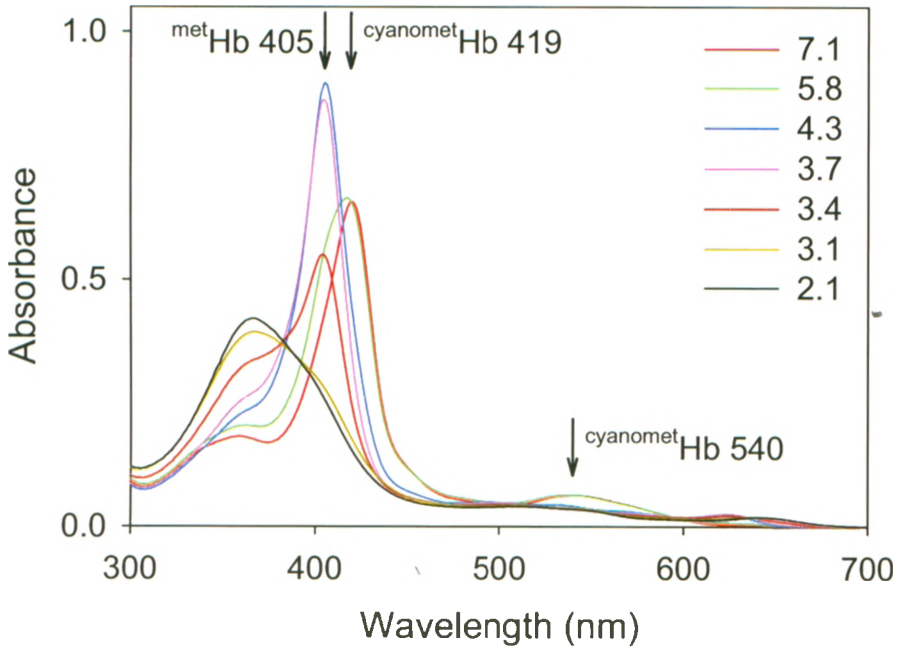

Figure 2.5: UV-Vis spectral changes accompanying the acid-induced denaturation of freshly prepared ^{cyanomet}Hb. Also shown are the characteristic absorption maxima for ^{met}Hb and ^{cyanomet}Hb [43].

Acidification induces a gradual shift of the distribution, until at pH 3.5 the base peak corresponds to the mass of unligated $(\alpha^h\beta^h)_2$. Because protonation is an integral part of the ionization process, it is possible that some cyanide is released in the form of HCN during ESI. Thus, the distributions depicted in Figure 2.6 likely under-represent the actual cyanide binding levels in bulk solution. No cyanide binding was observed for dimeric or monomeric globins.

A key conclusion from the acid-induced denaturation data presented so far (especially those in Figures 2.1, 2.2) is that the α and β subunits of freshly prepared Hb exhibit a highly symmetric behavior. In other words, the changes in association state, heme binding, and conformation exhibited by α globin are closely mirrored by the β subunit. Based on Figure 2.2, the denaturation process can be summarized by the following simplified scheme (ignoring the possible involvement of higher order aggregates):

$$(\alpha^h\beta^h)_2 \rightarrow 2\,\alpha^h\beta^h \rightarrow$$
$$2\,\alpha^h_{\text{folded}} + 2\,\beta^h_{\text{folded}} \rightarrow \qquad \text{(Scheme 1)}$$
$$2\,\alpha^a_{\text{unfolded}} + 2\,\beta^a_{\text{unfolded}} + 4\ \text{heme}$$

This result contrasts the data previously obtained on commercial ^{met}Hb, which indicate a highly asymmetric behavior of the two subunits, as discussed in the Introduction section [39].

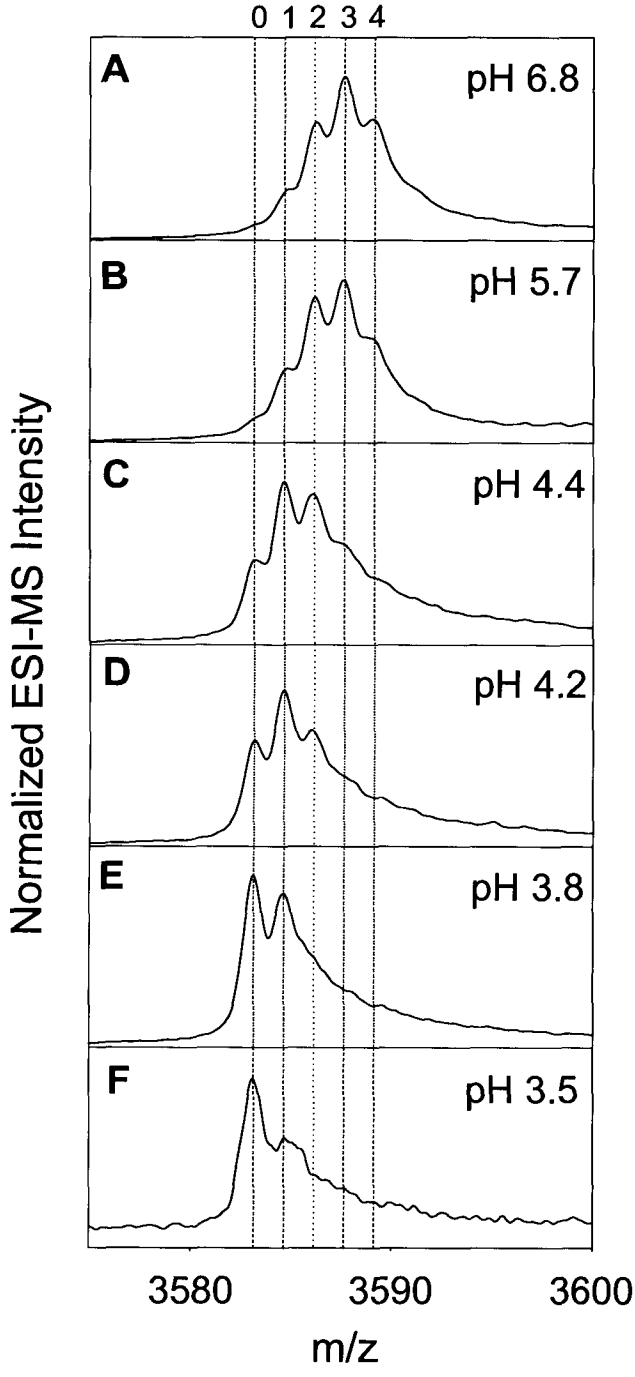

Figure 2.6: Partial ESI mass spectra showing the $(\alpha^h\beta^h)_2$ 18+ region of freshly prepared ^{cyanomet}Hb at different pH values. Dotted lines numbered 0 through 4 indicate the number of cyano groups bound to the protein tetramer. Changes in the overall spectrum as a function of pH are very similar to those depicted in Figure 2.2.

A particularly striking result in previous studies on commercial ^{met}Hb was the observation of an $\alpha^h\beta^a$ dimer during acid-induced denaturation. It was proposed that this species represents a mechanistically important intermediate during the (dis)assembly process of the native tetramer [28, 39, 40]. The spectrum depicted in Figure 2.1A confirms the existence of a heme-deficient heterodimer for the commercial protein at pH 6.8, albeit with a +32 Da modification. MS/MS experiments verified the composition of this species as $\alpha^h\beta^a{}_{ox}$, ruling out other possible combinations that would result in the same mass, such as $\alpha^a{}_{ox}\beta^h$ [73]. Importantly, none of the freshly prepared Hb species investigated here exhibits significant levels of heme-deficient dimers when studied under native solvent conditions (Figure 2.1B-D). The same result is obtained when exposing the freshly prepared protein to semi-denaturing conditions. In the case of ^{oxy}Hb this has already been demonstrated by the data in Figure 2.2. A direct comparison of ESI mass spectra for commercial and freshly prepared ^{met}Hb (*i.e.*, using the same iron oxidation state in both cases) confirms the lack of $\alpha^h\beta^a$ and $\alpha^h\beta^a{}_{ox}$ for the freshly prepared protein, as exemplified for pH 5.8 (Figure 2.7A, B) and pH 4.2 (Figure 2.7C, D). Moreover, these data demonstrate that the commercial protein is less resistant to acid-denaturation, as seen from the much higher intensity of monomeric globin chains in Figure 2.7C than in Figure 2.7D.

It is concluded that the asymmetric behavior [39] of the α and β subunits during acid-induced denaturation of commercial ^{met}Hb represents an artifact, likely caused by structural damage of the protein during isolation and/or storage. This apparent asymmetry seems to be largely caused by substantial levels of chemically altered β-globin (termed β_{ox}).

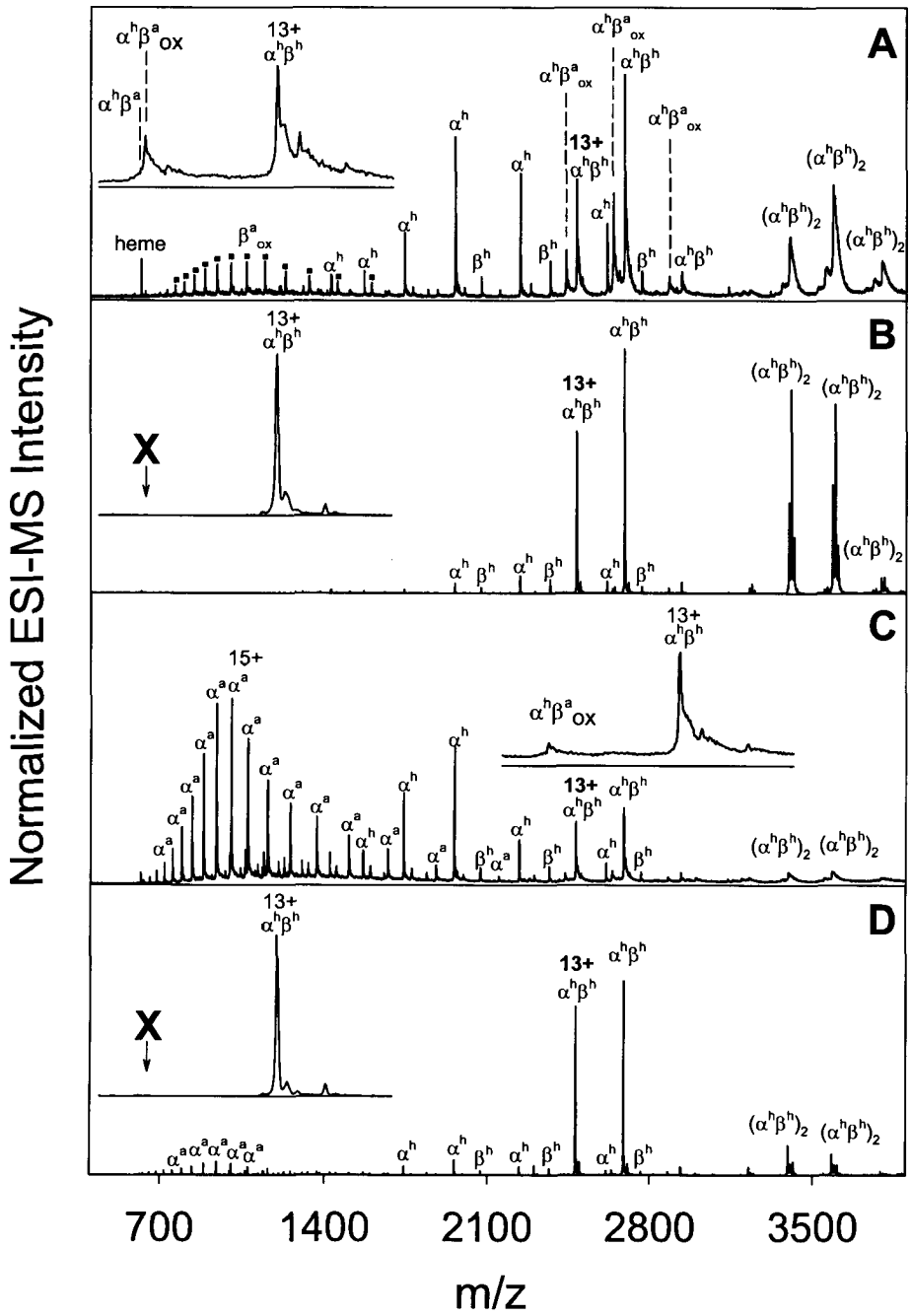

Figure 2.7: ESI mass spectra of commercially obtained ^{met}Hb (A) and freshly prepared ^{met}Hb (B) recorded at pH 5.8. Also shown are the corresponding data for pH 4.2 (C, commercial ^{met}Hb; D, freshly prepared ^{met}Hb. Insets focus on the m/z range corresponding to 13+ hetero-dimer. The expected peak positions for $\alpha^h\beta^a{}_{ox}{}^{13+}$ and $\alpha^h\beta^{a\,13+}$ are indicated as vertical dashed lines in the inset of panel (A). Arrows marked with "X" in (B) and (D) highlight the lack of $\alpha^h\beta^a$ and/or $\alpha^h\beta^a{}_{ox}$ in the spectra of freshly prepared ^{met}Hb.

The existence of $\alpha^h\beta^a_{ox}$ complexes implies that β_{ox} is still able to form noncovalent contacts with α^h, while exhibiting a greatly reduced heme affinity. However, the presence of a considerable fraction of free β^a_{ox} under native conditions (Figure 2.1A) suggests that the interaction between α^h and β^a_{ox} is relatively weak. Since the overall α:β stoichiometry in the sample is unity [66], the existence of free β^a_{ox} necessarily leads to the presence of unbound α globin. The latter maintains a compact heme-bound conformation, as seen by the low ESI charge states of α^h. In contrast, the lack of heme in β^a_{ox} traps modified β chains in a non-native conformation [3] that is characterized by high ESI charge states (labeled with black squares in Figure 2.1A).

2.3.3 Identification of Oxidation Sites in Commercial ^{met}Hb

Deconvoluted mass distributions of acid-denatured ^{met}Hb provide an estimate of the overall level of covalent modifications. As expected from the data discussed above, the β-subunit of the commercial protein exhibits a dominant satellite peak that is shifted by +32 Da (Figure 2.8A). In addition, the β-globin mass distribution in Figure 2.8A exhibits less intense signals at +16 and +48 Da. These observations are attributed to the incorporation of one, two, or three oxygen atoms [74]. Signals corresponding to up to three oxidation events also appear in the mass distribution of α-globin, albeit at lower levels. The most intense satellite peak for α-globin corresponds to a mass shift of +16 Da. In contrast, the mass distributions of freshly prepared ^{met}Hb subunits recorded under identical conditions show only trace levels of these oxidative modifications (Figure 2.8B).

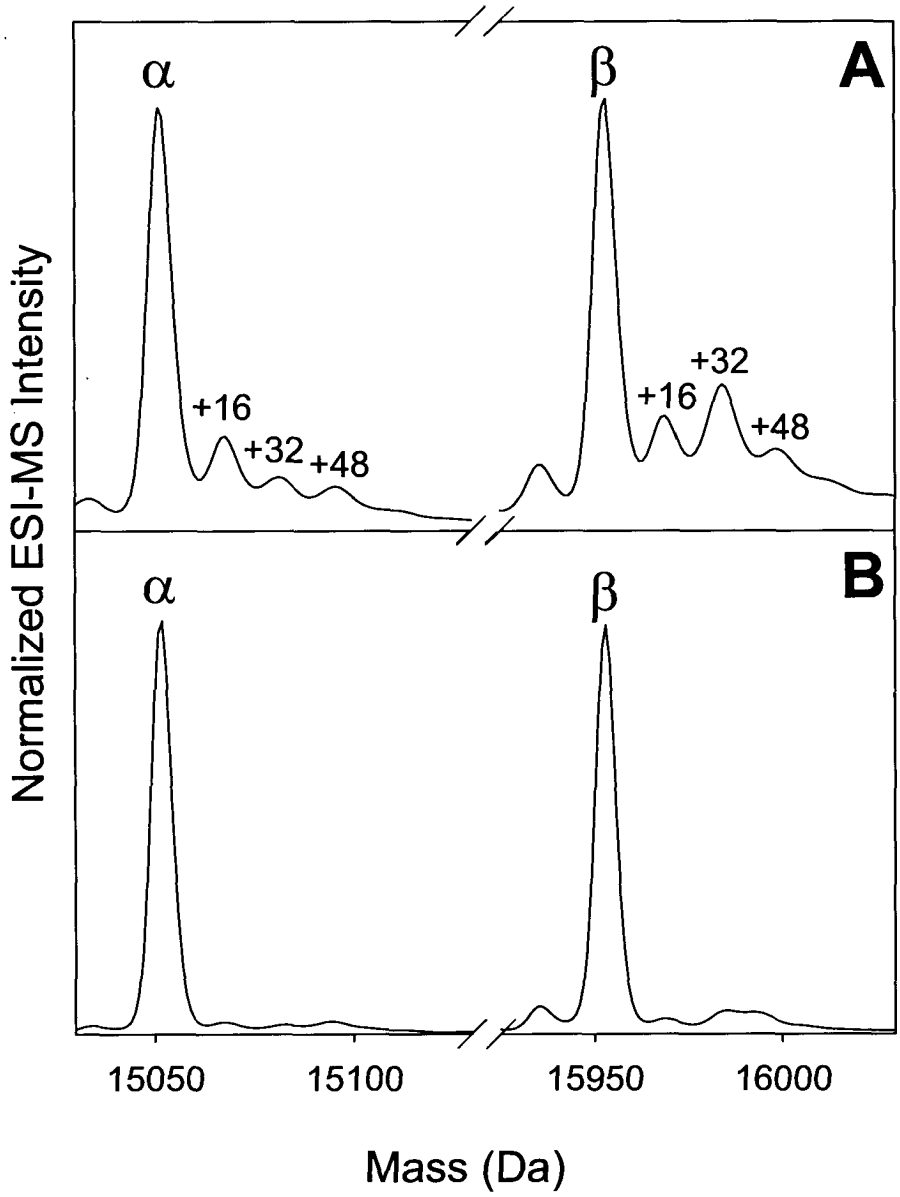

Figure 2.8: Deconvoluted mass distributions of α- and β-globin, obtained for acid-denatured ^{met}Hb at pH 2.1. (A) Commercial protein; (B) freshly prepared protein. The main peaks observed for each distribution correspond to the masses of unmodified α- and β-globin. Mass shifts of the observed covalent modifications are indicated.

Tryptic peptide mapping was carried out in order to identify the locations of oxidation sites in commercial ^{met}Hb. Shown below are the sequences of bovine α- and β-globin, with trypsin cleavage sites indicated as spaces [55].

α-globin:

VLSAADK GNVK AAWGK VGGHAAEYGAEALER MFLSFPTTK TYFPHFDLSHGSAQVK GHGAK VAAALTK AVEHLDDLPGALSELSDLHAHK LRVDPVNFK LLSHSLLVTLASHLPSDFTPAVHASLDK FLANVSTVLTSK YR

β-globin:

MLTAEEK AAVTAFWGK VK VDEVGGEALGR LLVVYPWTQR FFESFGDLSTADAVMNNPK VK AHGK K VLDSFSNGMK HLDDLK GTFAALSELHCDK LHVDPENFK LLGN VLVVVLAR NFGK EFTPVLQADFQK VVAGVANALAHR YH

LC-MS revealed that all four methionine-containing tryptic peptides (one for α, three for β) were accompanied by derivatized variants carrying a +16 Da modification. None of the other peptides were found to carry +16 Da additions or multiples thereof. The oxidized species eluted at lower acetonitrile concentrations than the corresponding unmodified peptides (data not shown). This behavior is consistent with the fact that incorporation of oxygen increases the overall hydrophilicity of the modified peptides, resulting in less favorable interactions with the reverse-phase column than for the

corresponding unmodified forms [74]. It was found that the intensity of the satellite peaks in Figure 2.8A depends somewhat on the experimental conditions, with higher ESI voltages leading to elevated oxidation levels. This phenomenon is attributed to redox reactions occurring during the ionization process, a common occurrence in ESI-MS [75]. Importantly, however, the fact that oxidized and non-oxidized peptides can be separated on an LC column demonstrates the existence of oxidative modifications in bulk solution. Tandem mass spectrometry was used to confirm methionine as the site of oxidation in all four modified peptides. As an example, MS/MS data for the modified and unmodified peptide β6 are depicted in Figure 2.9. The masses of the C-terminal fragment ions up to y"4 are identical in both cases, whereas all fragments from y"5 on show a mass shift of +16 Da. This confirms that methionine, the fifth residue from the C-terminus, carries the oxygen atom.

The observation of oxidized methionine residues is not particularly surprising, given the well known susceptibility of this residue to oxidative damage by sulfoxide formation ($R\text{-}S\text{-}CH_3 \rightarrow R\text{-}SO\text{-}CH_3$) [76]. It is interesting to note that no modifications were found for the peptide β12, which contains cysteine as another potential oxidation site. However, this cysteine residue appears buried in the X-ray structure of the protein, whereas all three methionines in the β subunit are partially solvent accessible. It is noted that low levels of non-methionine residues must be affected by oxidation as well, otherwise α-globin (carrying only one single Met) could not exhibit weak +32 and +48 Da signals. Unfortunately, the identity of these low-level oxidation sites could not be uncovered in our MS/MS experiments. In summary, it appears that partial methionine oxidation is chiefly responsible for the different behavior of commercial and freshly

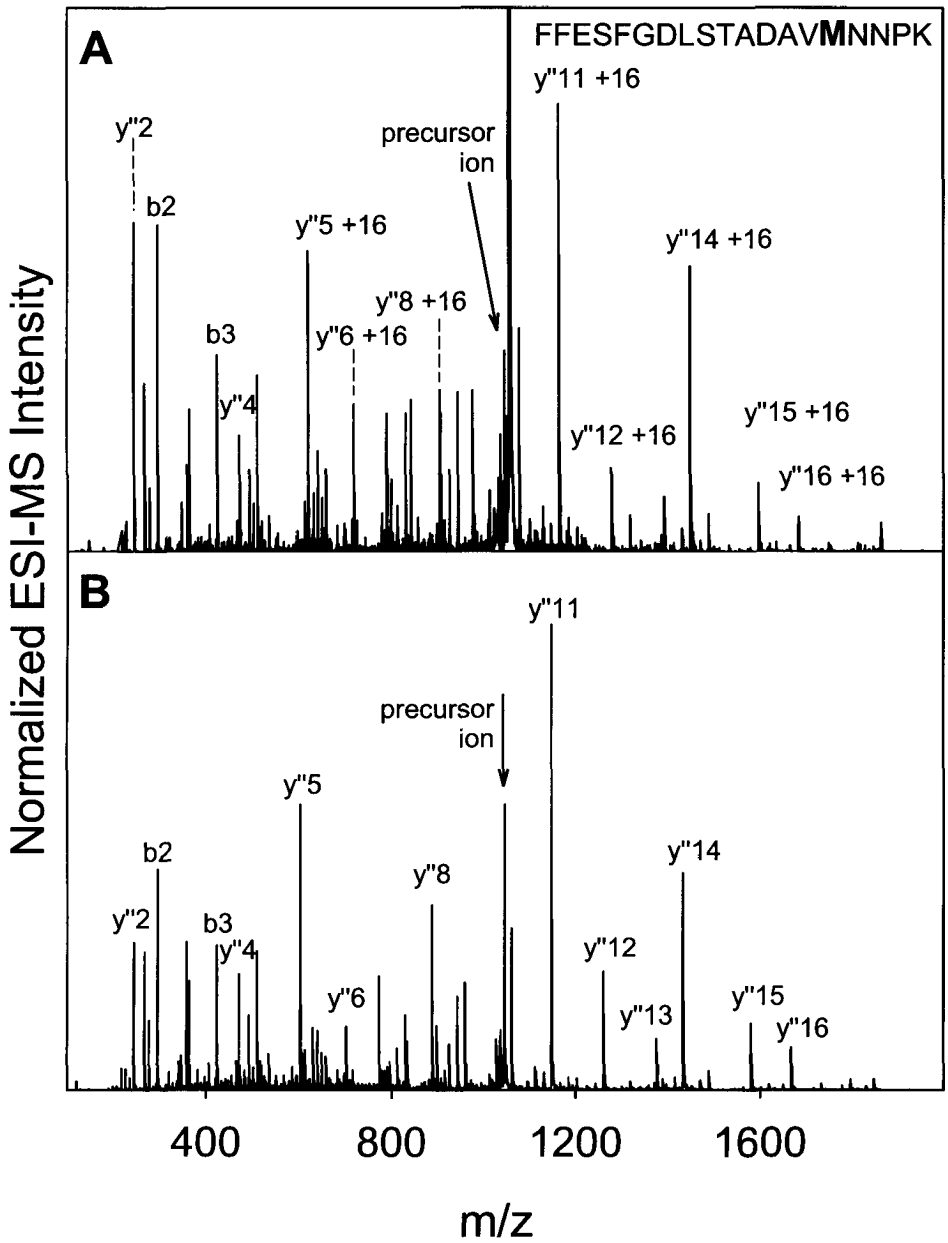

Figure 2.9: MS/MS spectra of the singly oxidized (A) and unmodified (B) tryptic peptide β6 obtained from commercial ^{met}Hb. Signals attributed to the doubly charged precursor ions (m/z 1053.47 and m/z 1045.48) are indicated, along with major singly charged fragment ions.

prepared Hb during acid-induced denaturation. Oxidation of βMet54 (Figure 2.9A), located close to the $\alpha_1\beta_1$ interface, has previously been shown to destabilize the structure of $(\alpha^h\beta^h)_2$ [77]. This provides an explanation for the significant level of monomeric globin chains for commercial ^{met}Hb under the conditions of Figure 2.1A. Our results suggest that methionine oxidation also interferes with binding of β globin to heme, evident from the presence of β^a_{ox} and $\alpha^h\beta^a_{ox}$ in the spectra of the commercial protein (Figure 2.1A).

2.4 Conclusions

Earlier ESI-MS experiments sought to gain insights into the Hb assembly and disassembly mechanism by studying the protein at increasing acid concentrations [39]. The results of that study suggested major differences in the behavior of α- and β-globin during pH denaturation. Based on those data it was proposed that the assembly of $(\alpha^h\beta^h)_2$ follows a highly asymmetric mechanism. Unfortunately, the fact that those experiments were based on commercial ^{met}Hb casts doubts on the general validity of the conclusions reached. Our data reveal significant levels of oxidative damage in commercial ^{met}Hb. In contrast, oxidative modifications were almost absent in freshly prepared samples (Figure 2.8). Experiments on three freshly prepared Hb derivatives in the current study demonstrate that the responses of α and β to changes in pH are remarkably similar, as summarized in Scheme 1. Thus, our work does not confirm the presence of a highly asymmetric Hb disassembly pathway upon acid denaturation.

It is not immediately clear whether experiments on the acid-induced denaturation of Hb *in vitro* have direct implications for the assembly of this protein complex at near-neutral pH and/or in a cellular environment, as suggested in ref. [39]. The data presented here, therefore, do not rule out the possible occurrence of asymmetric (dis)assembly pathways under different conditions. In particular, the existence of a chaperone protein that specifically interacts with α-globin is consistent with an asymmetric mechanism *in vivo* [14-20]. It appears that ESI-MS should be well suited to provide detailed insights into the exact way in which this chaperone assists the assembly process of Hb in RBC precursors.

2.5 References

1. Shaeffer, J. R., McDonald, M. J. & Bunn, H. F. (1981) Assembly of normal and abnormal human hemoglobins, *Trends Biochem. Sci. 6*, 158-161.

2. Rose, M. Y. & Olson, J. S. (1983) The Kinetic Mechanism of Heme Binding to Human Apohemoglobin, *J. Biol. Chem. 258*, 4298-4303.

3. Leutzinger, Y. & Beychok, S. (1981) Kinetics and mechanism of heme-induced refolding of human α-globin, *Proc. Natl. Acad. Sci. USA. 78*, 780-784.

4. Adachi, K., Zhao, Y. & Surrey, S. (2003) Effects of heme addition on formation of stable human globin chains and hemoglobin subunit assembly in a cell-free system, *Arch. Biochem. Biophys. 413*, 99-106.

5. Hernan, R. A. & Sligar, S. G. (1995) Tetrameric hemoglobin expressed in *Escherichia coli*, *J. Biol. Chem. 270*, 26257-26264.

6. Joshi, A. A. & McDonald, M. J. (1994) Role of α and β Carboxyl-terminal Residues in the Kinetics of Human Oxyhemoglobin Dimer Assembly, *J. Biol. Chem. 269*, 8549-8553.

7. McGovern, P., Reisberg, P. & Olson, J. S. (1976) Aggregation of Deoxyhemoglobin Subunits, *J. Biol. Chem. 251*, 7871-7879.

8. McDonald, M. J., Turci, S. M., Mrabet, N. T., Himelstein, B. P. & Bunn, H. F. (1987) The Kinetics of Assembly of Normal and Variant Human Oxyhemoglobins, *J. Biol. Chem. 262*, 5951-5956.

9. Kawamura, Y., Hasumi, H. & Nakamura, S. (1982) Kinetic Studies on the Reconstitution of Deoxyhemoglobin from Isolated α and β Chains, *J. Biochem. 92*, 1227-1233.

10. Adachi, K., Yang, Y., Joshi, A. A., Vasudevan, G., Morris, A. & McDonald, M. J. (2001) Consequences of β16 and β112 Replacements on the Kinetics of Hemoglobin Assembly, *Biochem. Biophys. Res. Comm. 289*, 75-79.

11. Bunn, H. F. & McDonald, M. J. (1983) Electrostatic interactions in the assembly of haemoglobin, *Nature. 306*, 498-500.

12. Mrabet, N. T., McDonald, M. J., Turci, S., Sarkar, R., Szabo, A. & Bunn, H. F. (1986) Electrostatic Attraction Governs the Dimer Assembly of Human Hemoglobin, *J. Biol. Chem. 261*, 5222-5228.

13. Yamaguchi, T., Yang, Y., McDonald, M. J. & Adachi, K. (2000) Surface and Interface β-Chain Residues Synergistically Affect Hemoglobin Assembly, *Biochem. Biophys. Res. Comm. 270*, 683-687.

14. Luzzatto, L. & Notaro, R. (2002) Haemoglobin's chaperone, *Nature. 417*, 703-704.

15. Kihm, A. J., Kong, Y., Hong, W., Russel, J. E., Rouda, S., Adachi, K., Simon, M. C., Blobel, G. A. & Weiss, M. J. (2002) An abundant erythroid protein that stabilizes free α-haemoglobin, *Nature. 417*, 758-763.

16. Baudin-Creuza, V., Vasseur-Godbillon, C., Pato, C., Prehu, C., Wajcman, H. & Marden, M. C. (2004) Transfer of Human α- to β-Hemoglobin via its Chaperone Protein, *J. Biol. Chem. 279*, 36530-36533.

17. Santiveri, C. M., Perez-Canadillas, J. M., Viadivelu, M. K., Allen, M. D., Rutherford, T. J., Watkins, N. A. & Bycroft, M. (2004) NMR structure of the α-Hemoglobin Stabilizing Protein, *J. Biol. Chem. 279*, 34963-34970.

18. Hodge, D., Coghill, E., Keys, J., Maguire, T., Hartman, B., McDowall, A., Weiss, M., Grimmond, S. & Perkins, A. (2006) A global role for EKLF in definitive and primitive erythropoiesis, *Blood. 15*, 3359-3370.

19. Feng, L., A., G. D., Zhou, S., Gu, L., Kong, Y., Li, J., Hu, M., Yan, N., Lee, C., Rich, A. M., Armstrong, R. S., Lay, P. A., Gow, A. J., Weiss, M. J., Mackay, J. P. & Shi, Y. (2004) Molecular Mechanism of AHSP-Mediated Stabilization of α-Hemoglobin, *Cell. 119*, 629-640.

20. Feng, L., Zhou, S., Gu, L., Gell, D. A., Mackay, J. P., Weiss, M. J., Gow, A. J. & Shi, Y. (2005) Structure of oxidized α-haemoglobin bound to AHSP reveals a protective mechanism for haem, *Nature. 435*, 697-701.

21. Boys, B. L. & Konermann, L. (2007) Folding and Assembly of Hemoglobin Monitored by Electrospray Mass Spectrometry Using an On-line Dialysis System, *J. Am. Soc. Mass Spectrom. 18*, 8-16.

22. Schaeffer, J. R., McDonald, M. J., Turci, S. M., Dinda, D. M. & Bunn, H. F. (1984) Dimer-Monomer Dissociation of Human Hemoglobin A, *J. Biol. Chem. 259*, 14544-14547.

23. Komar, A. A., Kommer, A., Krasheninnikov, I. A. & Spirin, A. S. (1997) Cotranslational folding of globin, *J. Biol. Chem. 272*, 10646 - 10651.

24. Komar, A. A., Kommer, A., Krasheninnikov, I. A. & Spirin, A. S. (1993) Cotranslational heme binding to nascent globin chains, *FEBS Lett. 326*, 261-263.

25. Vasudevan, G. & McDonald, M. J. (2002) Ordered heme binding ensures the assembly of fully functional hemoglobin: a hypothesis, *Curr. Prot. Pept. Sci. 3*, 461-466.

26. Vasudevan, G. & McDonald, M. J. (1997) Spectral demonstration of semihemoglobin formation during CN-hemin incorporation into human apohemoglobin, *J. Biol. Chem. 272*, 517 - 524.

27. Vasudevan, G. & McDonald, M. J. (2006) Soret spectral and bioinformatic approaches provide evidence for a critical role of the α-subunit in assembly of tetrameric hemoglobin, *T. Protein. J. 25*, 45-56.

28. Griffith, W. P. & Kaltashov, I. A. (2007) Protein Conformational Heterogeneity as a Binding Catalyst: ESI-MS Study of Hemoglobin H Formation, *Biochemistry. 46*, 2020-2026.

29. Kawamura-Konishi, Y. & Suzuki, H. (1985) Binding Reaction of Hemin to Globin, *J. Biochem. 98*, 1181-1190.

30. Kawamura-Konishi, Y., Chiba, K., Kihara, H. & Suzuki, H. (1992) Kinetics of the reconstitution of hemoglobin from semihemoglobins α and β with heme, *Eur. Biophys. J. 21*, 85-92.

31. Kaltashov, I. A. & Eyles, S. J. (2002) Studies of Biomolecular Conformations and Conformational Dynamics by Mass Spectrometry, *Mass Spectrom. Rev. 21*, 37-71.

32. Heck, A. J. R. & Van den Heuvel, R. H. H. (2004) Investigation of intact protein complexes by mass spectrometry, *Mass Spectrom. Rev. 23*, 368-389.

33. Loo, J. A. (2005) Noncovalent Protein-Ligand Complexes in *The Encyclopedia of Mass Spectrometry* (Gross, M. L. & Caprioli, R. M., eds) pp. 289-299, Elsevier, Amsterdam.

34. Ruotolo, B. T. & Robinson, C. V. (2006) Aspects of native proteins are retained in vacuum, *Curr. Op. Chem. Biol. 10*, 402-408.

35. Smith, A. M., Jahn, T. R., Ashcroft, A. E. & Radford, S. E. (2006) Direct Observation of Oligomeric Species formed in the Early Stages of Amyloid Formation using Electrospray Ionization Mass Spectrometry, *J. Mol. Biol. 364*, 9-19.

36. Potier, N., Donald, L. J., Chernushevich, I., Ayed, A., Ens, W., Arrowsmith, C. H., Standing, K. G. & Duckworth, H. W. (1998) Study of a noncovalent trp repressor: DNA operator complex by electrospray ionization time-of-flight mass spectrometry, *Protein Sci. 7*, 1388-1395.

37. Grandori, R., Matecko, I. & Muller, N. (2002) Uncoupled analysis of secondary and tertiary protein structure by circular dichroism and electrospray ionization mass spectrometry, *J. Mass Spectrom. 37*, 191-196.

38. Konermann, L. (2007) A Minimalist Model for Exploring Conformational Effects on the Electrospray Charge State Distribution of Proteins, *J. Phys. Chem. B. 111*, 6534-6543.

39. Griffith, W. P. & Kaltashov, I. A. (2003) Highly asymmetric interactions between globin chains during hemoglobin assembly revealed by electrospray ionization mass spectrometry, *Biochemistry. 42*, 10024 - 10033.

40. Griffith, W. P. & Kaltashov, I. A. (2006) Mass Spectrometry in the Study of Hemoglobin: from Covalent Structure to Higher Order Assembly, *Curr. Org. Chem. 10*, 535-553.

41. Simmons, D. A., Wilson, D. J., Lajoie, G. A., Doherty-Kirby, A. & Konermann, L. (2004) Subunit Disassembly and Unfolding Kinetics of Hemoglobin Studied by Time-resolved Electrospray Mass Spectrometry, *Biochemistry. 43*, 14792-14801.

42. Hossain, B. M. & Konermann, L. (2006) Pulsed Hydrogen/Deuterium Exchange MS/MS for Studying the Relationship between Noncovalent Protein Complexes in Solution and in the Gas Phase after Electrospray Ionization, *Anal. Chem. 78*, 1613-1619.

43. Antonini, E. & Brunori, M. (1971) *Hemoglobin and Myoglobin in Their Reactions With Ligands*, North-Holland Publishing Company, Amsterdam, London.

44. Shreffler, D. C. & Salisbury, G. W. (1959) Distribution of Inheritance of Hemoglobin Variants in American Cattle, *J. Dairy Sci. 42*, 1147-1156.

45. Paul, K. G., Theorell, H. & Akeson, A. (1953) The Molar Light Absorption of Pyridine Ferroprotoporphyrin (Pyridine Haemochromogen), *Acta Chem. Scand. 7*, 1284-1287.

46. Crosby, W. H. & Houchin, D. N. (1957) Preparing Standard Solutions of Cyanmethemoglobin, *Blood. 12*, 1132-1136.

47. Haematology, I. C. f. S. i. (1978) Recommendations for reference method for haemoglobinometry in human blood (ICSH Standard EP 6/2:1977) and specifications for international haemiglobincyanide reference preparation (ICSH Standard EP 6/3:1977), *J. Clinical Path. 31*, 139-143.

48. Breepoel, P. M., Kreuzer, F. & Hazevoet, M. (1981) Interaction of Organic Phosphates with Bovine Hemoglobin, *Pflugers Arch. 389*, 219-225.

49. Bunn, H. F. (1971) Differences in the Interaction of 2,3-Diphosphoglycerate with Certain Mammalian Hemoglobins, *Science. 172*, 1049-1050.

50. Moore, G. L. & et_al. (1992) Evaluation of Methemoglobin Formation During the Storage of Various Hemoglobin Solutions, *Artif. Organs. 16*, 513-518.

51. Evelyn, K. A. & Malloy, H. T. Microdetermination of Oxyhemoglobin, Methemoglobin, and Sulfhemoglobin in a Single Sample of Blood, *J. Biol. Chem. 126*, 655-662.

52. Leahy, T. & Smith, R. (1960) Notes on Methemoglobin Determination, *Clin. Chem. 6*, 148-152.

53. Cruz-Laneira, A., Bal, B. J., Quintela, O. & Lopez-Rivadulla, M. (2002) Determination of Methemoglobin and Total Hemoglobin in Toxicological Studies by Derivative Spectrophotometry, *J. Anal. Tox. 26*, 67-72.

54. Versluis, C. & Heck, A. J. R. (2001) Gas-phase dissociation of hemoglobin, *Int. J. Mass Spectrom. 210/211*, 637-649.

55. Mueser, T. C., Rogers, P. H. & Arnone, A. (2000) Interface Sliding as Illustrated by the Multiple Quaternary Structures of Liganded Hemoglobin, *Biochemistry. 39*, 15353 - 15364.

56. Ackers, G. K. & Halvorson, H. R. (1974) The linkage between oxygenation and subunit dissociation in human hemoglobin, *Proc. Natl. Acad. Sci. U.S.A. 71*, 4312-4316.

57. Lunelli, L., Paola, Z. & Baldini, G. (1994) Evidence of hemoglobin dissociation, *Biopolymers. 34*, 747-757.

58. White, S. L. (1975) The molecular dissociation of ferrihemoglobin derivatives, *J. Biol. Chem. 250*, 1263-1268.

59. Riggs, A. F. (1998) Self-association, cooperativity and supercooperativity of oxygen binding by hemoglobins, *J. Exper. Biol. 201*, 1073-1084.

60. Peschke, M., Verkerk, U. H. & Kebarle, P. (2004) Features of the ESI Mechanism that Affect the Observation of Multiply Charged Noncovalent Protein Complexes and the Determination of the Association Constant by the Titration Method, *J. Am. Soc. Mass Spectrom. 15*, 1424-1434.

61. Sun, J., Kitova, E. N., Wang, W. & Klassen, J. S. (2006) Method for Distinguishing Specific from Nonspecific Protein-Ligand Complexes in Nanoelectrospray Ionization Mass Spectrometry, *Anal. Chem. 78*, 3010-3018.

62. Green, B. N. & Vinogradov, S. N. (2004) An Electrospray Ionization Mass Spectrometric Study of the Subunit Structure of the Giant Hemoglobin from the Leech *Nephelopsis oscura*, *J. Am. Soc. Mass Spectrom. 15*, 22-27.

63. McKay, A. R., Ruotolo, B. T., Ilag, L. L. & Robinson, C. V. (2006) Mass Measurements of Increased Accuracy Resolve Heterogeneous Populations of Intact Ribosomes, *J. Am. Chem. Soc. 128*, 11433-11442.

64. Sen, U., Dasgupta, J., Choudhury, D., Datta, P., Chakrabarti, A., Chakrabarty, S. B., Chakrabarty, A. & Dattagupta, J. K. (2004) Crystal Structure of HbA_2 and HbE and Modeling of Hemoglobin δ_4: Interpretation of the Thermal Stability and the Antisickling Effect of HbA_2 and Identification of the Ferrocyanide Binding site in Hb, *Biochemistry. 43*, 12477-12488.

65. Dobo, A. & Kaltashov, I. A. (2001) Detection of Multiple Protein Conformational Ensembles in Solution via Deconvolution of Charge-State Distributions in ESI MS, *Anal. Chem. 73*, 4763-4773.

66. Kuprowski, M. C., Boys, B. L. & Konermann, L. (2007) Analysis of Protein Mixtures by Electrospray Mass Spectrometry: Effects of Conformation and Desolvation Behavior on the Signal Intensities of Hemoglobin Subunits, *J. Am. Soc. Mass Spectrom. 18*, 1279-1285.

67. Sogbein, O. O., Simmons, D. A. & Konermann, L. (2000) The Effects of pH on the Kinetic Reaction Mechanism of Myoglobin Unfolding Studied by Time-Resolved Electrospray Ionization Mass Spectrometry, *J. Am. Soc. Mass Spectrom. 11*, 312-319.

68. Adams, P. A. (1976) The Kinetics and Mechanism of the Recombination Reaction between Apomyoglobin and Haemin, *Biochem. J. 159*, 371-376.

69. Shikama, K. (2006) Nature of FeO_2 bonding in myoglobin and hemoglobin: A new molecular paradigm, *Progr. Biophys. Mol. Biol. 91*, 83-162.

70. Sage, J. T., Morikis, D. & Champion, P. M. (1991) Spectroscopic Studies of Myoglobin at Low pH: Heme Structure and Ligation, *Biochemistry. 30*, 1227-1237.

71. Sage, J. T., Li, P. & Champion, P. M. (1991) Spectroscopic Studies of Myoglobin at Low pH: Heme Ligation Kinetics, *Biochemistry. 30*, 1237-1247.

72. Konermann, L., Rosell, F. I., Mauk, A. G. & Douglas, D. J. (1997) Acid-Induced Denaturation of Myoglobin Studied by Time-Resolved Electrospray Ionization Mass Spectrometry, *Biochemistry. 36*, 6448-6454.

73. Simmons, D. A., Dunn, S. D. & Konermann, L. (2003) Conformational Dynamics of Partially Denatured Myoglobin Studied by Time-Resolved Electrospray Mass Spectrometry With Online Hydrogen-Deuterium Exchange, *Biochemistry. 42*, 5896-5905.

74. Takamono, K. & Chance, M. R. (2006) Radiolytic Protein Footprinting with Mass Spectrometry to Probe the Strucuture of Macromolecular Complexes, *Annu. Rev. Biophys. Biomol. Struct. 35*, 251-276.

75. Chen, M. & Cook, K. D. (2007) Oxidation Artifacts in the Electrospray Mass Spectrometry of Aβ Peptide, *Anal. Chem. 79*, 2031-2036.

76. Creighton, T. E. (1993) *Proteins*, W. H. Freeman & Co, New York.

77. Amiconi, G., Ascoli, F., Barra, D., Bertollini, A., Matarese, R. M., Verzili, D. & Brunori, M. (1989) Selective Oxidation of Methionine β(55)D6 at the α1β1 Interface in Hemoglobin Completely Destabilizes the T-state, *J. Biol. Chem. 264*, 17745-17749.

Chapter 3 - Protein Oxidative Modifications During Electrospray Ionization: Solution Phase Electrochemistry or Corona Discharge-Induced Radical Attack?

3.1 Introduction

Oxidative modifications of proteins represent a focal point of research. *In vivo* oxidation has been linked to disease mechanisms and ageing [1, 2]. The oxidation of amino acid side chains can be induced by exposure to hydroxyl radicals (·OH) and other reactive oxygen species (ROS). Many laboratories employ oxidative labeling *in vitro* for mapping protein structures and interactions in "footprinting" experiments. Studies of this kind provide information on tertiary structure and binding interfaces, because the reactivity of each residue is modulated by its solvent exposure [3-13]. The types of covalent modifications generated during oxidative labeling *in vitro* are largely identical to those induced under conditions of oxidative stress in living organisms [14-16]. Electrospray ionization (ESI) mass spectrometry (MS) [17] represents the most widely used analytical tool for monitoring protein oxidation. ROS exposure usually culminates in the formation of covalent +16 Da adducts, but side products exhibiting other mass shifts may be formed as well [18]. The exact location of modification sites within a protein can be determined by tryptic peptide mapping in combination with liquid chromatography (LC) and ESI-MS/MS [3-12, 19].

A potential problem with these ESI-MS-based studies is the fact that oxidation can also occur during the ESI process itself. As a result, it may be difficult to assess how well the observed ions reflect the actual oxidation levels in bulk solution [20]. Two

fundamentally different oxidation mechanisms can be envisioned, namely (i) processes linked to electron transfer at the metal/liquid interface of the ESI emitter, or (ii) reactions induced by ROS generated in a corona discharge. It is useful to briefly review the operation of an ESI source, with emphasis on these two factors. We will restrict our discussion to the commonly used positive ion mode.

An ESI source represents a controlled-current electrochemical flow cell (black elements in Figure 3.1) [21-23]. Analyte solution is infused into a stainless steel capillary that is held at high positive potential V_0 vs. ground. The capillary exit is separated from the mass spectrometer by an atmospheric pressure gap. Positively charged solvent droplets are emitted from the tip of a Taylor cone. Solvent evaporation and droplet fission culminate in the formation of gas phase analyte ions (denoted as A^+ in Figure 3.1). These species then migrate towards the mass spectrometer, the potential of which is at ground [24]. The emission of positive charge from the Taylor cone necessitates the occurrence of charge balancing oxidation processes at the metal/liquid interface, e.g., oxidation of the solvent, the analyte, or the capillary material [25-28]. The electrons released in this way constitute the current I_{ESI} that flows through a wire to the high voltage power supply, and ultimately to the mass spectrometer where charge recombination takes place. In this series circuit the ESI capillary represents the working electrode (anode), and the mass spectrometer constitutes the counter electrode (cathode) [24, 29].

The interfacial potential drop $V_{M/L}$ at the metal liquid interface of the ESI capillary reflects the extent to which an electric double layer has formed, thereby determining whether oxidation of a given species at the electrode surface is thermodynamically possible [25]. Van Berkel et al. demonstrated the oxidation of substances with potentials up to almost 1.5 V vs. SCE (saturated calomel electrode) [30]. Computational studies [31]

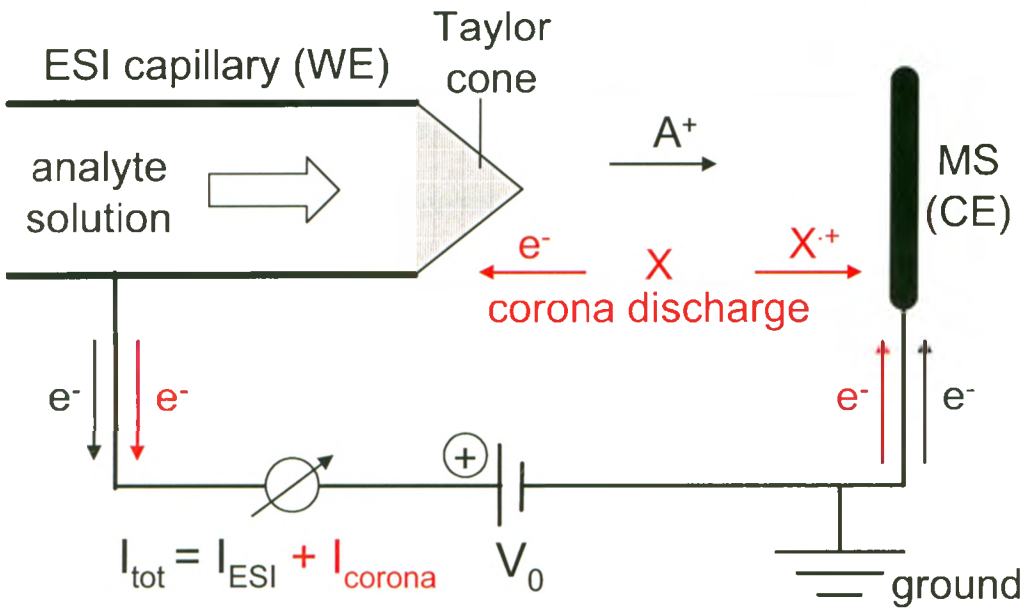

Figure 3.1: Schematic depiction of an ESI source in positive ion mode (**black**). Positively charged solvent droplets and analyte ions (A^+) are ejected from the tip of the Taylor cone. Flow directions of charge carriers are indicated by thin arrows. Shown in **red** are the *additional* current contributions under corona discharge conditions, where neutral gas molecules X break down to form X^+ and free electrons. MS, mass spectrometer; CE, counter electrode; WE, working electrode; V_0, capillary voltage.

and microelectrode measurements [32-34] revealed that $V_{M/L}$ is not uniform along the capillary length, and that even higher potentials may be present at the emitter tip. Oxidation of the capillary material has a tendency to lower $V_{M/L}$ [20, 35], but this redox buffering effect is diminished by the formation of a protective oxide layer on the stainless steel surface [26, 36-38]. The conditions within the ESI capillary should therefore, in principle, allow the oxidation of a wide range of organic and biological species, including several amino acid side chains (e.g., Cys, Met, Trp, Tyr, His) [39]. However, $V_{M/L}$ is not a fixed value but depends on a range of parameters such as the composition and flow rate v_f of the solution, as well as the applied voltage V_0. Also, overpotentials and relatively unfavorable mass transfer in tubular emitters [25, 40] may limit the extent of oxidation for any given species. As a result, it is not always easy to predict the nature of the charge-balancing reactions within the ESI capillary [25].

The second aspect that has to be considered is the possible occurrence of a corona discharge in the ion source region. Most ESI sources employ a coaxial flow of nebulizer gas (not shown in Figure 3.1) to enhance solvent dispersion and evaporation. This gas fills the gap separating the positively charged emitter tip from the counter electrode. Dielectric breakdown of gas molecules X takes place once the capillary voltage V_0 exceeds a critical value, generating a plasma that consists of radical cations and free electrons ($X \rightarrow X^{\cdot+} + e^-$) [41, 42]. The former migrate towards the mass spectrometer and the latter towards the capillary tip (Figure 3.1, red elements). The onset of corona discharge is usually marked by a sharp increase in overall current I_{tot} [20, 43], which now represents the sum of the two contributions

$$I_{tot} = I_{ESI} + I_{corona} \qquad (1)$$

I_{corona} is not associated with charge-balancing reactions at the metal/liquid interface. At very high V_0 it is easy to recognize the occurrence of a discharge by its light emission [44]. This regime leads to sub-optimal ESI performance and is usually avoided. Gas phase electrons liberated in the discharge are accelerated and induce the formation of OH radicals through inelastic collisions in the vicinity of the emitter tip ($H_2O + e^- \rightarrow H\cdot + \cdot OH + e^-$) [45]. Hydroxyl radicals and other ROS produced in the plasma can induce various oxidation processes [44, 46].

It is important to delineate the extent to which ESI-induced protein oxidation is linked to redox reactions at the metal/liquid interface, or to discharge-related processes. The answer to this question remains elusive, as previous studies (to our knowledge) have not examined this issue systematically from both directions. A correlation between the onset of corona discharge at elevated V_0 and the oxidation of Met, Trp, and Tyr was first noticed by Morand and coworkers [44]. In related work by Downard et al., an ESI source was operated at very high voltage (V_0 = 8 kV) and with oxygen nebulizer gas for protein footprinting by "radical probe-MS" [8, 46]. Analyte oxidation in those cases was attributed to corona-generated ROS. However, elevated values of V_0 that induce a discharge should also increase the rate of charge-balancing reactions and the interfacial potential drop $V_{M/L}$, thereby enhancing redox processes at the metal/liquid interface [25]. Notably, protein oxidation in electrochemical flow cells occurs at potentials comparable to those encountered during ESI, albeit under conditions that provide more efficient mass transfer, and with the possible involvement of secondary (indirect) processes [10, 47, 48]. Bateman attributed protein oxidation in nanoESI-MS to purely electrochemical factors [49] More recently, Chen and Cook [20] tentatively ascribed methionine sulfoxide

(MetO) formation at V_0 = 4.5 kV to corona discharge, but they noted that the exact oxidation mechanism remains unknown.

This work explores the mechanism of ESI-induced protein oxidation by focusing on bovine hemoglobin (Hb) as a model system. The native state of Hb represents a noncovalently bound $\alpha_2\beta_2$ tetramer [50]. In previous work we found that the β subunit of this protein (βHb) undergoes spontaneous MetO formation during storage. Those oxidation events have major implications for subunit interactions, and for the assembly of the native tetramer [51, 52]. Note that MetO formation is unrelated to reversible oxygen binding under physiological conditions [53]. During the course of our experiments [51, 52] we noticed that βHb is also highly susceptible to ESI-induced oxidation. Interestingly, these modifications were found to occur even under fairly normal operating conditions, i.e., they did not require extreme capillary voltage and oxygen nebulizer gas as in radical probe-MS [8, 46]. This unexpected phenomenon prompted us to examine whether corona-induced ROS significantly contribute to protein oxidation under regular ESI conditions, or whether the effect is a manifestation of heterogeneous electrochemistry.

3.2 Experimental

3.2.1 Materials

Ammonium acetate and formic acid were purchased from Fluka (Buchs, Switzerland). H_2O was purified by distillation of reverse osmosis water. Bovine Hb was prepared from fresh hemolysate via standard procedures [52, 54]. 1.6 mM Hb stock solution was flash frozen in liquid nitrogen, and stored at -80 °C in 10 mM ammonium acetate (pH 6.8). Acid-denatured Hb was prepared by diluting this stock solution to a protein concentration of 1 μM (as tetramer), i.e., 2 μM αHb and 2 μM βHb, in 10 mM ammonium acetate and 2% (v/v) formic acid (pH 2). This solution was used for all experiments. Heme loss, subunit dissociation, as well as extensive unfolding occur under these acidic conditions for both subunits [51, 52, 55]. Commercially available Hb was not used due to high levels of background oxidation [52].

3.2.2 Mass Spectrometry

Mass spectra were recorded on a Q-TOF Ultima API (Waters/Micromass, Manchester, UK) utilizing a standard Z-spray ESI source in positive ion mode. The commercial probe was modified to allow measurements of I_{tot}. For this purpose a Fluke 189 multimeter was isolated from ground and operated in series with the ESI power supply as indicated in Figure 3.1 (safety note: this arrangement may expose the operator to inadvertent electric shock). ESI capillaries were cut and polished in house from type 304 stainless steel hypodermic tubing (Small Parts, Miramar, FL) to a length of 18.5 cm (i.d. 140 μm, o.d. 235 μm). The probe tip was oriented 10 mm back and 3 mm lateral from the ion sampling

cone. The cone voltage was held at 70 V, and the RF lens 1 was at 40 V for all acquisitions. Various capillary voltages were tested, up to $V_0 = 5$ kV, which represents the highest possible value on our instrument. The TOF analyzer was calibrated with CsI. The nebulizer gas pressure was held at 100 psi, resulting in a flow of ca. 0.5 L min^{-1}. N_2 was purified in house with a Whatman nitrogen generator; O_2 (medical grade), Ar (ultra high purity 5.0) and SF_6 (99.9% purity) were purchased from Praxair (Mississauga, Ont., Canada). Samples not requiring desalting were infused into the mass spectrometer via a syringe pump. These direct infusion measurements were carried out in the absence of an upstream ground to avoid the occurrence of external currents that might otherwise complicate data interpretation [25, 26]. Samples exposed to off-line electrolysis were analyzed by LC/ESI-MS using a 1525μ HPLC pump (Waters) and a Symmetry 300 C4 column (2.1 × 100 mm, Waters) at a flow rate of 100 μL min^{-1} to reduce the extent of salt contamination introduced through the reference electrode (see below). The water and acetonitrile/propanol (50:50 v/v) mobile phase contained 0.1% v/v formic acid. The organic content was ramped from 0% to 90% within 6 min. All data were acquired and analyzed using MassLynx 4.0 software provided by the instrument manufacturer. Consistent with previous reports [56], the subunit masses were found to be 15053 and 15954 Da for αHb and βHb, respectively.

3.2.3 Off-Line Electrolysis

Hb solution was electrolyzed using a three-electrode setup (Figure 3.2). Protein solution was enclosed in a 2.5 × 3.5 × 0.34 cm^3 Slide-A-Lyzer dialysis cassette (Pierce, Rockford, IL) with a 7 kDa molecular weight cut-off. The solution was rapidly circulated through the cassette via a peristaltic pump at a flow rate of 15 mL min^{-1} in order to facilitate mass

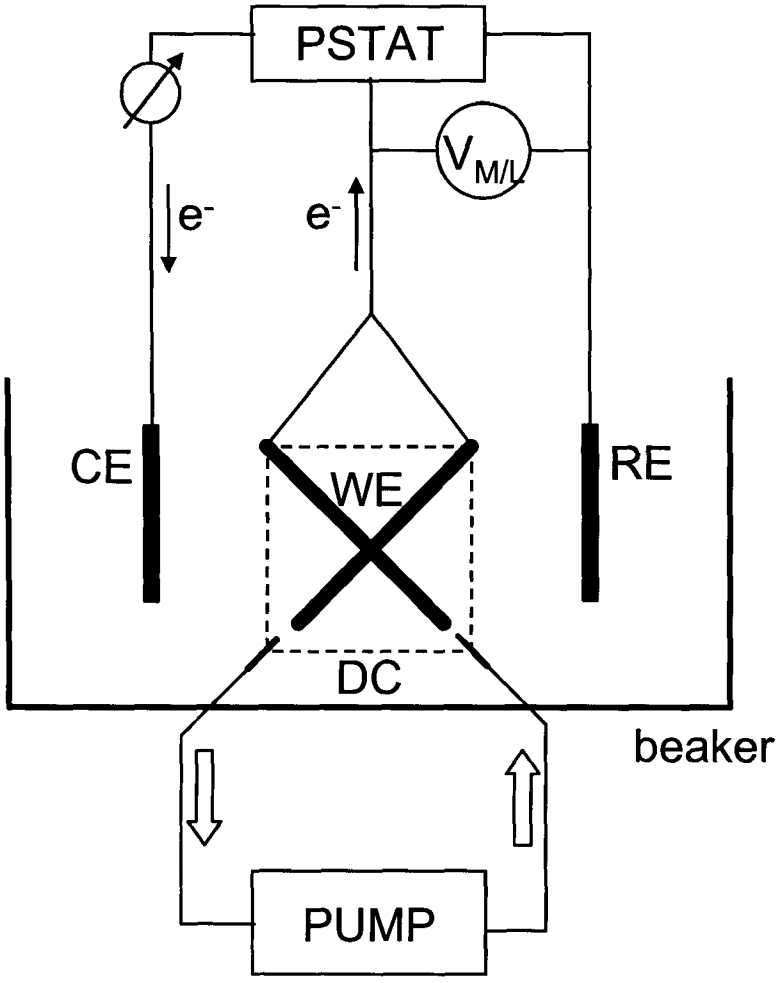

Figure 3.2: Schematic representation of the setup used for protein electrolysis. A peristaltic pump circulates the protein solution through a dialysis cassette (DC) which contains the working electrode (WE). Block arrows indicate the direction of liquid flow. The interfacial potential drop $V_{M/L}$ at WE is set relative to a saturated calomel reference electrode (RE) by a potentiostat (PSTAT), which ensures adequate electron flow (I) from WE to the Pt counter electrode (CE). No current flows between WE and RE, thereby allowing an accurate measurement of the interfacial potential drop at WE. DC and all three electrodes are submersed in electrolyte solution.

transfer. The total volume of protein solution in the system was 3 mL. The working electrode within the cassette consisted of two crossed stainless steel 304 wires with a diameter of 235 μm (Small Parts) with an exposed length of 3 cm. The orientation of these wires relative to the circulation inlet and outlet is indicated in Figure 3.2. The interfacial potential drop $V_{M/L}$ at the working electrode was measured with respect to a reference SCE. A Pt sheet with a total surface area of 12.5 cm^2, welded to a Pt wire, served as counter electrode. The dialysis cassette was submersed along with the three electrodes in a supporting electrolyte solution matching the solvent used for the protein (10 mM ammonium acetate in water, 2% v/v formic acid, pH 2). Applied potentials were controlled, and current responses recorded, with a Solartron model 1287 potentiostat (Farnborough Hampshire, UK). The entire electrochemical setup was placed in a grounded Faraday cage. LC/ESI-MS analysis of Hb after off-line electrolysis was performed as outlined above. Control experiments carried out at an extremely high value of $V_{M/L}$ (2.5 V vs. SCE) resulted in almost complete protein oxidation (fraction unmodified [57] < 10%) within three minutes, demonstrating that mass transfer limitations become insignificant for $t > 3$ min (data not shown).

3.3 Results and Discussion

3.3.1 Protein Oxidation under Normal Operating Conditions

ESI-MS analysis of 1 μM Hb at a capillary voltage of V_0 = 2.0 kV, a solution flow rate of v_f = 10 μL min^{-1}, and with N_2 nebulizer gas results in the mass distribution depicted in Figure 3.3A. Signals for both αHb and βHb appear at their expected mass values, with no indication of protein oxidation. Minor sodium adducts of the type seen in Figure 3.3A are commonly encountered in ESI-MS [58]. An entirely different picture is obtained when analyzing the same sample at V_0 = 3.5 kV and v_f = 1 μL min^{-1} (Figure 3.3B). Under these conditions βHb is heavily oxidized, with a mass distribution that is dominated by molecules that have incorporated two oxygen atoms (+32 Da). Additional oxidation products are observed as well, up to at least [βHb + 4O]. In contrast, αHb shows hardly any evidence of oxidation. This different behavior can be attributed to the higher number of easily oxidizable amino acids in βHb (1 Cys and 3 Met, vs. 0 Cys and 1 Met for αHb) [52, 59]. The data in Figure 3.3A prove that the base amount of oxidation in bulk solution is minimal for the protein samples employed here. Yet, a moderate change in ESI conditions (as in Figure 3.3B) results in extensive βHb oxidation. ESI-MS users unaware of this type of artifact might therefore be misled when assessing the properties of a protein sample.

For suppressing βHb oxidation it was not necessary to change both V_0 and v_f. Instead, data comparable to those in Figure 3.3A could be obtained by modifying just one of these parameters. Also, increasing the protein concentration by a factor of ten at V_0 = 3.5 kV and v_f = 1 μL min^{-1} had a similar effect (data not shown). The mass distributions

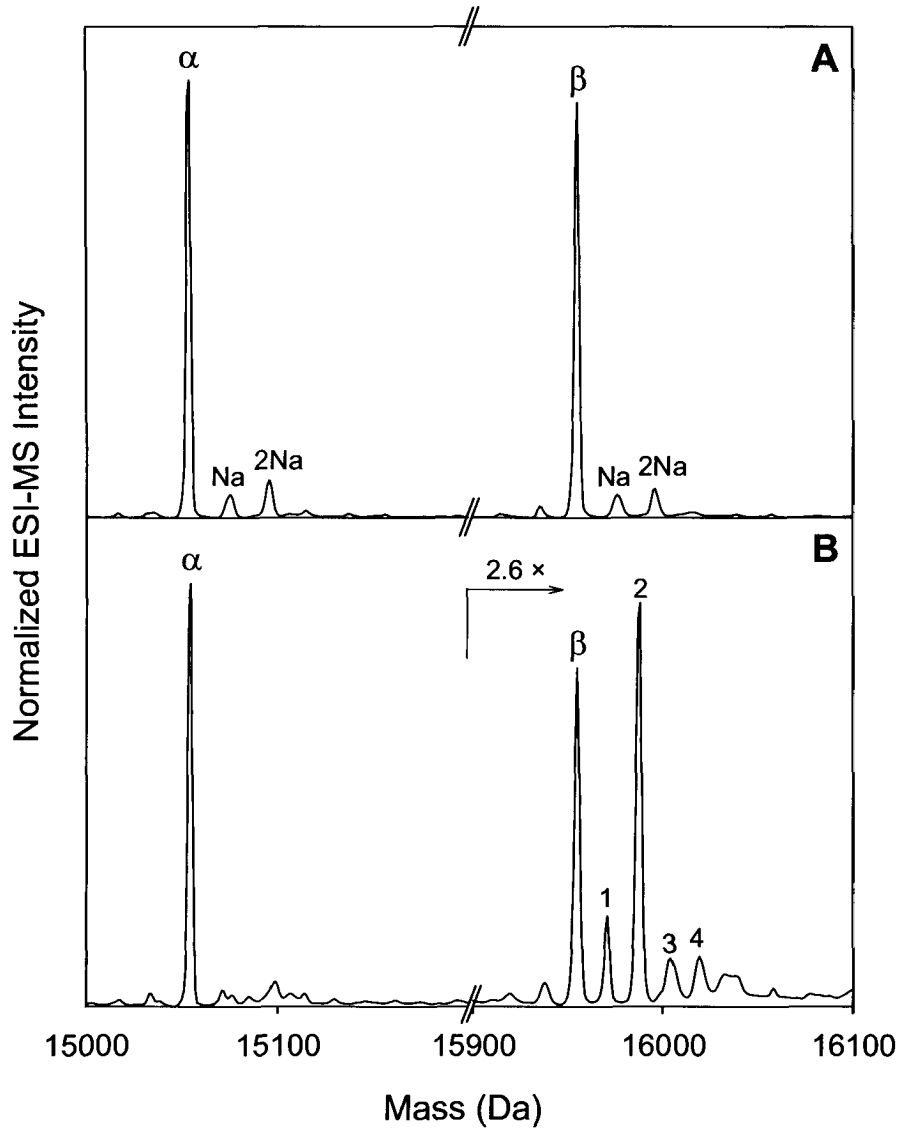

Figure 3.3: Deconvoluted ESI mass spectra of acid-denatured hemoglobin, with signals corresponding to both subunits (αHb and βHb). (A) V_0 = 2.0 kV, solution flow rate 10 μL min^{-1}. (B) V_0 = 3.5 kV, solution flow rate 1 μL min^{-1}. Minor satellite peaks in panel A represent sodium adducts. Selected peaks in panel B are labeled according to the number of incorporated oxygen atoms (1 - 4). Nitrogen was used as nebulizer gas for both spectra.

in Figure 3.3 were highly reproducible over several months, and with capillaries that had been operated for different periods of time. A pronounced dependence of protein oxidation levels on capillary age, as reported in a previous study [20], was not apparent in our measurements.

The observation of extensive oxidation under the conditions of Figure 3.3B is surprising, considering that the capillary voltage used (3.5 kV) is well within the typical operating range recommended by the instrument manufacturer. This value of V_0 resulted in excellent signal stability and intensity. No luminescence was observable by visual inspection of the emitter tip under ambient light. This scenario is quite different from previous radical probe-MS experiments where proteins were oxidized under much harsher conditions, by operating the ESI source at 8 kV with O_2 nebulizer gas in the presence of a clearly visible discharge [3, 8, 46].

3.3.2 Corona Discharge with Different Nebulizer Gases

The voltage required to induce corona discharge depends on the dielectric strength of the gas separating the electrodes [60]. To eliminate experimental factors related to electrode geometry, the dielectric strength is usually reported relative to N_2, which is arbitrarily assigned a value of unity. On this scale the reported values of Ar, O_2, and SF_6 are 0.18, 0.92, and 2.6, respectively [60].

Measurements of the current I_{tot} vs. ESI capillary voltage V_0 are depicted in Figure 3.4. These data were recorded while infusing Hb solution at a flow rate of $v_f = 1$ μL min^{-1}. The onset of discharge for N_2 is marked by a conspicuous "kink" [44] at $V_0 \approx 3$ kV, followed by a steep rise in current up to $I_{tot} = 4.0$ μA at $V_0 = 5.0$ kV. Notably, light

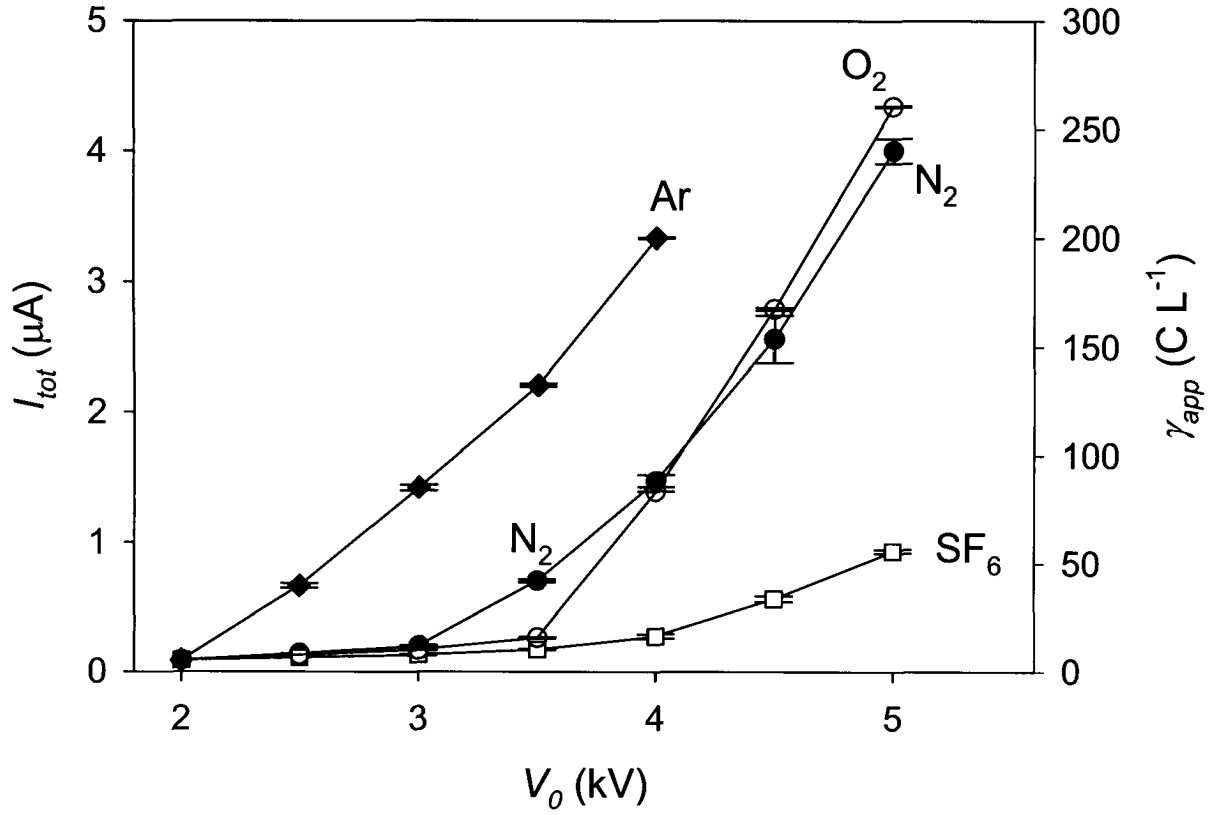

Figure 3.4: Total current I_{tot} as a function of capillary voltage for different nebulizing gases, measured while electrospraying 1μM Hb in 10 mM ammonium acetate with 2% (v/v) formic acid at v_f = 1 μL min^{-1}. Data points represent the average of 3-6 independent measurements, error bars indicate standard deviations. Also shown is the apparent electrolytic load γ_{app} (eq 4).

emission was not readily apparent up to at least 4 kV, demonstrating that visual inspection alone is not adequate for determining whether or not corona discharge occurs. Instead, voltage-current plots of the type displayed in Figure 3.4 are much better suited for this purpose. Discharge for Ar begins at a considerably lower voltage than for N_2, around 2 kV. In contrast, strong suppression of corona discharge occurs for SF_6, with I_{tot} values that are several fold lower than for N_2 in the range of 3.5 to 5 kV. Nonetheless, a weak discharge appears to be present for SF_6 upwards of around V_0 = 4 kV. These observations are in line with previous ESI-MS studies where SF_6 was used as nebulizer gas to suppress the extent of discharge [61, 62]. The behavior seen in Figure 3.4 for Ar, N_2, and SF_6 is qualitatively consistent with the dielectric strength values quoted above. Interestingly, the voltage-current curve for O_2 resembles that for N_2, except that the onset of discharge is shifted to ca. 3.5 kV, despite its slightly lower dielectric strength. This behavior can be attributed to the electron scavenging activity of molecular oxygen [45, 63].

As a side note, it is pointed out that oxidation of all βHb at the metal/liquid interface would result in I_{tot} = 12.8 nA at the flow rate used. This estimate assumes that (i) four electrons are released from each βHb (corresponding to two Met → MetO conversions), (ii) mass transfer is not limiting, (iii) I_{corona} = 0, and (iv) βHb oxidation is the only charge-balancing redox reaction. The measured I_{tot} values are much larger than 12.8 nA, even for capillary voltages that do not result in corona discharge, for example I_{tot} = 140 nA with N_2 at 2.5 kV. This demonstrates that even extensive electrochemical protein oxidation could provide only a very minor contribution to the charge-balancing current I_{ESI}. Consistent with this notion is the observation of cyclic voltammograms that

are indistinguishable when recorded with and without 1 μM Hb (data not shown). The major charge-balancing reaction under the conditions of our work is likely the oxidation of water ($2\ H_2O \rightarrow 4\ H^+ + O_2 + 4\ e^-$, $E^0 = 0.9$ V vs. SCE at pH 2)[64], an assertion that is in line with earlier studies [26, 65].

3.3.3 Dependence of ESI-Induced Oxidation on Nebulizer Gas and V_0

ESI mass spectra of 1 μM Hb were recorded at $v_f = 1$ μL min^{-1} for the various voltages and nebulizer gases examined in Figure 3.4. We will restrict our discussion to βHb because of its greater oxidation susceptibility. Representative data are depicted in Figure 3.5, highlighting that the extent of oxidation increases as the capillary voltage is raised. Compared to the behavior observed for N_2 (Figure 3.5A-D), oxidation for SF_6 is much less prevalent and remains virtually undetectable up to ca. 4.0 kV (Figure 3.5E-H). O_2 provides less oxidation than N_2 at 3.5 kV (Figure 3.5J), whereas the situation is reversed at 5.0 kV (Figure 3.5L). Of the four gases studied, only Ar yields significant oxidative modifications at 2.5 kV (Figure 3.5M), but no oxidation is observable at 2.0 kV (data not shown). Ar spectra acquired at $V_0 > 2.5$ kV are not included in Figure 3.5 due to their unacceptable S/N ratio, which might be the result of oxidative backbone cleavage.

We now return to the question whether protein oxidation during ESI is predominantly due to corona discharge-generated ROS, or whether the effect is linked to heterogeneous electron transfer at the metal/liquid interface. Cursory inspection of the data in Figures 3.4, 3.5 immediately points to a correlation between discharge and oxidation, suggesting a causative relationship between the two factors. Still, alternative explanations cannot be discounted without additional considerations. Specifically, an

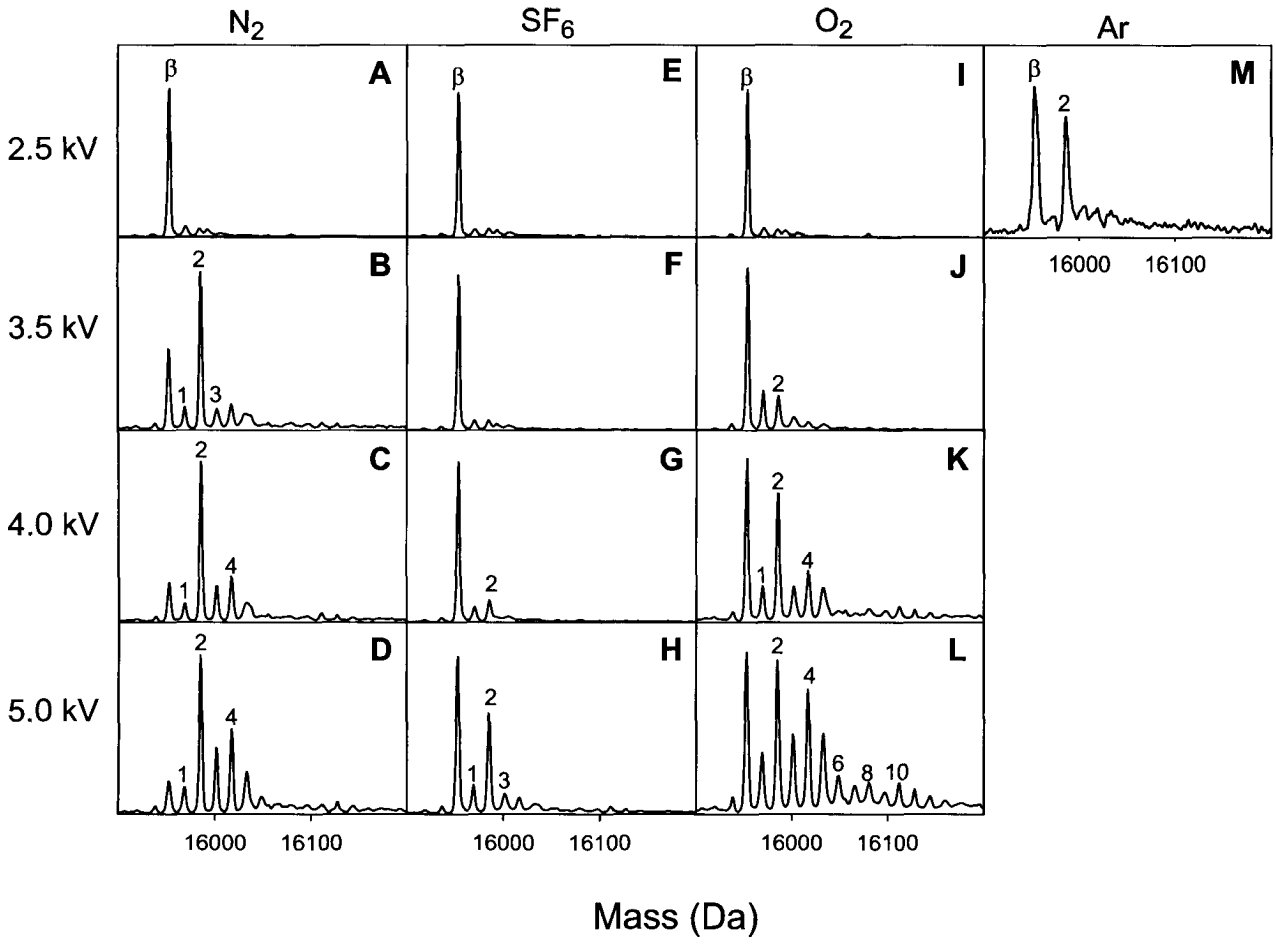

Figure 3.5: Deconvoluted ESI mass spectra of 1 μM βHb acquired as a function of capillary voltage (2.5 - 5.0 kV; indicated on the left hand side) for different nebulizer gases (N_2, SF_6, O_2, and Ar; indicated along the top) at a flow rate of 1 μL min^{-1}. Selected peaks are labeled according to the number of incorporated oxygen atoms (1 - 10).

increase in V_0 applied in order to induce discharge might at the same time render the conditions for electrochemical protein oxidation more favorable, e.g., by enhancing $V_{M/L}$ and I_{ESI} [25]. But can such a scenario be sufficient to account for a dramatic rise in βHb oxidation? This issue can be addressed by comparing spectra recorded with and without corona discharge under otherwise identical conditions. For example, a corona is absent with SF_6 at 3.5 kV (Figure 3.4), and no protein oxidation is observed under these conditions (Figure 3.5F). In contrast, repeating the measurement with N_2 under otherwise identical conditions induces significant oxidation (Figure 3.5B) as well as discharge (Figure 3.4). If we assume that the electrochemical conditions within the ESI capillary are largely the same in both experiments, it follows that charge-balancing redox reactions can *not* account for the observed βHb oxidation. Instead, the occurrence of oxidative modifications in Figure 3.5B must be attributed to the presence of the corona discharge. Analogous conclusions can be drawn by comparing other data sets, e.g., N_2 and O_2 (Figure 3.5B/J), or N_2 and Ar (Figure 3.5A/M).

In summary, the discussion presented above supports a mechanism whereby ESI-induced protein oxidation is mediated solely by ROS that are generated in the plasma of the discharge. However, the analysis relies on the assumption that the electrochemical conditions inside the metal capillary are largely the same with and without discharge, as long as all other parameters (V_0, solution composition, flow rate, etc.) do not change. Because this assertion may not always be valid we sought to corroborate our conclusions based on an alternative strategy.

3.3.4 Protein Electrolysis in Bulk Solution

The electrolysis cell depicted in Figure 3.2 was used in an attempt to mimic electrochemical processes occurring at the metal/liquid interface of the ESI capillary. For describing the extent to which a solution has been exposed to oxidative conditions it is convenient to define an "electrolytic load" γ which describes how many Coulombs of electrons have been removed from a given volume, i.e.

$$\gamma = (electron\ charge\ extracted) / volume \qquad (2)$$

In an ESI source this value is given by

$$\gamma = I_{ESI} / v_f \qquad (3)$$

As noted above, the magnitude of I_{ESI} in the presence of a corona discharge cannot be determined directly, but only the value of I_{tot} which includes the contribution I_{corona} (eq 1). We thus define an "apparent" electrolytic load γ_{app} as

$$\gamma_{app} = I_{tot} / v_f \qquad (4)$$

with $\gamma_{app} \geq \gamma$. The two parameters are equal only in the absence of corona discharge. Although the electrolytic cell depicted in Figure 3.2 uses the same solvent system and working electrode material as our ESI experiments, it is clear that such an off-line device does not perfectly reproduce the geometry, potential distribution, and mass transfer

properties of an actual ESI source. Nonetheless, relevant information can be obtained when comparing results for the two systems based on their electrolytic load.

Following off-line electrolysis of 1 μM Hb solution, mass distributions were measured by LC/ESI-MS under conditions that are free of artifactual in-source oxidation (Figure 3.6A). We will initially focus on off-line data obtained for a working electrode potential drop of $V_{M/L}$ = 1.5 V vs. SCE, which represents a typical value that might be encountered within an ESI capillary [30]. The electrolytic load γ of the solution in the cell can be controlled by adjusting the electrolysis time t. Off-line electrolysis does not result in discernible protein oxidation up to ca. γ = 90 C L^{-1} (t = 3.7 min, Figure 3.6B). To put this into context, extensive oxidative modifications are observed for the ESI-MS data in Figure 3.5C which were recorded under corona discharge conditions with $\gamma_{app} \approx$ 90 C L^{-1} (the actual electrolytic load in the latter case is considerably below 90 C L^{-1} because $\gamma_{app} > \gamma$). This comparison implies that electrochemical oxidation at the metal/liquid interface of the ESI capillary is *not* capable of accounting for the protein oxidation observed under the conditions of Figure 3.5C. In other words, protein oxidation observed in the ESI-MS measurement (Figure 3.5C) must be ascribed to the effects of ROS generated in the corona discharge of the ion source.

As noted above, water oxidation (E^0 = 0.9 V vs. SCE at pH 2) [64] likely represents the major charge-balancing reaction within the ion source under the conditions of our work. The values of $V_{M/L}$ for the ESI-MS measurements in Figure 3.5 might therefore be expected to remain considerably below 1.5 V due to redox buffering [35, 38]. Cyclic voltammetry using our electrolysis system (Figure 3.2) showed the minimum $V_{M/L}$ required for water oxidation to be around 1.3 V vs. SCE (data not shown). This relatively

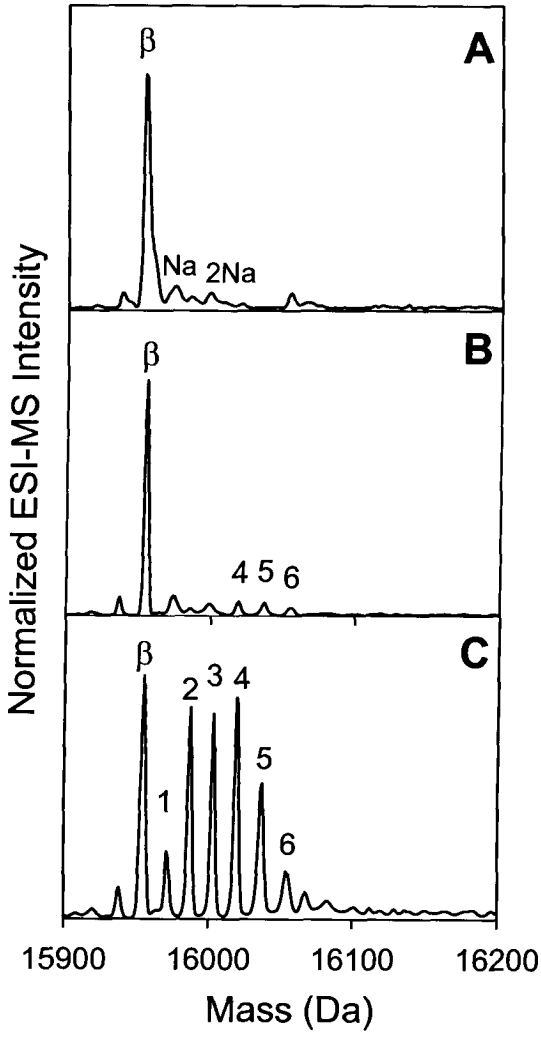

Figure 3.6: Deconvoluted ESI mass spectra of 1 μM βHb after electrolysis using the cell depicted in Figure 3.2. (A) no potential applied, circulation time t = 1 h, γ = 0 (control); (B) $V_{M/L}$ = 1.5 V vs. SCE, t = 3.7 minutes, γ = 90 C L^{-1}; (C) $V_{M/L}$ = 1.5 V vs. SCE, t = 44 minutes, γ = 1000 C L^{-1}.

high value can be attributed to an overpotential [37]. Nonetheless, off-line electrolysis experiments analogous to that in Figure 3.6B were repeated at lower $V_{M/L}$ in order to test if these conditions resulted in more extensive protein oxidation (e.g., $V_{M/L}$ = 1.0 V, t = 2 h, γ = 90 C L^{-1}). Protein solutions treated in this way showed very little oxidation, yielding mass distributions comparable to that in Figure 3.6B (data not shown). These results demonstrate that our conclusions do not depend on the specific choice of $V_{M/L}$ during off-line electrolysis.

Finally, it is pointed out that substantial βHb oxidation can be induced under off-line conditions by using a much larger electrolytic load, e.g., t = 44 min at 1.5 V, corresponding to γ = 1000 C L^{-1} (Figure 3.6C). These data confirm that electrochemical protein oxidation at a metal/liquid interface is possible in principle, thus reiterating that the question posed in the title of this work is not unreasonable. Nonetheless, our results clearly demonstrate that such an electrochemical mechanism cannot account for covalent oxygen adducts formed under typical ESI operating conditions.

3.4 Conclusions

The occurrence of protein oxidative modifications in radical probe-MS is well established. In those experiments, oxygen incorporation into amino acid side chains is induced by operating an ESI source at extremely high capillary voltage and with O_2 nebulizer gas in the presence of a clearly visible corona discharge [3, 8, 46]. The current work demonstrates that considerable oxidation can take place even under standard operating conditions, i.e., with nitrogen nebulizer gas and at much lower capillary voltage. The extent of oxidation is protein-dependent, e.g., αHb is less susceptible than βHb, presumably due to the greater number of Met and Cys residues in the latter (Figure 3.3). To our knowledge, this study represents the first attempt to systematically explore the basis of ESI-induced protein oxidation. Corona discharge-induced hydroxyl radicals are commonly cited as the causative agent, but a possible role of heterogeneous electrochemistry has never been explicitly ruled out. Our results confirm that ROS formed in the plasma of a corona discharge are responsible for protein oxidation, even at low capillary voltage where the presence of a discharge can easily go undetected. This conclusion is based on measurements of I_{tot} in the ESI circuit (Figure 3.4), comparative ESI-MS experiments with nebulizer gases of different dielectric strength (Figure 3.5), and off-line electrochemical studies (Figure 3.6). The occurrence of charge-balancing oxidation reactions at the metal/liquid interface of the ESI capillary is undisputed [22, 25, 26]. While those processes do not lead to the formation of covalent (+16 Da) modifications on proteins, they may be responsible for other effects such as the $Fe^{2+} \rightarrow Fe^{3+}$ oxidation of protein-bound heme groups [27, 28].

Careful control of artifactual protein oxidation has considerable practical implications, particularly for studies that use oxidative labeling for exploring solvent accessibility [3, 4] and for experiments aimed at monitoring the level of oxidative damage in bulk solution [1, 2]. For example, the Hb model chosen for this work illustrates a possible quality control issue for medical blood supplies. One possible strategy for avoiding oxidation artifacts is to operate the ESI source without corona discharge by lowering the capillary voltage. However, very low values of V_0 will compromise sensitivity, and therefore this course of action is not always advisable. Detecting the onset of discharge by measuring I_{tot} as a function of V_0 is simple, but unfortunately most commercial mass spectrometers are not equipped with an ammeter at the appropriate point in the ESI circuit (Figure 3.1). Our results demonstrate that a discharge can be present long before it is detectable by visual inspection of the emitter tip under ambient light conditions. The use of N_2 nebulizer gas for eliminating oxidation artifacts is not a viable strategy. In fact, due to its electron scavenging activity [45, 63] O_2 suppresses the onset of corona discharge, thereby reducing the extent of oxidation at moderate capillary voltage compared to N_2 (Figure 3.5B, J). Consistent with this finding is the fact that oxygen atoms incorporated into protein side chains originate from water, not from molecular oxygen [20, 49]. Suppression of corona discharge-induced oxidation by using SF_6 nebulizer gas is most effective, but associated with considerable cost. Argon and other noble gases have to be avoided due to their extremely low dielectric strength (Figure 3.4).

Corona discharge-induced oxidation can be strongly reduced by increasing the solution flow rate v_f and/or the protein concentration. This relationship may be rationalized based on the molar protein : ROS ratio [15], but the actual origin of such a

"dilution strategy" is likely more complicated [57]. Previous work indicated that repolishing the ESI capillary tip after accumulation of an oxide layer can also suppress protein oxidation [20]. This effect appears to be instrument-dependent since we did not notice a pronounced dependence of capillary age on the Hb spectra. The addition of radical scavengers [57] or redox buffers [20] represents another possibility, although such a strategy may lead to nonspecific adduct formation or ion suppression. It appears that ESI-MS experiments aimed at characterizing protein oxidation levels in bulk solution should always involve easily oxidizable test proteins as internal standards. Polypeptide chains containing multiple Met residues, such as βHb, are most suitable for this purpose. Possible implications of our findings for the mechanism of analyte oxidation during desorption-ESI (DESI)-MS [66] will have to await further investigations.

3.5 References

1. Soskic, V., Groebe, K. & Schrattenholz, A. (2008) Nonenzymatic posttranslational protein modifications in ageing, *Exp. Gerontol. 43*, 247-257.

2. Chao, C.-C., Ma, Y.-S. & Stadtman, E. R. (1997) Modification of protein surface hydrophobicity and methionine oxidation by oxidative systems, *Proc. Natl. Acad. Sci. U.S.A. 94*, 2969-2974.

3. Xu, G. & Chance, M. R. (2007) Hydroxyl Radical-Mediated Modification of Proteins as Probes for Structural Proteomics, *Chem. Rev. 107*, 3514-3543.

4. Pan, Y., Stocks, B. B., Brown, L. & Konermann, L. (2009) Structural Characterization of an Integral Membrane Protein in its Natural Lipid Environment by Oxidative Methionine Labeling and Mass Spectrometry, *Anal. Chem. 81*, 28-35.

5. Stocks, B. B. & Konermann, L. (2009) Structural Characterization of Short-Lived Protein Unfolding Intermediates by Laser-Induced Oxidative Labeling and Mass Spectrometry, *Anal. Chem. 81*, 20-27.

6. Nukuna, B. N., Sun, G. & Anderson, V. E. (2004) Hydroxyl Radical Oxidation of Cytochrome c by Aerobic Radiolysis, *Free Radical Biol. Med. 37*, 1203-1213.

7. Charvatova, O., Foley, B. L., Bern, M. W., Sharp, J. S., Orlando, R. & Woods, R. J. (2008) Quantifying Protein Interface Footprinting by Hydroxyl Radical Oxidation and Molecular Dynamics Simulation: Application to Galectin-1, *J. Am. Soc. Mass Spectrom. 19*, 1692-1705.

8. Maleknia, S. D. & Downard, K. (2001) Radical Approaches to Probe Protein Structure, Folding, and Interactions by Mass Spectrometry, *Mass Spectrom. Rev. 20*, 388-401.

9. Sharp, J. S., Becker, J. M. & Hettich, R. L. (2004) Analysis of protein solvent accessible surfaces by photochemical oxidation and mass spectrometry, *Anal. Chem. 76*, 672-683.

10. McClintock, C., Kertesz, V. & Hettich, R. L. (2008) Development of an Electrochemical Oxidation Method for Probing Higher Order Protein Structure with Mass Spectrometry, *Anal. Chem. 80*, 3304-3317.

11. Hambly, D. M. & Gross, M. L. (2005) Laser Flash Photolysis of Hydrogen Peroxide to Oxidize Protein Solvent-Accessible Residues on the Microsecond Timescale, *J. Am. Soc. Mass Spectrom. 16*, 2057-2063.

12. Sharp, J. S. & Tomer, K. B. (2006) Effects of Anion Proximity in Peptide Primary Sequence on the Rate and Mechanism of Leucine Oxidation, *Anal. Chem. 78*, 4885-4893.

13. West, G. M., Tang, L. & Fitzgerald, M. C. (2008) Thermodynamic Analysis of Protein Stability and Ligand Binding Using a Chemical Modification- and Mass Spectrometry-Based Strategy, *Anal. Chem. 80*, 4175-4185.

14. Manzanares, D., Rodriguez-Capote, K., Liu, S., Haines, T., Ramos, Y., Zhao, L., Doherty-Kirby, A., Lajoie, G. & Possmayer. (2007) Modification of Tryptophan and Methionine Residues Is Implicated in the Oxidative Inactivation of Surfactant Protein B, *Biochemistry. 46*, 5604-5615.

15. Shum, W.-K., Maleknia, S. D. & Downard, K. M. (2005) Onset of oxidative damage in α-crystallin by radical probe mass spectrometry, *Anal. Biochem. 344*, 247-256.

16. Sharp, J. S. & Tomer, K. B. (2007) Analysis of the Oxidative Damage-Induced Conformational Changes of Apo- and Holocalmodulin by Dose-Dependent Protein Oxidative Surface Mapping, *Biophys. J. 92*, 1682-1692.

17. Fenn, J. B. (2003) Electrospray Wings for Molecular Elephants (Nobel Lecture), *Angew. Chem. Int. Ed. 42*, 3871-3894.

18. Takamoto, K. & Chance, M. R. (2006) Radiolytic Protein Footprinting with Mass Spectrometry to Probe the Strucuture of Macromolecular Complexes, *Annu. Rev. Biophys. Biomol. Struct. 35*, 251-276.

19. Bridgewater, J. D., Lim, J. & Vachet, R. W. (2006) Transition Metal-Peptide Binding Studied by Metal-Catalyzed Oxidation Reactions and Mass Spectrometry, *Anal. Chem. 78*, 2432-2438.

20. Chen, M. & Cook, K. D. (2007) Oxidation Artifacts in the Electrospray Mass Spectrometry of Aβ Peptide, *Anal. Chem. 79*, 2031-3036.

21. Van Berkel, G. J. & Zhou, F. (1995) Characterisation of an Electrospray Ion Scource as a Controlled-Current Electrolytic Cell, *Anal. Chem. 67*, 2916-1923.

22. Blades, A. T., Ikonomou, M. G. & Kebarle, P. (1991) Mechanism of Electrospray Mass Spectrometry. Electrospray as an Electrolysis Cell, *Anal. Chem. 63*, 2109-2114.

23. Van Berkel, G. J., De La Mora, J. F., Enke, C. G., Cole, R. B., Martinez-Sanchez, M. & Fenn, J. B. (2000) Electrochemical processes in electrospray ionization mass spectrometry, *J. Mass Spectrom. 35*, 939-952.

24. Kebarle, P. & Tang, L. (1993) From ions in solution to ions in the gas phase: The mechanism of electrospray mass spectrometry, *Anal. Chem. 65*, 972A-986A.

25. Van Berkel, G. J. & Kertesz, V. (2007) Electrochemistry/spray Ion Source, *Anal. Chem. 79*, 5511-5520.

26. Konermann, L., Silva, E. A. & Sogbein, O. F. (2001) Electrochemically Induced pH Changes Resulting in Protein Unfolding in the Ion Source of an Electrospray Mass Spectrometer, *Anal. Chem. 73*, 4836-4844.

27. McLafferty, F. W., Guan, Z., Haupts, U., Wood, T. D. & Kelleher, N. L. (1998) Gaseous Conformational Structures of Cytochrome c, *J. Am. Chem. Soc. 120*, 4732-4740.

28. He, F., Hendricksen, C. L. & Marshall, A. G. (2000) Unequivocal Determination of Metal Atom Oxidation State in Naked Heme Proteins: Fe(III)Myoglobin, Fe(III)Cytochrome c, Fe(III)Cytochrome b5, and Fe(III) Cytochrome b5 L47R, *J. Am. Soc. Mass Spectrom. 11*, 120-126.

29. Jackson, G. S. & Enke, C. G. (1999) Electrical Equivalence of Electrospray Ionization with Conducting and Nonconducting Needles, *Anal. Chem. 71*, 3777-3784.

30. Van Berkel, G. J., McLuckey, S. A. & Glish, G. L. (1992) Electrochemical Origin of Radical Cations Observed in Electrospray Ionization Mass Spectra, *Anal. Chem. 64*, 1586-1593.

31. Van Berkel, G. J., Giles, G. E., Bullock, J. S. & Gray, L. J. (1999) Computational Simulation of Redox Reactions within a Metal Electrospray Emitter, *Anal. Chem. 71*, 5288-5296.

32. Li, Y., Pozniak, B. P. & Cole, R. B. (2003) Mapping of Potential Gradients within the Electrospray Emitter, *Anal. Chem. 75*, 6987-6994.

33. Pozniak, B. P. & Cole, R. B. (2007) Current Measurements within the Electrospray Emitter, *J. Am. Soc. Mass Spectrom. 18*, 737-748.

34. Pozniak, B. P. & Cole, R. (2007) Ambient Gas Influence on Electrospray Potential as Revealed by Potential Mapping within the Electrospray Capillary, *Anal. Chem. 79*, 3383-3391.

35. Kertesz, V., Van Berkel, G. J. & Granger, M. C. (2005) Study and Application of a Controlled-Potential Electrochemistry-Electrospray Emitter for Electrospray Mass Spectrometry, *Anal. Chem. 77*, 4366-4373.

36. Moini, M., Cao, P. & Bard, A. J. (1999) Hydroquinone as a Buffer Additive for Supression of Bubbles Formed by Electrochemical Exidation of the CE Buffer at the Outlet Electrode in Capillary Electrophoresis/Electrospray Ionization-Mass Spectrometry, *Anal. Chem. 71*, 1658-1661.

37. Sedriks, A. J. (1996) *Corrosion of Stainless Steels*, 2nd edn, John Wiley & Sons, Inc., New York.

38. Van Berkel, G. & Kertesz, V. (2001) Redox buffering in an electrospray ion source using a copper capillary emitter, *J. Mass Spectrom. 36*, 1125-1132.

39. Brabec, V. & Mornstein, V. (1980) Electrochemical Behavior of Proteins at Graphite Electrodes. II. Electrooxidation of Amino Acids, *Biophys. Chem. 12*, 159-165.

40. Van Berkel, G. J. (2000) Insights into Analyte Electrolysis in an Electrospray Emitter from Chronopotentiometry Experiments and Mass Transport Calculations, *J. Am. Soc. Mass Spectrom. 11*, 951-960.

41. Morrow, R. (1997) The theory of positive glow corona, *J. Phys. D: Appl. Phys. 30*, 3099-3114.

42. Chen, J. & Davidson, J. H. (2002) Electron Density and Energy Distributions in the Positive DC Corona: Interpretation for Corona-Enhanced Chemical Reactions, *Plasma Chem. Plasma Process. 22*, 199-224.

43. Yamashita, M. & Fenn, J. B. (1984) Electrospray Ion Source. Another variation on the Free-Jet Theme, *J. Phys. Chem. 88*, 4451-4459.

44. Morand, K., Talbo, G. & Mann, M. (1993) Oxidation of Peptides During Electrospray Ionization, *Rapid Commun. Mass Spectrom. 7*, 738-743.

45. Wang, W., Wang, S., Liu, F., Zheng, W. & Wang, D. I. C. (2006) Optical study of OH radical in a wire-plate pulsed corona discharge, *Spectrochimica Acta Part A. 63*, 477-482.

46. Maleknia, S. D., Chance, M. R. & Downard, K. M. (1999) Electrospray-assisted Modification of Proteins: a Radical Probe of Protein Structure, *Rapid Commun. Mass Spectrom. 13*, 2352-2358.

47. Van Berkel, G., Kertesz, V. & Ford, M. J. (2004) Efficient Analyte Oxidation in an Electrospray Ion Source Using a Porous Flow-Through Electrode Emitter, *J. Am. Soc. Mass Spectrom. 15*, 1755-1766.

48. Permentier, H. P. & Bruins, A. P. (2004) Electrochemical oxidation and cleavage of proteins with on-line mass spectrometric detection: Development of an instrumental alternative to enzymatic protein digestion, *J. Am. Soc. Mass Spectrom. 15*, 1707-1716.

49. Bateman, K. P. (1999) Electrochemical Properties of Capillary Electrophoresis-Nanoelectrospray Mass Spectrometry, *J. Am. Soc. Mass Spectrom. 10*, 309-317.

50. Perutz, M. F. (1970) Stereochemistry of Cooperative Effects in Haemoglobin, *Nature. 228*, 726-739.

51. Boys, B. L. & Konermann, L. (2007) Folding and Assembly of Hemoglobin Monitored by Electrospray Mass Spectrometry Using an On-line Dialysis System, *J. Am. Soc. Mass Spectrom. 18*, 8-16.

52. Boys, B. L., Kuprowski, M. C. & Konermann, L. (2007) Symmetric Behaviour of Hemoglobin α- and β- Subunits during Acid-Induced Denaturation Observed by Electrospray Mass Spectrometry, *Biochemistry. 46*, 10675-10684.

53. Eaton, W. A., Henry, E. R., Hofrichter, J. & Mozzarelli, A. (1999) Is cooperative oxygen binding by hemoglobin really understood, *Nat. Struct. Biol. 6*, 351 - 358.

54. Antonini, E. & Brunori, M. (1971) *Hemoglobin and Myoglobin in Their Reactions With Ligands*, North-Holland Publishing Company, Amsterdam, London.

55. Griffith, W. P. & Kaltashov, I. A. (2003) Highly asymmetric interactions between globin chains during hemoglobin assembly revealed by electrospray ionization mass spectrometry, *Biochemistry. 42*, 10024 - 10033.

56. Versluis, C. & Heck, A. J. R. (2001) Gas-phase dissociation of hemoglobin, *Int. J. Mass Spectrom. 210/211*, 637-649.

57. Tong, X., Wren, J. C. & Konermann, L. (2007) Effects of Protein Concentration on the Extent of γ-Ray-Mediated Oxidative Labeling Studied by Electrospray Mass Spectrometry, *Anal. Chem. 79*, 6376-6382.

58. Verkerk, U. H. & Kebarle, P. (2005) Ion-Ion and Ion-Molecule Reactions at the Surface of Proteins Produced by Nanospray. Information on the Number of Acidic Residues and Control of the Number of Ionized Acidic and Basic Residues, *J. Am. Soc. Mass Spectrom. 16*, 1325-1341.

59. Mueser, T. C., Rogers, P. H. & Arnone, A. (2000) Interface Sliding as Illustrated by the Multiple Quaternary Structures of Liganded Hemoglobin, *Biochemistry. 39*, 15353 - 15364.

60. Lide, D. R. (2001) *CRC Handbook of Chemistry and Physics*, 82nd edn, CRC Press, Boca Raton, London, New York, Washington.

61. Ikonomou, M. G., Blades, A. & Kebarle, P. (1991) Electrospray Mass Spectrometry of Methanol and Water Solutions Supression of Electric Discharge with SF6 Gas, *J. Am. Soc. Mass Spectrom. 2*, 497-505.

62. Smith, R. D., Loo, J. A., Loo, R. R. O., Busman, M. & Udseth, H. R. (1991) Principles and practice of electrospray ionization-mass spectrometry for large polypeptides and proteins, *Mass Spectrom. Rev. 10*, 359-451.

63. Zheng, W., Zhang, L., Liu, Y., Wang, W. & Wang, X. (2009) Modeling of the production of OH and O radicals in a positive pulsed corona discharge plasma, *Vacuum. 83*, 238-243.

64. Pourbaix, M. (1966) *Atlas of Electrochemical Equilibria in Aqueous Solutions*, Pergamon Press, Oxford.

65. Van Berkel, G. J., Zhou, F. & Aronson, J. T. (1997) Changes in Bulk solution pH Caused by the Inherent Controlled-Current Electrolytic Process of an Electrospray Ion Source, *Int. J. Mass Spectrom. Ion Proc. 162*, 55-67.

66. Pasilis, S. P., Kertesz, V. & Van Berkel, G. (2008) Unexpected Analyte Oxidation during Desorption Electrospray Ionization-Mass Spectrometry, *Anal. Chem. 80*, 1208-1214.

Chapter 4 – Conclusions

4.1 Summary

Hb was used as a model system for the study of multi-subunit protein-protein interactions under equilibrium unfolding conditions. The acid-induced denaturation of freshly prepared bovine Hb was monitored via ESI-MS and UV-Vis spectroscopy. The ability of ESI-MS to simultaneously detect coexisting species and conformers in solution and to readily distinguish intramolecular contacts from intermolecular interactions make it particularly well suited for this type of analysis. The effects of posttranslational oxidative modifications on protein stability and folding reactions were found to be severe in the case of Hb (Chapter 2). Awareness of the potential for ESI-induced oxidation artifacts is examined in Chapter 3.

The results of Chapter 2 discredited the notion of the obligatory intermediate $\alpha^h\beta^a$ or 'semi-hemoglobin' in the (dis)assembly pathway for bovine ^{met}Hb. The presence of unfolded β^a, folded α^h, and $\alpha^h\beta^a$ in the mass spectra of commercially obtained protein triggered the proposition that during Hb assembly, unfolded β^a requires a folded α^h-scaffold with which to 'snap' it into a proper conformation so as to facilitate heme acquisition. Thus, $\alpha^h\beta^a$ was seen as an obligatory intermediate in the Hb assembly pathway, ensuring the correct folding of the native $(\alpha^h\beta^h)_2$ tetramer. It was shown herein that such pathways are a result of oxidatively damaged β-globin. Indeed, freshly prepared ^{oxy}Hb with no apparent oxidative modifications exhibits highly symmetric disassembly and unfolding characteristics for both α- and β- globin chains.

The objective of Chapter 3 was to shed light on the potential for ESI-induced analyte oxidation under 'typical' operating conditions. Chapter 2 highlighted the importance of knowing the oxidation status of solution phase proteins if reliable information regarding (dis)assembly and (un)folding reactions were to be obtained. Method-induced analyte oxidation would complicate analysis. It was discovered that during ESI, corona-discharge regimes are often present. When susceptible analytes are electrosprayed in the presence of even a weak corona-discharge, significant oxidation may result. Although it was demonstrated that oxidation patterns observed during 'harsh' electrospray conditions could be mimicked via solution phase electrolysis, the magnitude of the charge density required to accomplish this was such that heterogeneous solution phase electrochemistry was ruled out. This was corroborated by observing the stark increase in ESI-induced analyte oxidation when nebulizing gases of low dielectric strength were used, thus suggesting a corona-discharge mediated oxidation mechanism.

The utility of ESI-MS for elucidation of multi-subunit protein folding reactions is demonstrated. A potential pitfall relating to ESI-induced analyte oxidation was acknowledged. The mechanism of ESI-induced oxidation was determined, facilitating appropriate prevention strategies aimed at avoiding corona-discharge mediated oxidation. These include (1) monitoring the total current I_{tot}, (2) use of a nebulizing gas of high dielectric strength, (3) incorporation of radical scavengers into solutions, and (4) increasing protein concentration and flow rates when studying susceptible analytes.

4.2 Future Work

4.2.1 Hemoglobin Assembly

Much work remains to be done pertaining to the folding and assembly mechanism of Hb. The results of Chapter 2 were based on *in vitro* acid-induced equilibrium unfolding experiments. Although such *in vitro* studies are thought to provide insight into the behaviour of protein folding pathways [1], it is not immediately clear whether such experiments on the acid-induced denaturation of Hb *in vitro* have direct implications for the assembly of this protein complex at near-neutral pH and/or in a cellular environment [2]. The data presented here, therefore, do not rule out the possible occurrence of asymmetric (dis)assembly pathways under different conditions. In particular, the existence of a chaperone protein that specifically interacts with α-globin is consistent with an asymmetric mechanism *in vivo* [3-9]. It appears that ESI-MS should be well suited to provide detailed insights into the exact way in which this chaperone assists the assembly process of Hb in RBC precursors.

Furthermore, the distal coordination site and oxidation state of the iron in the heme groups of Hb have a profound effect on the observed tetramer-dimer dissociation constant [10, 11]. It would be interesting to conduct similar equilibrium unfolding studies as done herein under anaerobic conditions, where the tetramer-dimer dissociation constant is five orders of magnitude lower than under aerobic conditions. Additionally, it was noticed that upon aerobic unfolding, rapid heme oxidation from ferrous to ferric occurs. Such a one electron oxidation would result in the bound oxygen molecule leaving as a reactive super-oxide radical, which could quickly oxidize susceptible residues in the

Hb molecule from which it was created. It would be interesting to see if Hb denatured under anaerobic conditions would result in less baseline protein oxidation when compared to aerobic conditions.

4.2.2 Higher-Order Hemoglobin Assembly

Many high flying avian are thought to contain Hb types which demonstrate higher-order assemblies, i.e., tetramer-octamer equilibriums [10]. This phenomenon is thought to give rise to a form of 'supercooperativity'. ESI-MS would be well suited for the oxygen dependent analysis of potentially 'supercooperative' Hb varieties. Hydrogen/deuterium exchange studies monitored via ESI-MS could resolve solution phase higher-order structures from artifacts of the ESI process [12].

4.3 References

1. Dobson, C. M. (2004) Experimental investigation of protein folding and misfolding, *Methods. 34*, 4-14.

2. Griffith, W. P. & Kaltashov, I. A. (2003) Highly asymmetric interactions between globin chains during hemoglobin assembly revealed by electrospray ionization mass spectrometry, *Biochemistry. 42*, 10024 - 10033.

3. Luzzatto, L. & Notaro, R. (2002) Haemoglobin's chaperone, *Nature. 417*, 703-704.

4. Kihm, A. J., Kong, Y., Hong, W., Russel, J. E., Rouda, S., Adachi, K., Simon, M. C., Blobel, G. A. & Weiss, M. J. (2002) An abundant erythroid protein that stabilizes free α-haemoglobin, *Nature. 417*, 758-763.

5. Baudin-Creuza, V., Vasseur-Godbillon, C., Pato, C., Prehu, C., Wajcman, H. & Marden, M. C. (2004) Transfer of Human α- to β-Hemoglobin via its Chaperone Protein, *J. Biol. Chem. 279*, 36530-36533.

6. Santiveri, C. M., Perez-Canadillas, J. M., Viadivelu, M. K., Allen, M. D., Rutherford, T. J., Watkins, N. A. & Bycroft, M. (2004) NMR structure of the α-Hemoglobin Stabilizing Protein, *J. Biol. Chem. 279*, 34963-34970.

7. Hodge, D., Coghill, E., Keys, J., Maguire, T., Hartman, B., McDowall, A., Weiss, M., Grimmond, S. & Perkins, A. (2006) A global role for EKLF in definitive and primitive erythropoiesis, *Blood. 15*, 3359-3370.

8. Feng, L., A., G. D., Zhou, S., Gu, L., Kong, Y., Li, J., Hu, M., Yan, N., Lee, C., Rich, A. M., Armstrong, R. S., Lay, P. A., Gow, A. J., Weiss, M. J., Mackay, J. P. & Shi, Y. (2004) Molecular Mechanism of AHSP-Mediated Stabilization of α-Hemoglobin, *Cell. 119*, 629-640.

9. Feng, L., Zhou, S., Gu, L., Gell, D. A., Mackay, J. P., Weiss, M. J., Gow, A. J. & Shi, Y. (2005) Structure of oxidized α-haemoglobin bound to AHSP reveals a protective mechanism for haem, *Nature. 435*, 697-701.

10. Riggs, A. F. (1998) Self-association, cooperativity and supercooperativity of oxygen binding by hemoglobins, *J. Exper. Biol. 201*, 1073-1084.

11. White, S. L. (1975) The molecular dissociation of ferrihemoglobin derivatives, *J. Biol. Chem. 250*, 1263-1268.

12. Hossain, B. M. & Konermann, L. (2006) Pulsed Hydrogen/Deuterium Exchange MS/MS for Studying the Relationship between Noncovalent Protein Complexes in Solution and in the Gas Phase after Electrospray Ionization, *Anal. Chem. 78*, 1613-1619.

Appendix 1 – Permissions

American Chemical Society's Policy on Theses and Dissertations

If your university requires a signed copy of this letter see contact information below.

Thank you for your request for permission to include **your** paper(s) or portions of text from **your** paper(s) in your thesis. Permission is now automatically granted; please pay special attention to the implications paragraph below. The Copyright Subcommittee of the Joint Board/Council Committees on Publications approved the following:

> Copyright permission for published and submitted material from theses and dissertations
> ACS extends blanket permission to students to include in their theses and dissertations their own articles, or portions thereof, that have been published in ACS journals or submitted to ACS journals for publication, provided that the ACS copyright credit line is noted on the appropriate page(s).
>
> Publishing implications of electronic publication of theses and dissertation material
> Students and their mentors should be aware that posting of theses and dissertation material on the Web prior to submission of material from that thesis or dissertation to an ACS journal may affect publication in that journal. Whether Web posting is considered prior publication may be evaluated on a case-by-case basis by the journal's editor. If an ACS journal editor considers Web posting to be "prior publication", the paper will not be accepted for publication in that journal. If you intend to submit your unpublished paper to ACS for publication, check with the appropriate editor prior to posting your manuscript electronically.

If your paper has **not** yet been published by ACS, we have no objection to your including the text or portions of the text in your thesis/dissertation in **print and microfilm formats**; please note, however, that electronic distribution or Web posting of the unpublished paper as part of your thesis in electronic formats might jeopardize publication of your paper by ACS. Please print the following credit line on the first page of your article: "Reproduced (or 'Reproduced in part') with permission from [JOURNAL NAME], in press (or 'submitted for publication'). Unpublished work copyright [CURRENT YEAR] American Chemical Society." Include appropriate information.

If your paper has already been published by ACS and you want to include the text or portions of the text in your thesis/dissertation in **print or microfilm formats**, please print the ACS copyright credit line on the first page of your article: "Reproduced (or 'Reproduced in part') with permission from [FULL REFERENCE CITATION.] Copyright [YEAR] American Chemical Society." Include appropriate information.

Submission to a Dissertation Distributor: If you plan to submit your thesis to UMI or to another dissertation distributor, you should not include the unpublished ACS paper in your thesis if the thesis will be disseminated electronically, until ACS has published your paper. After publication of the paper by ACS, you may release the entire thesis (**not the individual ACS article by itself**) for electronic dissemination through the distributor; ACS's copyright credit line should be printed on the first page of the ACS paper.

Use on an Intranet: The inclusion of your ACS unpublished or published manuscript is permitted in your thesis in print and microfilm formats. If ACS has published your paper you may include the manuscript in your thesis on an intranet that is not publicly available. Your ACS article cannot be posted electronically on a publicly available medium (i.e. one that is not

password protected), such as but not limited to, electronic archives, Internet, library server, etc. The only material from your paper that can be posted on a public electronic medium is the article abstract, figures, and tables, and you may link to the article's DOI or post the article's author-directed URL link provided by ACS. This paragraph does not pertain to the dissertation distributor paragraph above.

Questions? Call +1 202/872-4368/4367. Send e-mail to copyright@acs.org or fax to +1 202-776-8112.
10/10/03, 01/15/04, 06/07/06